EXPLORATION AND OPTIMIZATION OF SEPARATION TECHNIQUES FOR THE REMOVAL OF MICROPLASTICS FROM MARINE SEDIMENTS DURING DREDGING OPERATIONS

Michiel Van Melkebeke

Student number: 01407604

Promotors: Prof. Dr. Ir. Steven De Meester and Prof. Dr. Colin Janssen

GHENT
UNIVERSITY

Declaration of authorship

Gent, juni 2019

Promotors,   The author,

Prof. Dr. Ir. Steven De Meester & Prof. Dr. Colin Janssen   Michiel Van Melkebeke

Preface

With pride I present you my master dissertation titled *"Exploration and Optimization of Separation Techniques for the Removal of Microplastics from Marine Sediments during Dredging Operations"*. It is the result of a challenging education program in bioscience engineering at the University of Ghent, which I started doubtful and anxious but finished passionate and determined. This work is a product of that growing ambition to improve the world we live in to the best of my ability, one step at a time. And as was proven along the way, a great dream requires a great team.

First and foremost, I want to thank Prof. Dr. Colin Janssen to introduce me into the world of marine microplastics and enable me to embark on this fascinating journey. His international contribution to raise both scientific and public awareness of the issue is remarkable. It never gets old to indulge in his seminars and speeches where he repeatedly succeeds to convince others to participate in the fight against marine plastic pollution. He encouraged me to participate in cross-disciplinary events, which added value that goes beyond the scope of a traditional academic dissertation. His involvement was both an essential and a memorable part of my thesis.

For the supervision, support and feedback I would like to express my sincere appreciation to Prof. Dr. Ir. Steven De Meester. His pleasant guidance and critical advice were fundamental to the realisation of this work. In addition, he offered the means to perform a significant part of my research at Campus Kortrijk, where I met Ruben Demets, Pieter Knockaert, Nicolas Mys, Dave Manhaeghe and Martijn Roosen. Each of them played an important role during my thesis. Ruben for his continuous support and expert advice in plastic flotation systems, Pieter for his time and effort invested in the construction of the novel flotation design, Nicolas for his guidance at Zwijnaarde science park, Dave for sharing its expertise in algae growth and Martijn for facilitating the valuable collaboration with the Matter project.

Within the GhenToxLab at Campus Coupure, which also housed a significant part of my research, I would like to stress my gratitude towards Nancy De Saeyer. She provided technical support and offered practical solutions whenever required. I will remember Nancy as a kind-hearted person with an admirable hands-on attitude. From research group PaInT, I would like to thank Prof. Dr. Ir. Paul Van der Meeren for his expert advice in particle technology and Dr. Ir. Marjolein Vanoppen for proofreading my literature review.

For the fruitful collaboration with the dredging industry, I would like to thank Emile Lemey and Pieterjan Waeyaert from Jan De Nul, and Frank Verschraegen and Tomas Sterckx from DEME. Their involvement revealed a potential synergy between the dredging industry and the remediation of marine microplastics.

Last but not least, my parents Connie and Gunther deserve some words of appreciation for their unconditional support, both financial and emotional. My mom gave me the opportunity to explore my passions and the means to do so in an untroubled and enjoyable way, for which I am very thankful. Gunther is one of the most genuine and thoughtful people I know, whose impact on my life I will never take for granted. During these past few months, they supported me every step of the way and carried me through the pitfalls of my research, one at a time. Finally, I want to thank my girlfriend Elyssia for lifting my spirits when my morale was low and for her encouraging, loving personality. Thank you!

Michiel Van Melkebeke   Ghent, June 2019

Table of Contents

Abbreviations

AC	Acrylate
BCS	Best-case scenario
DAF	Dissolved air flotation
DDT	Dichlorodiphenyltrichloroethane
GESAMP	Joint Group of Experts on the Scientific Aspects of Marine Environmental Protection
HCl	Hydrogen chloride
HDPE	High-density polyethylene
LDPE	Low-density polyethylene
LMPs	Large microplastics
LR-SMPs	Lower range small microplastics
NaCl	Sodium chloride
N/A	Not available or Not applicable
PA	Polyamide
PAH	Polycyclic aromatic hydrocarbon
PC	Polycarbonate
PCB	Polychlorinated biphenyl
PES	Polyester
PET	Polyethylene terephthalate
POP	Persistent organic pollutant
PP	Polypropylene
PS	Polystyrene
PSD	Particle size distribution
PUR	Polyurethane
PVC	Polyvinyl chloride
PVDC	Polyvinylidene chloride
SMPs	Small microplastics
TSHD	Trailing suction hopper dredger
UR-SMPs	Upper range small microplastics
WCS	Worst-case scenario
WWTP	Wastewater treatment plant

Nomenclature

Symbol	Description	SI unit
a	Longest particle principal axis	m
a_c	Centrifugal accelaration	m s^{-2}
A	Cross sectional area	m^2
A_o	Particle surface area occupied by a single bubble	m^2
A_p	Particle surface area	m^2
A_{bp}	Bio-fouled particle surface area	m^2
A_{sph}	Surface area of the volume-equivalent sphere	m^2
b	Intermediate particle principal axis	m
Bo	Bond number	-
β	Particle shape factor	-
c	Shortest particle principal axis	m
C_D	Drag coefficient	-
$C_{D,calc}$	Theoretically calculated drag coefficient	-
$C_{D,meas}$	Measured drag coefficient	-
$C_{D,ref}$	Drag coefficient of reference spheres	-
$C_{D,sphere}$	Drag coefficient of a sphere	-
CSF	Corey Shape Factor	-
χ	Particle circularity	-
d_c	Smallest particle circumscribed circle	m
d_i	Largest particle inscribed circle	m
d_o	Bubble hemisphere diameter	m
d_p	Volume-equivalent sphere diameter	m
d_{bu}	Bubble diameter	m
$d_{p,50}$	Particle diameter with 50 % separation efficiency or critical diameter	m
$d_{p,100}$	Particle diameter with 100 % separation efficiency	m
d_*	Nominal diameter according to Dietrich (1982)	-
d_{**}	Nominal diameter according to Camenen (2007)	-
D	Pipe diameter	m
D_b	Bowl diameter of a decanter	m
D_w	Weir diameter of a decanter	m
e	Particle elongation	-

Symbol	Description	SI unit
E_1	Energy barrier for particle-bubble attachment	J
E_{d_p}	Grade efficiency	-
E_k	Kinetic energy of collision	J
ϵ	Solids volume fraction	-
f_w	Wall factor	-
F_c	Centrifugal force	N
F_D	Drag force	N
F_N	Newton shape factor	-
F_S	Stokes shape factor	-
$\mathcal{F}$	Particle flatness	-
g	Gravitational acceleration	m s^{-2}
γ_c	Critical surface tension	N m^{-1}
γ_{lv}	Liquid-vapor interfacial tension	N m^{-1}
γ_{sl}	Solid-liquid interfacial tension	N m^{-1}
γ_{sv}	Solid-vapor interfacial tension	N m^{-1}
h_p	Height of a flattened cubic particle	m
h_{bp}	Height of a flattened cubic bio-fouled particle	m
$H_{recycle}$	Position of the recycle inlet	m
H_{sieve}	Position of the sieve plate	m
K	Particle bubble-coverage percentage	-
K_1	Stokes shape factor	-
K_2	Newton shape factor	-
K_S	Stokes drag corrector	-
K_N	Newton drag corrector	-
l_p	Length of a flattened cubic particle	m
l_{bp}	Length of a flattened cubic bio-fouled particle	m
L_b	Total bowl length of a decanter	m
L_{cyl}	Cylindrical length of a decanter	m
m_b	Biofilm mass	kg
m_p	Particle mass	kg
μ	Dynamic viscosity	Pa s
n	Speed	rpm
N	Number	-
$N_{venturi}$	Number of venturi spargers	-
ν	Kinematic viscosity	m^2 s^{-1}
Ω	Angular velocity	s^{-1}
P	Powers Index	-
P	Particle collection probability	-

Symbol	Description	SI unit
P_a	Particle-bubble adhesion probability	-
P_c	Particle-bubble collision probability	-
P_d	Particle-bubble detachment probability	-
Φ	Particle sphericity	-
Φ_K	Particle sphericity proposed by Krumbein (1941)	-
Φ_R	Particle sphericity proposed by Riley (1941)	-
$\Phi_{S\&F}$	Particle sphericity proposed by Sneed and Folk (1958)	-
Ψ	Particle shape factor	-
Q	Flow rate	m^3 s^{-1}
Q_{air}	Venturi air inlet flow rate	m^3 s^{-1}
Q_{in}	Decanter inlet flow rate	m^3 s^{-1}
r	Radial distance	m
r_i	Radial distance to where the feed mixture is located	m
R	Radius of a centrifugal drum	m
Re_p	Particle Reynolds number	-
Re_{bu}	Bubble Reynolds number	-
Re_{start}	Initial prediction of the particle Reynolds number	-
R_b	Bowl radius of a decanter	m
R_w	Weir radius of a decanter	m
R_H	Hindered settling function	-
RC	Relative centrifgual force	-
ρ'	Particle to fluid density ratio	-
ρ_a	Particle-bubble aggregate density	kg m^{-3}
ρ_b	Biofilm density	kg m^{-3}
ρ_f	Fluid density	kg m^{-3}
ρ_p	Particle density	kg m^{-3}
ρ_{bp}	Bio-fouled particle density	kg m^{-3}
t_a	Residence time	s
T	Temperature	K
T_b	Biofilm thickness	m
θ	Contact angle	°
θ_a	Advancing contact angle	°
θ_r	Receding contact angle	°
θ_Y	Young's contact angle	°
u_c	Centrifugal settling velocity	m s^{-1}
u_t	Terminal settling velocity	m s^{-1}
u_{bu}	Terminal bubble rising velocity	m s^{-1}
$u_{t,calc}$	Theoretically calculated terminal settling velocity	m s^{-1}

Symbol	Description	SI unit
$u_{t,meas}$	Measured terminal settling velocity	m s^{-1}
u_*	Nominal settling velocity	-
v_θ	Tangential velocity	m s^{-1}
V_b	Biofilm volume	m^3
V_p	Particle volume	m^3
V_{bp}	Bio-fouled particle volume	m^3
V_{bu}	Bubble volume	m^3
V_{eff}	Effective volume of a centrifuge	m^3
φ	Particle aspect ratio	-
W_{sc}	Screw Pitch	m

Abstract

Microplastic particles are ubiquitous pollutants in the marine environment, predominantly (i.e. > 90 %) accumulating in sediments worldwide. Numerous studies on sources, occurrence and potential impact of marine microplastics have been published, yet research on remediation is lacking. The aim of this work was to identify, develop and optimize a separation technique that isolates microplastics from marine sediments, while aspiring a synergy with the dredging industry. To that end, an explorative review of potential separation techniques was established. Based on this review as well as on a qualitative and quantitative characterisation of the target mixture of sediment and microplastic particles, two promising separation technologies were selected, namely centrifugal sedimentation and froth flotation. In order to appropriately evaluate their separation performance, the sinking behaviour of microplastic particles obtained by fragmentation of municipal plastic waste products was experimentally examined, and the drag model that best accounts for the particularly irregular shape of the corresponding particles was identified. In addition, the effect of marine biofouling on the surface of different plastic types was analyzed.

Separation by means of centrifugal sedimentation is concluded to be a potentially effective sediment remediation technique for low-density microplastics (i.e. floating in seawater) but appears ineffective for high-density microplastics (i.e. non-floating in seawater) based on theoretical calculations regarding a decanter centrifuge. These calculations included the newly identified drag model, which illustrates that both sphericity and circularity are essential shape descriptors to account for the different shape classes of microplastics such as spheres, fibres and foils. Moreover, the decanter grade efficiency curves of sediment and high-density microplastics revealed that centrifugal sedimentation seems to be an inappropriate separation technique for the remediation of high-density microplastics from marine sediments. This is primarily due to the significant overlap of the inherent particle diameter ranges of sediment and high-density microplastics, which can not be compensated by their considerable difference in density. On the other hand, successful remediation is expected for low-density microplastics. However, the phenomenon of marine biofouling might reverse this prediction for low-density microplastics in case the biofilms would not detach from the surface of bio-fouled microplastics during the separation process. This implies that in case low-density microplastics end up on the seabed due to density-modification caused by marine biofouling, the initial density must be restored during centrifugal operation to achieve successful remediation.

With respect to froth flotation, a novel installation is proposed and constructed primarily based on the principles of a cyclonic-static microbubble flotation column (FCSMC) applied in the mining industry. A microplastic recovery rate > 95 % is experimentally derived for high-density microplastics with a diameter > 2 mm from sediment mixtures associated with the mud fraction (i.e. particle size < 63 μm) or the sand fraction (i.e. particle size between 63 μm and 2 mm) at a concentration of 1000 microplastic particles/kg sediment. The corresponding sediment entrainment is independent of the microplastic concentration and equals less than 0.15 m% for the sand fraction, yet increases to approximately 5 m% for the mud fraction. For a concentration of 100 microplastic particles/kg sediment, which corresponds to the global average concentration of intertidal sediments, a microplastic recovery rate of approximately 85 % is found for high-density microplastics. With respect to low-density microplastics, a consistent recovery rate of 100 % is obtained. The results from the biofouling analysis show that bio-fouled microplastics shift from hydrophobic to hy-

drophilic behaviour (i.e. from contact angles $> 90°$ to $< 90°$), which is undesirable for separation by means of froth flotation. However, it is hypothesized that the corresponding biofilms will detach from the surface of the microplastics during the separation process, similarly as assumed in the calculations regarding the decanter centrifuge. Further research is required to experimentally examine the effect of marine biofouling on the microplastic recovery rate of the novel flotation installation and evaluate its separation performance in more detail.

The findings presented in this thesis provide fundamental information about the sinking behaviour of representative microplastics and their most appropriate shape descriptors. As a result, the first extensive evaluation of different drag models was performed and identified the shape-dependent drag law that best predicts the settling velocity of microplastic particles. Furthermore, the unknown effect of marine biofouling on the surface chemical properties of plastics was analyzed. These results are of paramount importance to understand the dynamic behaviour and fate of microplastic particles in the marine environment, and might serve as a stepping stone towards the development of promising remediation techniques, as demonstrated in this work with the design of the novel flotation installation.

To conclude, this thesis illustrates that successful remediation of microplastics from marine sediments is possible, yet further research is required to experimentally evaluate large-scale applications. Therefore, this work might serve as the foundation to trigger the development of innovative solutions to answer the global microplastic accumulation issue. In addition, the recognition of a potential synergistic collaboration with the dredging industry might act as a catalyst for short-term international remediation operations to help cope with the growing concerns about marine microplastic pollution.

Samenvatting

Microplastic deeltjes zijn alomtegenwoordige verontreinigende stoffen in het mariene milieu, die zich wereldwijd hoofdzakelijk (> 90 %) ophopen in sedimenten. Talrijke studies omtrent de oorsprong, het voorkomen en de potentiële impact van mariene microplastics zijn reeds gepubliceerd, echter onderzoek naar de remediatie ervan ontbreekt. Het doel van dit werk was het identificeren, ontwikkelen en optimaliseren van een scheidingstechniek die microplastics isoleert van mariene sedimenten en tegelijkertijd een synergie met de baggerindustrie beoogt. Daartoe werd een verkennend onderzoek naar potentiële scheidingstechnieken gerealiseerd. Op basis van deze beoordeling alsook van een kwalitatieve en kwantitatieve karakterisering van het doelmengsel van sediment en microplastic deeltjes, werden twee veelbelovende scheidingstechnologieën geselecteerd, namelijk centrifugale sedimentatie en schuimflotatie. Om hun scheidingsprestatie op gepaste wijze te evalueren, werd het bezinkingsgedrag van microplastic deeltjes, die verkregen werden door fragmentatie van gemeentelijk plastic-houdend afval, experimenteel onderzocht en werd het drag model dat het best de bijzonder onregelmatige vorm van deze deeltjes kwantificeert, geïdentificeerd. Daarnaast werd ook het effect van mariene biofouling op het oppervlak van verschillende plastic soorten geanalyseerd.

Scheiding door middel van centrifugale sedimentatie blijkt een potentieel effectieve sediment remediatie techniek te zijn voor lage-dichtheid microplastics (i.e. drijvend in zeewater), maar niet voor hoge-dichtheid microplastics (i.e. niet-drijvend in zeewater) op basis van theoretische berekeningen met betrekking tot een decanter centrifuge. Deze berekeningen omvatten het nieuw geïdentificeerde drag model, welke aantoont dat zowel sfericiteit als circulariteit essentiële vormfactoren zijn voor het beschrijven van de verschillende vormklassen van microplastics, zoals bollen, vezels en folies. Daarnaast onthulden de decanter grade efficiency curves van sediment en hoge-dichtheid microplastics, dat centrifugale sedimentatie niet geschikt is voor de remediatie van deze hoge-dichtheid microplastics uit mariene sedimenten. Dit is voornamelijk te wijten aan de significante overlap van de inherente partikeldiameter ranges van sediment en hoge-dichtheid microplastics, welke tevens niet gecompenseerd kan worden door hun aanzienlijk verschil in dichtheid. Anderzijds wordt voor lage-dichtheid microplastics wel een succesvolle remediatie verwacht. Echter, het natuurlijk fenomeen van mariene biofouling kan deze verwachting voor lage-dichtheid microplastics omkeren in het geval dat de biofilms tijdens het scheidingsproces niet zouden loskomen van het oppervlak van biofouled microplastics. Dit houdt in dat wanneer lage-dichtheid microplastics op de zeebodem terechtkomen als gevolg van dichtheidsmodificatie veroorzaakt door mariene biofouling, de initiële dichtheid moet worden hersteld tijdens centrifugatie om succesvolle remediatie te bereiken.

Met betrekking tot schuimflotatie is een nieuwe installatie voorgesteld en opgebouwd die hoofdzakelijk gebaseerd is op de werkingsprincipes van een cyclonic-static microbubble flotatiekolom (FCSMC) toegepast in de mijnindustrie. Een microplastic recuperatiegraad > 95 % is experimenteel bepaald voor hoge-dichtheid microplastics met een diameter > 2 mm voor sedimentmengsels behorende tot de modderfractie (i.e. partikelgrootte < 63 μm) of de zandfractie (i.e. partikelgrootte tussen 63 μm en 2 mm) bij een concentratie van 1000 microplastic deeltjes/kg sediment. Het overeenkomstig percentage aan sediment entrainment is onafhankelijk van de microplastic concentratie en blijkt minder dan 0.15 m% voor de zandfractie, maar neemt toe tot ongeveer 5 m% voor de modderfractie. Voor een concentratie van 100 microplastic deeltjes/kg sediment, hetgeen overeenkomt met de gemiddelde globale concentratie in intergetijde sedimenten,

is een microplastic recuperatiegraad van ongeveer 85 % vastgesteld voor hoge-dichtheid microplastics. Wat betreft lage-dichtheid microplastics, wordt een consistente recuperatiegraad van 100 % verkregen. De resultaten van de biofouling analyse tonen aan dat bio-fouled microplastics verschuiven van hydrofoob naar hydrofiel gedrag (i.e. van contacthoeken $> 90°$ naar $< 90°$), hetgeen ongewenst is voor scheiding met behulp van schuimflotatie. Er wordt echter verondersteld dat de overeenkomstige biofilms tijdens het scheidingsproces loskomen van het oppervlak van de microplastics, naar analogie met de gestelde aannames in de berekeningen van de decanter centrifuge. Verder onderzoek is vereist om het effect van mariene biofouling op de microplastic recuperatiegraad van de nieuwe flotatie installatie experimenteel na te gaan en de scheidingsprestatie uitvoeriger te evalueren.

De bevindingen gepresenteerd in deze thesis bieden fundamentele kennis over het bezinkingsgedrag van representatieve microplastics en over hun meest geschikte vormfactoren. Bijgevolg kon de eerste extensieve evaluatie van verschillende drag models worden uitgevoerd die de vormafhankelijke drag law identificeerde welke het best de bezinkingssnelheid van microplastic deeltjes voorspelt. Bovendien werd het tot noch toe ongekende effect van mariene biofouling op de chemische eigenschappen van plastic-oppervlakken geanalyseerd. Deze resultaten zijn van cruciaal belang om het dynamische gedrag en het lot van microplastic deeltjes in het mariene milieu te begrijpen. Daarnaast kunnen ze fungeren als een opstap naar de ontwikkeling van veelbelovende remediatie technieken, zoals aangetoond in dit werk met het ontwerp van de nieuwe flotatie installatie.

Tot slot toont deze thesis aan dat succesvolle remediatie van microplastics uit mariene sedimenten mogelijk is, doch verder onderzoek vereist is om grootschalige toepassingen experimenteel te evalueren. Bijgevolg kan dit werk fungeren als basis voor de ontwikkeling van innovatieve oplossingen als antwoord op de wereldwijde problematiek omtrent microplastic accumulatie. Bovendien kan de erkenning van een potentiële synergetische samenwerking met de baggerindustrie een katalysator zijn voor korte-termijn internationale remediatie activiteiten om zodoende gevolg te geven aan de toenemende bezorgdheid omtrent mariene microplastic verontreiniging.

1

Introduction

The thriving story of the plastic industry finds its origin in the early 1900s with the development of the first fully synthetic polymer, bakelite, by the Belgian-American chemist Leo Baekeland (Powers, 1993). Further improvements in chemical technology during World War I and World War II set the dawn of mass production in the 1950s. Henceforth, the die was cast for an extraordinarily rapid growth of global annual plastic production, from 15 million tons in 1964 to 335 million tons in 2016 (MacArthur Foundation, 2016; PlasticsEurope, 2018). The widespread use of this man-made material found its way to an increasing number of applications. Currently, the main market sectors are packaging (±40 %), building and construction (±20 %), as well as textiles (±15 %), followed by consumer and institutional products, transportation and electrical and electronic equipment, each representing under 10 % of the global market share (Biron, 2013; PlasticsEurope, 2018). At present, an estimated 8.3 billion tons of virgin plastics are produced worldwide since 1950. This remarkable trend led to approximately 6.3 billion tons of cumulative plastic waste generated up to 2015. Of this, only a small portion is recycled or incinerated, while the dominant fraction (79 %) is discarded and accumulating in landfills or the natural environment. Without improvement in waste management, this fraction will contribute to roughly 12 billion tons of plastic waste by 2050 (Geyer *et al.*, 2017). In terms of the marine environment, current practices add approximately 12 million tons of plastic every year of which the largest fraction (> 90 %) ends up on the seabed (Eunomia, 2016).

This inherent chain of events makes it reasonable to acknowledge that plastics form a permanent mark of human presence on Earth. Several scientists are even convinced of plastics' importance as a technofossil[1] to be used as a practical indicator of the Anthropocene epoch (Zalasiewicz *et al.*, 2016). A strong signal revealing the persistent characteristics of plastic and the urge to recognize and act appropriately to the global plastic accumulation issue. To that end, a growing awareness matured in the general public over the past decade. In particular, the highlighted impact and concerns about the marine environment gave life to numerous organizations making efforts to counteract the expanding accumulation of plastic litter. For instance, the "Plastic Attack Days" initiative rapidly became a global movement since its modest kick-off in London early 2018. Furthermore, the occurrence of "Beach Clean-ups" or "Coastal Clean-ups" rise every year and gather more voluntary participants as their concept gains attention. Perhaps the most famous yet arguable effort to solve the marine plastic accumulation is known as "The Ocean Clean-up" idealized by the Dutch entrepreneur Boyan Slat. And the list goes on: "Beat the Microbead", "Plastic-Free Tuesdays", "International Bag-Free Days", and many more environmentally oriented initiatives. Distasteful pictures of marine animals suffering the harsh consequences of marine litter are no longer an exception (Bergmann *et al.*, 2015). They serve as truthful, eye-catching tools aiding these organisations in their objective to raise

---

[1]The preservable material remains of the technosphere (Haff, 2014), driven by human purpose and transmitted cultural memory, with the dynamics of an emergent system (Zalasiewicz *et al.*, 2014).

public awareness and obtain the necessary political and financial support. Hence, in addition to revealing the drawbacks of a blooming plastic industry, the general recognition of the oceans as one of Earth's most valuable natural resources was rightfully emphasized. The oceans provide food sources, mineral sources, energy sources, transportation possibilities, recreation opportunities, and act as a climate buffer as well as an oxygen generator (European Union, 2018). They should under no circumstances operate as a sink for the end-of-life stage of man-made materials.

This renewed understanding of the importance of the oceans gave life to the 6th Belgian spearhead-cluster[2] in June 2018. It was founded as a central organ joining the knowledge and expertise of government institutions, scientific institutions and high-end companies. This *Blue Cluster* aims to boost innovative projects that support the growth of the maritime sector in a sustainable way (De Blauwe Cluster, 2018). Such blue growth initiatives, as labelled by the European Union in their policy to achieve the goals of the Europe 2020 strategy, include ideas that encompass the marine plastic accumulation (European Union, 2017). In this regard, the ideal setting is shaped for the outset of this thesis dealing with the widespread occurrence of marine microplastic particles and their frightening impact on marine life.

In recent years, new scientific interest led to numerous publications indicating the ubiquity of microplastic particles, while the first reports proving their existence date back to the early 1970s (Carpenter and Smith, 1972; Moore *et al.*, 2001; Thompson *et al.*, 2004; Law *et al.*, 2010; Claessens *et al.*, 2011). Consequently, the milestone is reached where the worldwide presence of microplastic particles, particularly in the marine environment, is undeniable. Yet very little research is performed on the removal of these pollutants. To that end, the objective of this thesis is to propose and engineer a technology that will separate, rather than analyse, microplastic particles from marine sediment. In particular, dredged sediment is suggested as target mixture. Since the displacement of sediment is part of the core business of dredging companies, this might prove to be an economic opportunity and allow for an interesting synergy. Particularly, considering that maintenance dredging in the Belgian coastal zone contributes annually to the relocation of approximately 10 million tons of dry material containing on average more than 4 trillion microplastic particles (Van den Eynde *et al.*, 2015; Claessens *et al.*, 2011). This sediment is mainly originating from the harbours and access channels of Zeebrugge, Ostend, Blankenberge and Nieuwpoort (De Brauwer *et al.*, 2005). Combining those routine dredging operations with an ingenious and efficient technique that successfully isolates microplastic particles from the dredged mixture, holds an elegant and promising vision. This thesis entails that vision by exploring, engineering and optimizing separation techniques by means of a theoretical and an experimental approach.

---

[2]Demand-driven, large-scale innovation platform that stimulates the collaboration between companies, knowledge institutions and government (triple-helix) to develop and implement long-term strategies regarding important domains within Flanders, which are internationally oriented (VLAIO, 2018).

2

Literature review

2.1 Plastics in general

2.1.1 Composition and production

Plastics are synthetic or semi-synthetic organic compounds, composed of a wide range of different polymers. These polymers are usually formed from chains of carbon atoms which can be connected to other atoms such as hydrogen, oxygen, nitrogen, chloride or sulphur (American Chemistry Council, 2005; Brazel and Rosen, 2012). Considering that plastics typically have a large molecular weight, this chain can easily consist of thousands of chemical bonds often with repeated characteristic groups of atoms. These groups are called repeating units and are not to be confused with monomers, which refer to the molecule(s) from which a polymer is synthesized (Figure 2.1). The polymer itself is classified as a thermoplastic when its atom-connections result in a linear or branched long chain, and is classified as a thermoset when its connections establish a two- and three-dimensional network (Ebewele, 2000). A more commonly used term for the long chain is the backbone of the polymer. In case this backbone exhibits a continuous link of carbon-to-carbon atoms, the structure is called homogenous. Heterogenous structures contain intermittent interruptions of the backbone carbon atoms by other atoms such as oxygen or nitrogen. In addition, a distinction is made between polymers consisting of identical monomers, namely homopolymers, and polymers produced by combining distinctive monomers, called copolymers (Ebewele, 2000; Brazel and Rosen, 2012). All these diversifications, together with the possibility of attaching different elements to the backbone as side-chains (e.g. fluorine addition in Teflon) and many more, permit the generation of tailor-made plastics with the desired properties and modify the intrinsic production process (Nicholson, 2017).
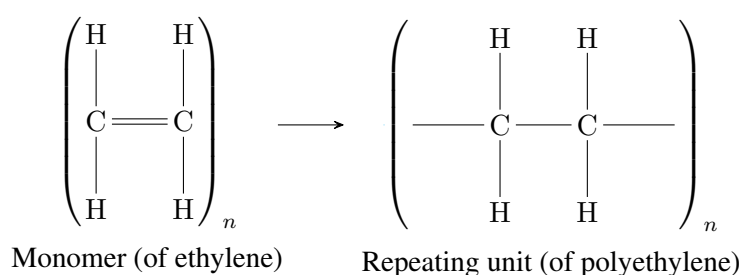

Monomer (of ethylene)   Repeating unit (of polyethylene)

Figure 2.1: The structural difference between monomers and repeating units.

The monomers utilized in the polymer or plastic production typically originate from petroleum, natural gas or coal. Routine manufacturing of plastics knows its outset with the distillation of crude oil in an oil refinery, as visually illustrated in Figure 2.2. This brings about different fractions of hydrocarbon mixtures with distinguishable chain size and structure. A reasonable illustrative sequence of the separated fractions with increasing boiling point starts with methane, ethane, propane, butane on through to naphtha, gasoline, kerosene, diesel, light mineral oils, heavy oils and paraffins to end with asphaltenes and carbon coke. The main raw material in plastic industry is naphtha that is subsequently treated in a steam cracker, where it is heated to very high temperatures (850°C) in the presence of water vapour. This reduces the molecular weight of the hydrocarbons and results in olefins (e.g. ethylene and propylene) and aromatics (e.g. benzene, toluene and xylene) (Ulrich, 1988; Elias, 2003; Karak, 2009). Thereafter, two main catalyst-driven processes are exploited, namely polyaddition and polycondensation. Polyaddition reactors are typically used with olefins (i.e. unsaturated hydrocarbons) and a peroxide catalyst to link monomers together to form long polymer chains and produce for instance polyethylene (PE), polystyrene (PS) or polyvinylchloride (PVC) without by-products. The objective of the catalysts used during a polycondensation process consists of making all monomers react with any adjacent monomer to form dimers. In the next stage, the dimers combine to form trimers and so on. Unlike in the polyaddition process, there is the constant generation of by-products (e.g. water) which have to be removed or recycled in order to produce the desired products in an efficient and sustainable way. Polyesters and polyamides (i.e. nylons) are two plastic-types constructed by polycondensation (Ebewele, 2000; Cowie and Arrighi, 2007; Nicholson, 2017).
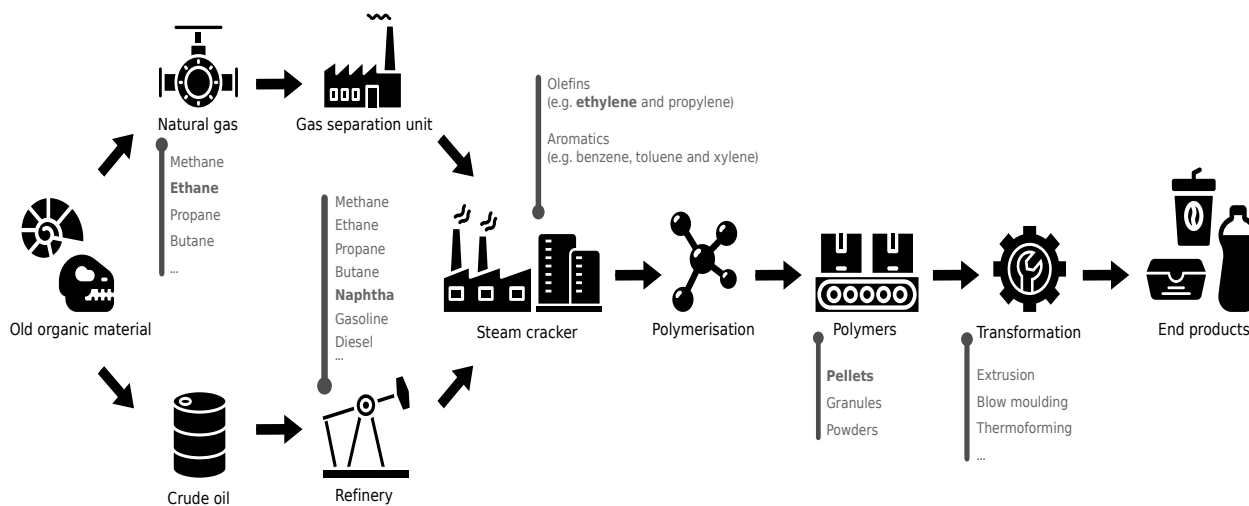

Figure 2.2: Conceptual illustration of the cradle-to-gate production process of plastic products (Adapted from NOVA Chemicals, 2017).

Considering the success of plastics across different industries, the manufacturing process has to cope with the versatile properties required for each individual application. To that end, additives can be incorporated to alter, improve or provide visual, mechanical, physical and chemical properties. Types of currently used additives are among others antioxidants, colorants, foaming agents, plasticizers, lubricants, anti-stats, antimicrobials and flame retardants (Saunders, 1988; Bolgar *et al.*, 2015).

Prior to delivering finished end-products, the manufactured polymers need to undergo a sequence of transformations (Figure 2.2). Afterwards, they will possess the colour, shape and precise properties according to its final application. The polymers leaving chemical factories as a result of the polymerisation reactions are usually shaped as granules, pellets or powders (Ebewele, 2000). This material can be subjected to numerous processing methods as described by, among others, Richardson (1974); Weir (1975); Ebewele (2000); Rosato *et al.* (2004) and NIIR Board of Consultants and Engineers (2006). Typically, an extruder is an essential part of the transformation process. For instance, extrusion is a continuous process where the

plastic material is fed into a long, heated cylindrical chamber (i.e. the extruder), which is equipped with one or two revolving screws. Melting of the plastic material is induced by the heat and the mechanical action of the screw(s). The molten plastic is forced out through a small opening (i.e. the die), forming its desired shape as it extrudes from the die. Subsequently, the material is cooled by immersion in water or by feeding onto rollers or belts. It is applied to produce plastic films, sheets, profiles, tubes and pipes. Other commonly applied transformation methods include injection moulding, blow moulding, rotational moulding and thermoforming.

As specified above, the vast majority of manufactured plastics are derived from virgin fossil feedstock claiming 6 % of the global oil consumption. Of this, approximately 50 % is utilized as material feedstock while the other 50 % is assigned to fuel the manufacturing process. Since the use of crude oil by the plastic industry is expected to increase equivalently to the growth of plastic production (i.e. 3.5 – 3.8 % annually), the share of global oil consumption attributed to the plastic industry will increase significantly (MacArthur Foundation, 2016). Notice the growth in overall oil demand is expected to increase by only 0.5 % annually (IEA and OECD, 2015). By 2050, estimations predict that the plastic industry will claim 20 % of the total oil consumption (MacArthur Foundation, 2016). This renders plastic products and their fate (Subsection 2.1.3) strongly dependent on the fluctuating, unpredictable oil prices. According to analysts, low oil prices suggest an economic advantage for manufacturing new plastic products rather than recycling the existing ones (WM, 2015).

2.1.2 Types and applications

The word *plastic* is derived from the Greek word *plastikos* which means "capable of being shaped or moulded". It relates to the physical property of plasticity which allows materials to be manipulated into a variety of shapes. This characteristic implies a first important classification in the permanence of plastics, namely the aforementioned diversification into thermoplastics and thermosets. When heat is applied to thermoplastics, their chemical composition remains identical thus allowing them to be transformed or moulded repeatedly. This renders them mechanically recyclable and enables reprocessing. In contrast, an irreversible chemical reaction takes place when heating thermosetting plastics during the shaping process, which makes them unable to be re-melted or re-formed. Therefore, thermosets are more resistant to high temperatures, but unsuitable for mechanical recycling (Ebewele, 2000; Nicholson, 2017).

A more familiar classification is given in Table 2.1 listing the different polymer types of plastic along with their abbreviations, densities and some discussed characteristics. The seven largest non-fibre polymer types according to the total worldwide primary plastic production up to 2015 are polypropylene (21.1 m%), low density polyethylene (19.8 m%), high density polyethylene (16.1 m%), polyvinylchloride (11.8 m%), polyethylene terephthalate (10.2 m%), polyurethane (8.4 m%) and polystyrene (7.7 m%). When taking polyester, polyamide and acrylic fibres into account, this fraction mounts up to 18.3 m%, indicating the significant share of fibrous polymers in the global primary plastic production (Geyer *et al.*, 2017).

Each polymer type holds unique physical and chemical properties as summarized in Appendix Table A.1. Due to this exceptional versatility, plastics are entrenched in nearly every industrial use sector as stated by Geyer *et al.* (2017). Examples of common applications relating to the plastic types along with their corresponding recycling codes are listed in Appendix Table A.2. Packaging industry is by far the largest industrial use sector, with 35.9 % of the total worldwide market share. Five other dominant sectors are building and construction (16.0 %), textiles (14.5 %), consumer and institutional products (10.3 %), transportation (6.6 %) as well as electrical and electronic equipment (4.4 %) (Geyer *et al.*, 2017).

Table 2.1: Overview of the most common plastic types along with their corresponding abbreviation, density range, chemical classification and prevailing polymerisation mechanism (Adapted from Andrady, 2011; Edmondson and Gilbert, 2017).

Polymer type	Abbreviation	Density [kg/m^3]	Chemical structure	Polymerisation mechanism
Polypropylene	PP	890 – 920	Thermoplastic	Polyaddition
Low-density polyethylene	LDPE	910 – 930	Thermoplastic	Polyaddition
High-density polyethylene	HDPE	930 – 970	Thermoplastic	Polyaddition
Polyvinyl chloride	PVC	1200 – 1700	Thermoplastic	Polyaddition
Polyethylene terephthalate	PET	1300 – 1400	Thermoplastic	Polycondensation
Polyurethane	PUR	870 – 1420	Thermoset or thermoplastic	Polyaddition
Polystyrene	PS	1040 – 1100	Thermoplastic	Polyaddition
Polyamide	PA	1020 – 1150	Thermoplastic	Polycondensation
Polycarbonate	PC	1150 – 1250	Thermoplastic	Polycondensation

2.1.3 Fate

Durability and resistance to degradation are both properties largely contributing to the versatility and success of plastics, yet making them nearly impossible for nature to assimilate. This enables three common scenarios for the fate of these polymers: different types of recycling, incinerating or discarding (Geyer *et al.*, 2017). Considering the leading plastic industrial use sector (i.e. packaging; Subsection 2.1.2), merely 14 m% of the worldwide plastic packaging material, which is predominantly single-use, is collected for recycling. Value losses during sorting and reprocessing plummets the fraction of recycled plastic utilized for secondary applications down to 5 m% (MacArthur Foundation, 2016). In general, 9 m% of global cumulative plastic waste up to 2015 was collected for recycling (Geyer *et al.*, 2017). By means of comparison, the estimated global recycling rate of paper equals 58 m% and that of steel 85 m% (ICFPA, 2015; BIR, 2018). Remarkably, the limited fraction of plastics that successfully gets recycled, usually yields lower-end applications thus rendering them unrecyclable in a next stage (i.e. downcycling). Furthermore, contamination and mixing of different types of polymers (and their individual additives) lowers the technical and economic value of secondary plastic products (MacArthur Foundation, 2016). Next to recycling, 12 m% of the cumulative plastic waste is incinerated (with or without energy recovery) and 79 m% is discarded in landfills or in the natural environment. Quantitatively, this last fraction represents 4.9 billion tons of plastic waste accumulated up to 2015 (Geyer *et al.*, 2017). A summarizing illustration is given in Figure 2.3.

To illustrate, the efforts done in producing bio-based and biodegradable plastics led to a global capacity of 2.05 million tons in 2017, which translates to less than 1 m% of the global annual plastic production (European Bioplastics, 2017). In addition, a significant portion of the currently biodegradable plastics are typically only biodegradable under controlled conditions as in specialized industrial composters. Consequently, the environmental advantage of biodegradable plastics when leaked into the natural environment is questionable (MacArthur Foundation, 2016). In particular, the noticeable lack of an effective and sustainable waste management system to cope with the growing accumulation of plastics, is raising concerns regarding the marine environment. Tiny plastic fragments appear to infiltrate and interact with the aquatic ecosystems. These particles form the subject of the next section.
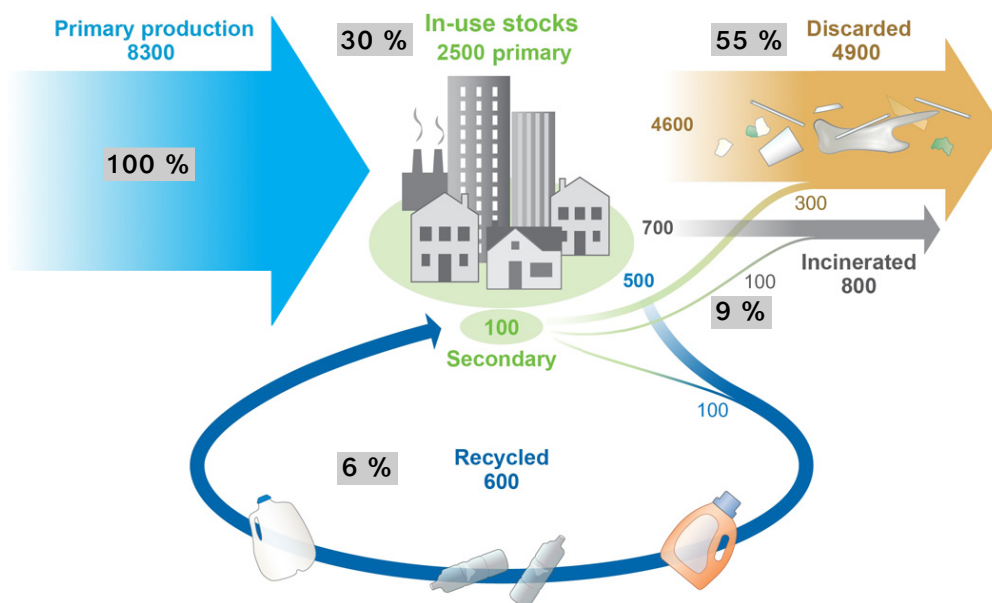
Figure 2.3: Global production, use and fate of plastic polymers from 1950 to 2015 expressed in million metric tons. The indicated percentages illustrate the corresponding mass-balance for the total worldwide plastic production, taking into account the in-use stocks but excluding secondary plastics (Adapted from Geyer *et al.*, 2017).

2.2 Microplastic particles

2.2.1 Definition

Since the exponential increase in scientific publications dedicated to marine plastic litter, a variety of definitions have been proposed to physically describe microplastic particles. Most of them propose a lower boundary that is dependent on the sensitivity of the applied sampling and extraction technique. This explains why Arthur *et al.* (2009), among others, have defined a lower boundary of 333 μm, the exact mesh size of the commonly used nets for sampling of plankton and debris in the water column. This causes an underestimation of the occurrence of microplastic particles during assessments based on in situ measurements. It was repeatedly illustrated that the number of microplastic particles smaller than 1 mm represents an important fraction (i.e. up to 35 to 90 %) of all present microplastics, presuming a size range between 1 μm and 5 mm (McDermid and McMullen, 2004; Browne *et al.*, 2010; Eriksen *et al.*, 2013; Song *et al.*, 2014; Zhao *et al.*, 2014). The Joint Group of Experts on the Scientific Aspects of Marine Protection (GESAMP, 2015) suggests an interval of 1 nm to 5 mm. Considering that the definition by GESAMP (2015) includes the dimensions of what has been defined as nanoparticles (Koelmans *et al.*, 2015), a more recognized lower boundary is that of 1 μm. The upper boundary of 5 mm originates from the definition described by Arthur *et al.* (2009) and is universally accepted (Lassen *et al.*, 2015). Therefore, this research will physically characterize microplastic particles within the range of 1 μm to 5 mm. This implies that macroplastics are those plastic particles that are larger than 5 mm (Figure 2.4).

A possible sub-classification distinguishes between small microplastics (i.e. from 1 μm to 1 mm) and large microplastics (i.e. from 1 mm to 5 mm), as proposed by MSFD Technical Subgroup on Marine Litter (2013) and illustrated in Figure 2.4. The 1 mm cut-off is justified by proving it to be the upper size boundary of particles that are readily available for planktonic species. Since those species constitute the base of the marine human food chain, lot of concern evolves around these small microplastics (Moore, 2008; Van Cauwenberghe, 2015).
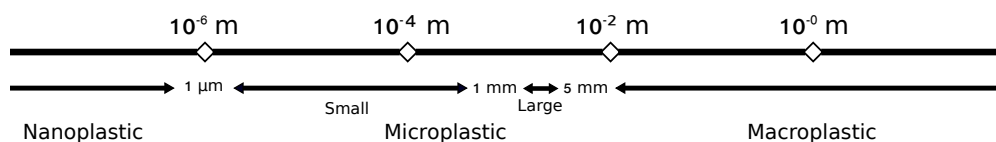
| 10⁻⁶ m | 10⁻⁴ m | 10⁻² m | 10⁻⁰ m |

10^{-6} m 10^{-4} m 10^{-2} m 10^{-0} m

1 μm   1 mm   5 mm

Nanoplastic   Small   Large   Macroplastic
         Microplastic

Figure 2.4: Definition of the plastic particle terminology applied in this thesis. The overall term *microplastic* is divided in *small* and *large* microplastic to differentiate between two other frequently used definitions of microplastics.

A complementary classification can been made between primary and secondary microplastic particles. Essentially, the former are plastics that are intentionally manufactured in the previously discussed size category (i.e. 1 μm – 5 mm) for direct use. For example, in facial-cleaners and cosmetics (Zitko and Hanlon, 1991), as air-blasting media (Gregory, 1996) or in medicine as vectors for pharmaceuticals (Patel *et al.*, 2009). Along with that, raw materials known as virgin plastic pellets are typically considered primary microplastic particles since their diameter usually fluctuates in the size range of 2 to 5 mm. Yet the allocation of virgin plastic pellets as primary microplastic particles is criticized (Costa *et al.*, 2010; Andrady, 2011). Contrarily, secondary microplastic particles originate from fragmentation and degradation processes of larger plastic products due to the cumulative effect of physical, biological and chemical mechanisms (Browne *et al.*, 2007). For example, prolonged exposure to ultraviolet radiation of sunlight causes photodegradation which reduces the structural integrity of the plastic material making it more susceptible to physical fragmentation by abrasion or wave-action (Barnes *et al.*, 2009).

2.2.2 Morphology

Aside from size, other parameters exist to describe microplastic particles (e.g. morphology, shape, colour and degree of erosion). Typically, the particles are categorized in 6 to 8 morphological groups: pellets (a.k.a. nibs, nurdles or mermaid tears), fragments, granules, filaments (a.k.a. sheets or flakes), films (a.k.a. foils), fibres and foams (Hidalgo-Ruz *et al.*, 2012). In some cases, a distinction is made between polymer foams and sponges (Zhou *et al.*, 2018). Every category will exhibit different physical and/or chemical behaviour, which highlights the importance of recognizing the morphological distinctions when considering (analytical) separation techniques. Figure 2.5 illustrates the aforementioned categories of microplastic particles. Note that for simplification purposes, granules are commonly described as fragments or pellets, depending on the sphericity of the particle.
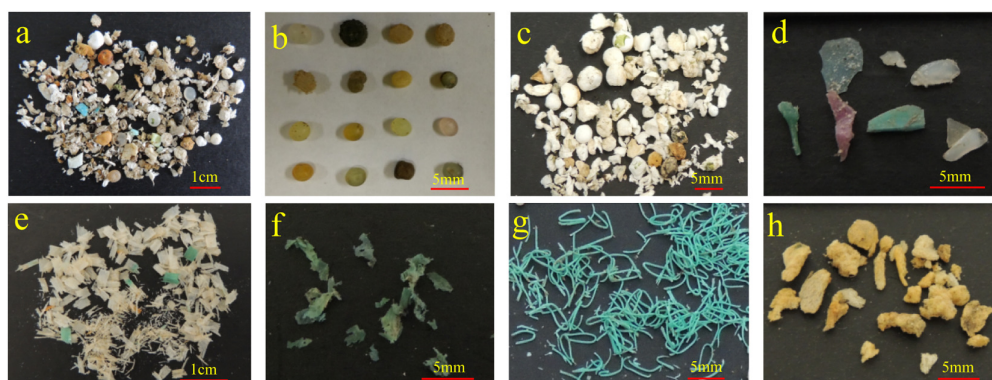

Figure 2.5: Images of different shapes of microplastic particles: (a) mixed, (b) pellets, (c) foams, (d) fragments, (e) flakes, (f) films, (g) fibres and (h) sponges (Zhou *et al.*, 2018).

2.2.3 Sources

This subsection will briefly discuss the major sources of marine plastic litter and their direct and indirect pathways by which they enter the Earth's oceans. The emphasis will be on microplastic particles where a clear distinction is made between primary and secondary microplastics as described in Subsection 2.2.1.

The main sources of marine plastic litter hold a land-based origin making up approximately 80 % of the total plastic inflow into the world's oceans (Andrady, 2011; Eunomia, 2016). This includes primary microplastic particles originating from (i) cosmetics such as microbeads used in toothpastes or exfoliating beads used in hygiene products (UNEP, 2015), (ii) abrasive media used as plastic blasting agents (McDevitt *et al.*, 2017), (iii) different types of paints (CCB, 2017), (iv) vectors used for pharmaceutical active ingredients (Cole *et al.*, 2011), and (v) virgin pellets used for the manufacturing of plastic products (Sundt *et al.*, 2014). However, many other applications further promote the release of primary microplastic particles into the marine environment (Lassen *et al.*, 2015). The secondary microplastic particles can be traced back (i) to city dust in part from the abrasion of automobile tyres (Sundt *et al.*, 2014), (ii) to textile fibres from, among other things, the washing of synthetic clothing (Browne *et al.*, 2011), or (iii) to general use and handling of plastic (waste)products, such as the wear and tear of agricultural films (Lassen *et al.*, 2015). To illustrate, Browne *et al.* (2011) found that cleaning 1 synthetic garment in a conventional laundry machine can discharge over 1900 microplastic fibres in the drain effluent. Considering that half of the world's population settles within 50 miles of the coast, microplastic particles that are daily used in personal care products or frequently released through washing activities of synthetic clothing, have a high potential to enter the marine environment (Cole *et al.*, 2011). Indeed, many researchers reported the significant contribution of rivers and wastewater effluents as pathways for marine plastic pollution. Despite the fact that a large fraction of domestic and industrial sewage enters wastewater treatment plants (WWTPs), an important fraction of the present microplastic particles escapes with the effluent, which will be elaborated in Subsection 2.2.4 (Magnusson and Norén, 2014; Talvitie and Heinonen, 2014; Gall and Thompson, 2015; Estahbanati and Fahrenfeld, 2016; Murphy *et al.*, 2016; Dyachenko *et al.*, 2017; Mintenig *et al.*, 2017). Furthermore, this implies that extreme weather conditions such as storms or floods can induce an elevated microplastic release into the marine environment. This hypothesis was repeatedly confirmed by in situ measurements (Barnes *et al.*, 2009; Moore, 2002; Lattin and Moore, 2004).

The remaining ±20 % of the total marine plastic inflow is associated with direct sources caused by coastal tourism, commercial and recreational fishing, marine industries such as aquaculture and oil-rigs, and by the loads of marine vessels. A typical source of secondary microplastic particles in this scenario originates from fishing gear, such as nets, lines and ropes. In the 1970s, the contribution of marine vessels was –in proportion to the global population– arguably larger, with an estimation of over 23,000 tons of plastic packaging material dumped by commercial fishing fleet (Pruter, 1987). The international agreement (MARPOL 73/78 Annex V) that was enacted in 1988 aimed to reduce dumping activities among fishermen and other marine parties. However, a lack of education and enforcement causes the marine fleet to remain a significant source of plastic pollution. Next to that, accidental spillages of microplastic particles used for manufacturing, such as virgin pellets and microbeads, are rather frequently reported. This partly explains the elevated levels of virgin pellets near harbours adjacent to plastic production facilities (Lozano and Mouat, 2009). Fair to mention is that a growing number and effect of initiatives are being observed that aid and support these companies to prevent plastic pellet losses during their operations (Law *et al.*, 2010; American Chemistry Council, 2011).

Table 2.2 provides a brief overview of the dominant sources of marine microplastic particles, including those mentioned above for both primary and secondary microplastic particles and their estimated main release pathways to the marine environment.

Table 2.2: Dominant sources of marine microplastics along with their estimated main release pathways to the marine environment. A distinction is made between primary and secondary microplastic particles (Adapted from Sundt *et al.*, 2014; Essel *et al.*, 2015).

Source	Description	Pathway
PRIMARY MICROPLASTIC PARTICLES		
Virgin pellets	Losses of plastic pellets by transportation, reloading, processing, etc.	Surface water, municipal sewage, industrial sewage, urban run-off
Cosmetics	Release of exfoliating microbeads by face and body wash with cosmetic scrubs and by using certain toothpastes	Municipal sewage
Abrasive media	Release due to plastic blasting at shipyards, offshore maintenance sites, bridges, etc. by atmospheric drift or cleaning of surfaces	Surface water, municipal sewage, industrial sewage, urban run-off
Paints	Release during usage of certain paints e.g. by cleaning brushes and other painting tools	Municipal sewage
Rubber granules	Release due to wear and tear of certain artificial turfs, running lanes, playgrounds, etc.	Soil, sewage
Pharmaceutical vectors	Release and losses of plastic vectors widely used in a range of medical and biological applications	Municipal sewage, industrial sewage
Others	Releases of microplastic particles used in professional dishwashing machines, as ironing beads for children and in printer toner.	Sewage
SECONDARY MICROPLASTIC PARTICLES		
Industrial and professional use	Release of plastic dust from cutting, polishing, and moulding plastic products e.g. in reparation works on boats or cars	Surface water, sewage
Household use	Release of plastic dust from abrasion, wear and tear or weathering of floor coverings, furniture, kitchen utensils, footwear, roof coverings, piping and tyres. Release of plastic fibres ripped loose from textiles as clothing, carpets and furniture e.g. in laundry machines.	Soil, surface water, urban run-off, sewage
Agriculture and aquaculture use	Releases due to weathering and abrasion of agricultural plastic films and fishing gear such as nets, ropes and other tools.	Soil, surface water
Painted surfaces	Release of plastic dust from paint application, abrasion and maintenance work	Soil, surface water, urban run-off, sewage
Waste handling	Release of plastic particles from shredding, dumping and fragmenting plastic waste and plastic contaminated waste	Soil, surface water, urban run-off, sewage
Environmental fragmentation	Fragmentation of macroplastic debris of terrestrial and maritime origin by biological, physical and chemical processes	Soil, surface water, urban run-off, sewage

2.2.4   Occurence

At present, the global omnipresence of microplastic particles in the marine environment is undeniable (Derraik, 2002; Lozano and Mouat, 2009; Ryan *et al.*, 2009). Numerous studies reported aquatic microplastic pollution, rendering huge amounts of data (e.g. Norén (2007); Claessens *et al.* (2011); Dubaish and Liebezeit (2013); Strand *et al.* (2013); Cole *et al.* (2014); Lusher *et al.* (2014) and Song *et al.* (2014)). However, comparing and extrapolating published results can be challenging since there is a lack of standardization in both sampling methods and measuring units (Claessens *et al.*, 2011; Lassen *et al.*, 2015). In addition, the inconsistency in terms of size-range defining microplastic particles (Subsection 2.2.1) yields discrepancies across studies (Nerland *et al.*, 2014). This is especially true due to the finding that small microplastics particles (i.e. < 1 mm) are much more abundant than the bigger ones (McDermid and McMullen, 2004; Browne *et al.*, 2010; Eriksen *et al.*, 2013; Song *et al.*, 2014; Zhao *et al.*, 2014). Measurements by Norén *et al.* (2014) indicate that using a mesh size of 50 μm instead of the common sampling nets of 333 μm yield abundance concentrations 2 to 5 orders of magnitude greater (Kang *et al.*, 2015). The importance of recognizing and resolving the missing plastic debris (i.e. the fraction of plastic particles that is not sampled) is described by Cozar *et al.* (2014). Therefore, estimated quantities of microplastic abundances should always be interpreted with caution.

2.2.4.1   Marine water

Regardless of the absence of uniformity in the methodological approach, valuable observations prove that microplastic particles are ubiquitous contaminants of the marine environment (Collignon *et al.*, 2012; Desforges *et al.*, 2014; Liebezeit and Dubaish, 2014). An average, rather conservative, theoretical concentration of 1.36 kg/m^2 is calculated by Everaert *et al.* (2018), representing the total amount of free-floating microplastics in the global sea surface layer (i.e. upper 5 m layer of the water column). This aligns with the concentration of 0.75 kg/m^2 provided by Eriksen *et al.* (2014) based on in situ observations, considering the previously described issues concerning sampling methods. Translated to a range expressed in number of particles per volumetric unit, 0.2 to 0.9 particles/m^3 was obtained (Everaert *et al.*, 2018). However, in situ observations are highly dependent on the geographical sampling site. For instance, Cole *et al.* (2014) identified a concentration of 0.27 particles/m^3 in the Western English Channel, while Desforges *et al.* (2014) reported a concentration of 7630 particles/m^3 in Queen Charlotte Sound near the South Island of New Zealand. The latter high level of microplastic particles appears to be the result of oceanographic conditions, which will be discussed in more detail in Subsection 2.2.5. Another rather recent study by Obbard *et al.* (2014) demonstrated that even the most remote marine areas are infiltrated by anthropogenic microplastic pollution. Analysis of ice cores taken from the Arctic Ocean revealed concentrations between 38 and 234 particles/m^3 (Obbard *et al.*, 2014). Successive studies suggest that Arctic sea ice might function as a temporal sink for microplastic particles due to in situ observations that exceeded the usual concentrations by several orders of magnitude (Bergmann *et al.*, 2017; Tekman *et al.*, 2017). Research examining the microplastic concentration in the Antarctic region is limited, yet on the rise (Waller *et al.*, 2017).

2.2.4.2   Freshwater

Although the majority (i.e. > 90 %) of the current microplastic pollution research is focused on the marine environment (Wagner *et al.*, 2014; Wagner and Lambert, 2018), increasing numbers of studies indicate that microplastic particles are equally ubiquitous in fresh (and brackish) waterbodies. In the Laurentian Great Lakes of the United States an average concentration of 43,000 particles/km^2 was reported by Eriksen *et al.*

(2013) in 2013. Similarly, one year later an average concentration of 20,300 particles/km^2 was derived by Free *et al.* (2014) for Lake Hovsgol in Mongolia. According to Mani *et al.* (2015), the river Rhine holds an average concentration of 893,000 particles/km^2. And another rather recent study found an average concentration of 193,000 particles/km^2 for Lake Winnipeg in Canada (Anderson *et al.*, 2017). In general, the reported averaged values in fresh water systems vary greatly from almost zero to several millions of particles per cubic meter (Li *et al.*, 2018). These differences are mainly attributed to the sampling locations, present human activities, inherent natural conditions and the applied sampling methodology (Eerkes-Medrano *et al.*, 2015). Remarkably, the effluent of wastewater treatment plants (WWTPs) seems to be a dominant "source" of microplastics (Magnusson and Norén, 2014; Talvitie and Heinonen, 2014; Gall and Thompson, 2015; Estahbanati and Fahrenfeld, 2016; Murphy *et al.*, 2016; Dyachenko *et al.*, 2017; Mintenig *et al.*, 2017). Even though some wastewater treatment facilities can remove up to 95 % of the microplastics (Talvitie and Heinonen, 2014; Talvitie *et al.*, 2017), a substantial amount escapes with the effluent. A conservative estimation of 8 billion microplastic particles being discharged through WWTPs every day in the USA was reported by Rochman *et al.* (2015). Considering that globally only 60 % of the municipal wastewater is being treated (Mateo-Sagasta *et al.*, 2015), each year an enormous amount of microplastic particles enter the natural environment through discharges from WWTPs. In that sense, WWTPs function as a collection-pool, rather than a source, of microplastic particles and currently fail to efficiently capture them.

2.2.4.3 Sediment and beaches

Next to floating microplastic particles, a substantial fraction settles, ends up on the seabed or washes up ashore. Several effects can cause a microplastic particle to vertically transport to the sediment surface. The most apparent reason is attributed to its intrinsic density. In case the intrinsic density of the polymer type (Table 2.1) exceeds the density of the surrounding seawater (i.e. 1020 – 1030 kg/m^3), the particle will naturally settle. However, even when the polymer's intrinsic density is strictly lower than the density of the surrounding water, the phenomenon of density-modification can cause a particle to settle. A common process of density-modification is bio-fouling, where biomass accumulates on the surface of the (micro)particle. This in turn induces settling behaviour of formerly floating particles. The latter process is believed to be one of the main reasons of the dominant presence of microplastic particles in marine sediments (Andrady, 2011; Reisser *et al.*, 2013; Zettler *et al.*, 2013; Kooi *et al.*, 2017). Furthermore, severe weathering in marine environments can cause leaching of additives, which likewise alters the microplastic's density (Talsness *et al.*, 2009). Recently, also the role of marine snows (i.e. organic-rich aggregates of faecal pellets, phytoplankton, particulate organic matter, etc.) in the vertical transport of buoyant polymers was quantitatively analyzed. Porter *et al.* (2018) found that the sinking rates of microplastic particles were enhanced when incorporated into marine snows. For common polyethylene particles the increase appeared to be 9.468 mm/s, which is very significant considering that these particles were formerly floating with a negative sinking rate of -0.002 mm/s (Porter *et al.*, 2018).

All these mechanisms lie at the core of the scientifically agreed upon estimation that at least 94 % of the total amount of plastic in the oceans (including microplastics) accumulates on the seabed (Eunomia, 2016). This translates to a global average microplastic concentration between 32 – 144 particles/kg dry sediment for intertidal (beach) areas and between 1.5 – 6.7 particles/kg dry sediment for deep sea areas (Everaert *et al.*, 2018). However, one has to acknowledge the strong spatial variation in sediment contamination (Subsection 2.2.5), but also the variation in applied cut-off size for microplastic particles during analysis. For instance, sediments in the North-East Atlantic held an average concentration of 421 particles/kg dry sediment using a lower boundary of 1 µm (Maes *et al.*, 2017), while Claessens *et al.* (2011) reported an average concentration of 97.2 particles/kg dry sediment for the Belgian Continental Shelf using a lower boundary of only 38 µm. The fraction that ends up on the beaches is approximately 5 % of the total amount

of marine plastic litter, yet the corresponding global average concentration is significantly higher compared to deep sea areas, as previously indicated (Eunomia, 2016; Everaert *et al.*, 2018).

As elaborated above, the fraction of marine microplastic particles that share the seabed as their final sink is dominating. Furthermore, since this thesis targets sediment as carrier of microplastic pollution, examining the major microplastic constituents of marine sediment regarding polymer type and physical characteristics seems appropriate. To that end, a table was constructed expressing the best available findings of scientists and researchers covering different marine areas. The results are translated to percentages where possible, as the main objective aims to illustrate distribution trends in the occurrence of microplastic particles in sediments (Appendix Table A.3). In addition, Hidalgo-Ruz *et al.* (2012) managed to put together a frequency of occurrence of different polymer types across 42 studies. Beside sediment samples also water samples containing microplastic particles were considered. Nonetheless, 79 % of the studies reported the presence of PE, 64 % of PP, 40 % of PS, 17 % of PA, 10 % of PES and 10 % of AC (Hidalgo-Ruz *et al.*, 2012).

2.2.5 Spatial and temporal trends

Aside from the lack in standardization as elaborated in Subsection 2.2.4, both spatial and temporal heterogeneity of microplastic abundances render extrapolation of local monitoring data very challenging (Goldstein and Goodwin, 2013). Therefore, it seems of high importance to assess the spatial scales at which microplastic particles enter, travel and accumulate in the marine environment with respect to the temporal trends (Nerland *et al.*, 2014). To that end, the role of major ocean currents was the topic of many publications. Kubota (1994) was one of the first to report the remarkable oceanic accumulation zones of floating marine debris and proposed a three-step process as explanation. The model used during this study was further improved and pinpointed a debris hotspot northeast of Hawaii, a location near the area currently known as the *Great Pacific Garbage Patch* (Kubota *et al.*, 2005). This *plastic island* holds abundance concentrations of plastics (in particular microplastic particles) that can be several orders of magnitude greater than in other areas of the marine environment (Law *et al.*, 2010; Doyle *et al.*, 2011; Maximenko *et al.*, 2012). Related studies concluded that the three-step process, as first described by Kubota, was responsible for the existence of the 5 notorious garbage patches (a.k.a. plastic–gyres or –islands; Figure 2.6) in the oceans (Martinez *et al.*, 2009). This three-step mechanism is strongly related to surface currents (i.e. Ekman drift and geostrophic current) and predominantly valid for all present garbage patches. Van Sebille *et al.* (2012) suggest the existence of a 6th garbage patch in the Barents Sea by including, among other things, seasonal variation in their model. Furthermore, on a smaller scale, spatial variation can be equally significant. As briefly mentioned in Subsection 2.2.4, local point sources are frequently reported. For instance, near densely populated coasts, WWTPs or plastic production facilities (Norén, 2007; Collignon *et al.*, 2012; Dubaish and Liebezeit, 2013).

Due to the fact that the microplastic concern is a relatively new area within marine research, very few long-term studies have been performed. In order to gain valuable insights into the temporal variation of marine microplastic particles, global standardization in the applied methodology is an urgent necessity (Nerland *et al.*, 2014). Recently, Beer *et al.* (2018) explored the long-term temporal changes of microplastic particles in the marine environment covering three decades from 1987 to 2015. Surprisingly, no significant concentration differences were reported in the Baltic Sea. However, analysis of the marine organism samples showed a clear seasonal correlation, suggesting an elevated microplastic level during spring months, most-likely associated with seasonal differences in feeding activity. A previous attempt to examine the temporal changes in microplastic abundance was done by Law *et al.* (2010). Analogously, no significant temporal changes were reported, this time regarding the Caribbean accumulation zone and the North Atlantic, over a timespan of 20 years. On the contrary, Thompson *et al.* (2004) were able to demonstrate a significant increase in the
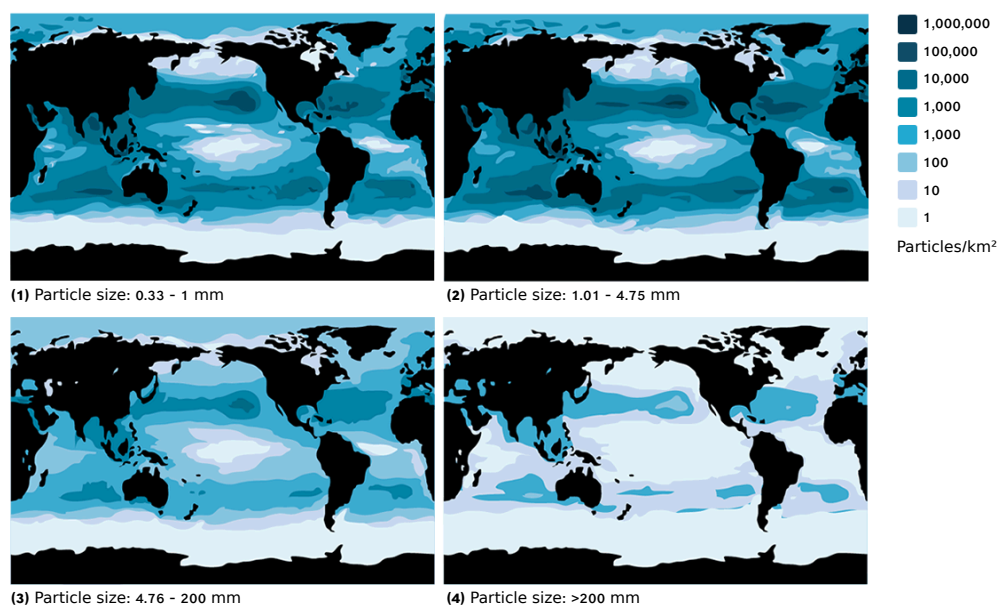
(1) Particle size: 0.33 - 1 mm	(2) Particle size: 1.01 - 4.75 mm
(3) Particle size: 4.76 - 200 mm	(4) Particle size: >200 mm

Legend: 1,000,000 / 100,000 / 10,000 / 1,000 / 1,000 / 100 / 10 / 1 — Particles/km²

Figure 2.6: Representation of the oceanic *garbage patches* by indicating plastic litter concentrations for 4 different particle size ranges (Adapted from Eriksen *et al.*, 2014).

abundance of microplastic particles in Scottish surface waters from the 1960s to the 1990s. Similar to the recent study by Beer *et al.* (2018), results were based on continuously archived samples of plankton. This suggests an insufficiency in qualitative data and underscores the need for better understanding of possible parameters influencing the spatial and temporal distribution of microplastic particles and their cycle through the marine environment (Thompson, 2015; Beer *et al.*, 2018).

2.2.6 Potential impact

Acknowledging the fact that horrifying pictures of marine animals impacted by the (mechanical) adverse effects of macroplastic particles triggers global awareness and concern adequately, a growing number of scientists believe that microplastic particles pose a greater threat to marine habitats and potentially even human health (Derraik, 2002; Thompson *et al.*, 2004; Ng and Obbard, 2006; Barnes *et al.*, 2009; Fendall and Sewell, 2009; Lozano and Mouat, 2009). As microplastic abundance and omnipresence in both pelagic and benthic ecosystems further increase, so will the probability of encounter and interaction of these small particles with marine organisms (Figure 2.7).

Although many factors influence the bioavailability of microplastic particles to marine organisms, particle size is a crucial one. Since small microplastic particles (SMPs) are similar in size to planktonic organisms, they become available for ingestion by lower trophic species (Van Cauwenberghe, 2015). These include zooplankton, but also other invertebrates such as amphipods (i.e. detrivores), lugworms and sea cucumbers (i.e. deposit feeders), and barnacles (i.e. filter feeders), which all have been reported to hold microplastic particles in their digestive system (Thompson *et al.*, 2004; Graham and Thompson, 2009; Cole *et al.*, 2011; Besseling *et al.*, 2013; Ugolini *et al.*, 2013; Wright *et al.*, 2013; Chua *et al.*, 2014). Voluntary uptake due to the organism's wrongful identification of microplastics as food is believed to be the main reason for these observations (Blight and Burger, 1997; Tourinho *et al.*, 2010; van Franeker *et al.*, 2011). However, trophic transfer of microplastic particles has been demonstrated on several occasions (Eriksen *et al.*, 2013; Murray and Cowie, 2011; Farrell and Nelson, 2013; Setälä *et al.*, 2014). Despite the currently
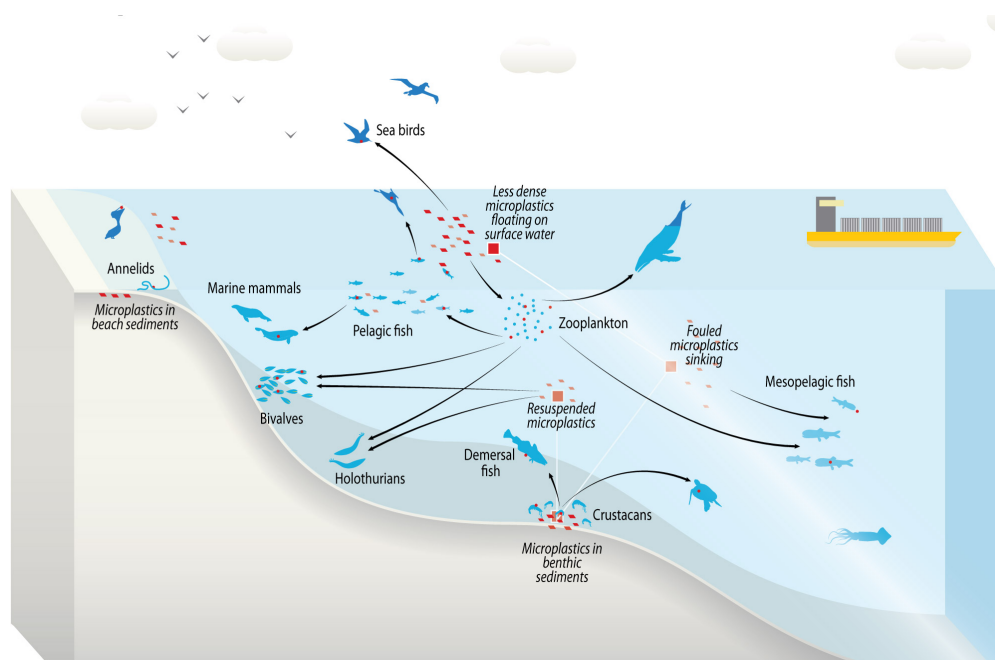
Figure 2.7: Conceptual illustration of the interaction pathways of many different organisms with marine microplastics (Lusher *et al.*, 2014).

unknown significance of this phenomenon, trophic transfer bears great concern. It allows infected organisms that make up the base of the food chain to introduce microplastic particles in its predator species, hence working its way up the food chain towards humans as apex predator (a.k.a. top or alpha predator), as illustrated in Figure 2.8. In other words, it potentially increases the exposure rate of aquatic organisms and all related predators (Carbery *et al.*, 2018).

Once ingested, microplastic particles may cause mechanical adverse effects, similar to those observed with macroplastic particles (e.g. blockage of feeding appendages, pseudo-satiation or hindered passage through intestinal tract) (Derraik, 2002; Thompson, 2006; Tourinho *et al.*, 2010). Furthermore, the potentially harmful particles can be egested or translocated within the organism (Browne *et al.*, 2008; Von Moos *et al.*, 2012). The ability to egest, and therefore avoid or greatly reduce detrimental effects, was demonstrated in lugworms by Thompson *et al.* (2004). However, research shows that microplastic particles have the potential to enter the circulatory system by translocating from the digestive system (Browne *et al.*, 2008; Fendall and Sewell, 2009). This was first observed by Browne *et al.* (2008) who used blue mussels to, among other things, indicate that small microplastic particles (SMPs) undergo translocation more readily than larger ones. A more recent study by Von Moos *et al.* (2012) was able to detect adverse biological effects (e.g. inflammatory response) due to the ingestion and subsequent translocation of microplastics in blue mussels.

Another aspect of concern relates to the phenomenon that is currently described as *pollution vectoring*. Since several toxic contaminants (e.g. PCB, PAH and DDT) have a hydrophobic nature, the affinity of these contaminants is greater for plastics than for seawater (Frias *et al.*, 2010; Hirai *et al.*, 2011; Heskett *et al.*, 2012; Antunes *et al.*, 2013). In addition, considering the large surface-area-to-volume ratio of microplastic particles, contaminant levels on its surface can reach up to several orders of magnitude greater compared to the ambient seawater (Mato *et al.*, 2001; Hirai *et al.*, 2011). In the event of ingestion of such heavily polluted microplastic particles, the process of biomagnification (a.k.a. bioaccumulation) comes into play. This mechanism leads to elevated contaminant concentrations in the tissues of the infected organism, posing a threat to the organism and potentially even human food safety (Van Cauwenberghe, 2015). Experimental trials
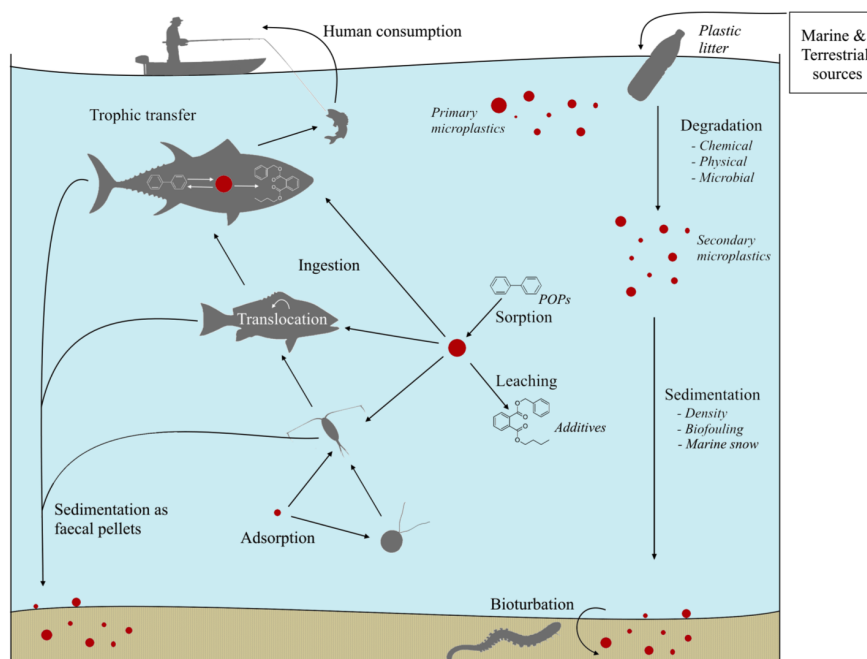
Figure 2.8: Conceptual model of microplastic pathways and the potentially harmful interactions with marine biota (Van Cauwenberghe, 2015).

with Japanese rice fish (a.k.a. medaka) revealed both endocrine disruption and hepatic stress after chronic exposure to naturally contaminated microplastics (Rochman *et al.*, 2013, 2014). Work done by Browne *et al.* (2013) demonstrated an accumulation of contaminants in the tissue of lungworms when exposed to presorbed microplastic particles. Interestingly, similar exposure to presorbed sand particles resulted in a contaminant accumulation more than 2-fold higher in the tissue of the lungworms (Browne *et al.*, 2013). Clarifying modelling work investigating the role of microplastics in the biomagnification of hydrophobic (and therefore persistent in the aquatic environment) organic pollutants (POPs) has been done by Gouin *et al.* (2011) and Koelmans *et al.* (2013). The importance of microplastic particles as *pollution-vectors* to marine organisms appeared limited. Furthermore, research indicates that the leaching of (micro)plastic additives (Subsection 2.1.1) might be a more significant threat to the organism (and its predators) than the accumulation of diffusely spread mix of contaminants on the surface of the microplastic (Koelmans *et al.*, 2014). A state-of-the-art review conducted by Ziccardi *et al.* (2016) underscores the lack of evidence to attribute the occurrence of adverse effects to aquatic life to the process of biomagnification caused by primary microplastic exposure. In addition, they stress the current insufficiency in qualitative data to state that secondary microplastic exposure (i.e. trophic transfer) can provoke significant ecological effects (whether or not correlated to biomagnification) to wildlife populations or human health (Ziccardi *et al.*, 2016).

Drawing an overall picture of the global impact of microplastic particles on marine ecosystems requires further research, preferably by means of an increased standardization. Currently, the vast majority of microplastic impact studies (including several referred above) administer extremely high concentrations of microplastics to demonstrate adverse effects. While this unrealistic approach might provide information about potential outcomes, testing at more relevant concentrations offers insights in the actual present and future risks (Van Cauwenberghe, 2015). The very first attempt to perform a generic environmental risk assessment for microplastics in the marine environment and to generate a safe concentration below which no adverse effects are expected to occur, was done by Everaert *et al.* (2018). They estimated that on average no direct adverse effects are likely to appear up to the year 2100 for the pelagic ecosystems. However, for the benthic ecosystems in the marine environment, adverse effects are expected to arise upward from 2050 (Ev-

eraert *et al.*, 2018). Therefore, the next section will discuss analytical and industrial separation techniques to explore their capabilities to prevent further accumulation of potentially harmful microplastic particles in marine sediments.

2.3 Removal of microplastic particles from sediment

2.3.1 Introduction

In this section a brief and concise overview of separation techniques is put together. It concerns an explorative review comprised of both analytical separation techniques used in microplastic research and proven industrial techniques applied to effectuate the separation of solid-solid or solid-liquid mixtures. The latter technologies are primarily inspired by the mining industry that aims to isolate a high value mineral at low concentration from a bulk sediment mixture. The following subsections will succinctly describe the operation principles of both batchwise as continuously operated installations or elaborate on the applied analytical separation methodology. Afterwards, the technologies will be evaluated against selection criteria to pinpoint the best fitting option as a research case for this thesis. This approach guarantees a broad perspective regarding potential separation techniques and therefore facilitates the generation of aspiring and innovative designs.

The following references are used throughout this section: Mineral Processing Design and Operations by Gupta and Yan (2016a), Unit Operations Of Chemical Engineering by McCabe *et al.* (2004), Perry's Chemical Engineers' Handbook by Perry and Green (1997) and Microplastic Pollutants by Crawford and Quinn (2017).

2.3.2 Visual separation

Visual separation and detection maintained to be fundamental analysis and separating techniques in microplastic research over the past few years. Regardless of the sample origin, a visual analysis approach is considered as essential to properly remove the inevitable contamination of variable debris structures such as naturally occurring organic fragments and all sorts of anthropogenic litter. Despite it receiving controversy due to its subjective character and elevated potential for bias initially, visual detection and separation by a human operator proves to be one of the most effective procedures to differentiate microplastic particles from the surrounding debris. During analysis, it is recommended to preliminary assign doubtful particles as (micro)plastic since underrepresentation is more difficult to identify than overrepresentation. The latter can be evaluated by subsequently using spectroscopic techniques to confirm whether the particles are comprised of plastic.

Visual examination for microplastic particles larger than 1 mm can be performed with the naked eye or with the use of binocular microscopy. For particles smaller than 1 mm, more advanced equipment is utilized such as high magnification fluorescence microscopy. The microplastic particles are usually identified based upon their physical characteristics, such as shape, size, texture, colour and lack of biological structures. Separation typically occurs by using tweezers. After visually sorting and categorizing the microplastics according to the standardized size and colour sorting system (SCS), further identification is possible by applying spectroscopic techniques such as Raman spectroscopy.

2.3.3 Filtration

Filtration is a physical or mechanical technique that is commonly applied for the analysis of water samples polluted with microplastics. However, in case the microplastic particles of interest are rather large while the present sediment particles are relatively small, filtration presents a viable analytical separation technique for sediment samples as well.

Fundamentally, separation occurs by use of a filter medium (a.k.a. septum) that allows passage of the liquid while retaining solid particles. In order to achieve successful microplastic separation in sediment samples, the size of the microplastic particles needs to be larger than the applied pore size, while the size of all other solid particles needs to be strictly smaller. During analysis, it is common to use a vacuum system as illustrated in Figure 2.9.
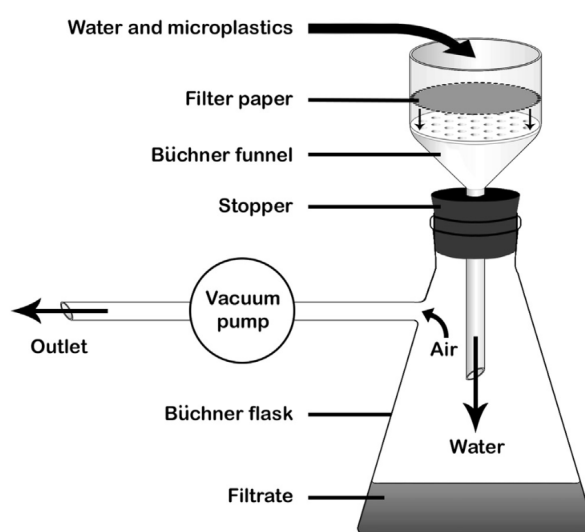

Figure 2.9: Representation of a vacuum filtration system frequently used to analytically isolate microplastic particles (Crawford and Quinn, 2017).

Filtration is a fairly simple and evident technique yet might encounter some important complications. Since samples are often contaminated with particulate matter or debris, the porous filter medium can clog quite rapidly. This hampers the effectiveness of the filtration process and increases the processing time significantly.

2.3.4 Sieving

Similar to filtration, sieving is an analytical separation technique mainly applied to water samples that can process sediment samples in case the physical dimensions of the involved particles align accordingly. In practice, separation is realized through the use of one or more sieve plates with a predefined mesh size. With the aid of an externally applied vibrational movement, the particles pass through the pores according to their size. In microplastic research, a multi-tier sieving installation is the most common setup as illustrated in Figure 2.10. This system brings about the separation of particles of different sizes by using a series of sieve plates with a decreasing mesh size from top to bottom.

Analogous to filtration, the frequently observed clogging of the pores in sieving systems renders the technique less efficient for heavily contaminated samples.
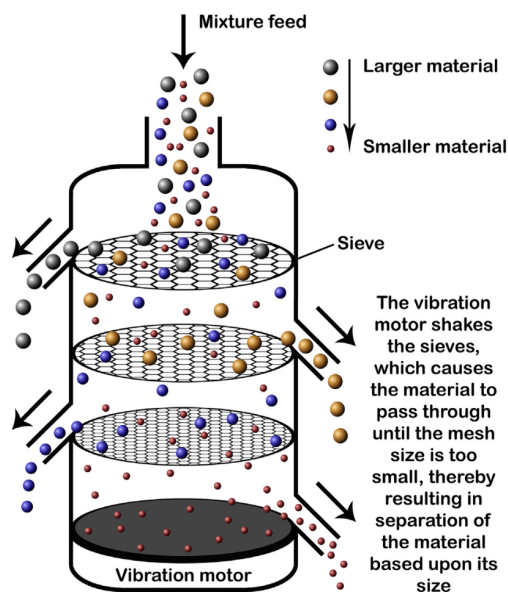
Figure 2.10: Representation of a multi-tier sieving system to illustrate its separating mechanism (Crawford and Quinn, 2017).

2.3.5   Density separation

Density separation is a technique commonly used to analytically separate microplastic particles from sediment. Furthermore, it is believed to be the most reliable method for this analytical separation.

A difference in density between the constituents of a sample mixture lies at the core of the separation mechanism. When particles of different densities are transferred to a liquid of intermediate density, the low-density particles will float, while the high-density particles will ultimately sink. Translated to microplastic analysis of sediment samples, plastic particles are assumed to be less dense than sediment particles. The latter typically bearing a particle density of approximately 2650 kg/m^3. In this regard, microplastics will float correspondingly to the selected liquid, which is commonly a saturated sodium chloride (NaCl) solution with a density of 1202 kg/m^3, although many other media are technically feasible and frequently reported. To illustrate, in case sodium chloride acts as the separating liquid, microplastic particles with a density strictly lower than 1202 kg/m^3 will rise to the surface where they are subsequently collected by decantation of the supernatant. This collection process is usually facilitated by a vacuum system. For instance, by means of a three-necked flask as illustrated in Figure 2.11.

However, care must be taken when selecting the separating liquid considering that the commonly used sodium chloride solution is unable to impose positive buoyancy to, among others, PET and PVC particles (Table 2.1). Furthermore, high-density solutions can establish a more exhaustive and efficient microplastic separation, but might cause other particles, such as light sediment grains, to start floating as well. The latter rendering the separation ineffective, thus an appropriate balance must be identified by experimental trial and error.

2.3.6   Elutriation

The technique of elutriation is based on density differences, but additionally on variations in size and shape. The separation is realized by applying a fluid stream (i.e. gas or liquid) counter current to the direction
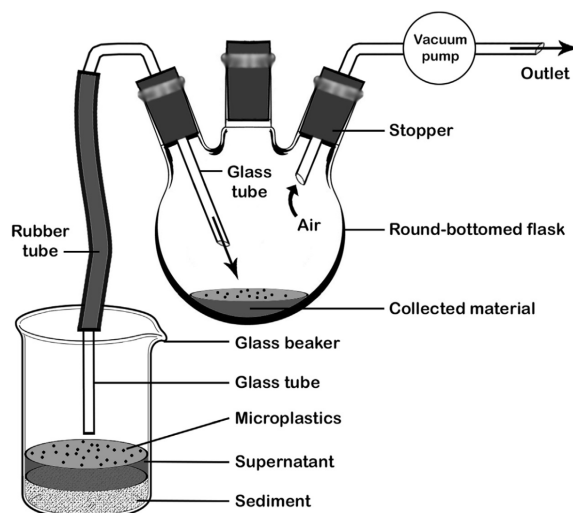
Figure 2.11: Representation of the experimental setup of a three-necked round-bottomed flask in combination with the technique of density separation for the analysis of microplastic particles (Crawford and Quinn, 2017).

of sedimentation. By creating an upward flow of water through a column containing a sediment sample contaminated with microplastics, fluidisation of the sediment is induced. Analytical elutriation is commonly applied to reduce the sample volume as a preceding step to density separation. The process of elutriation is demonstrated and further elaborated in Figure 2.12.
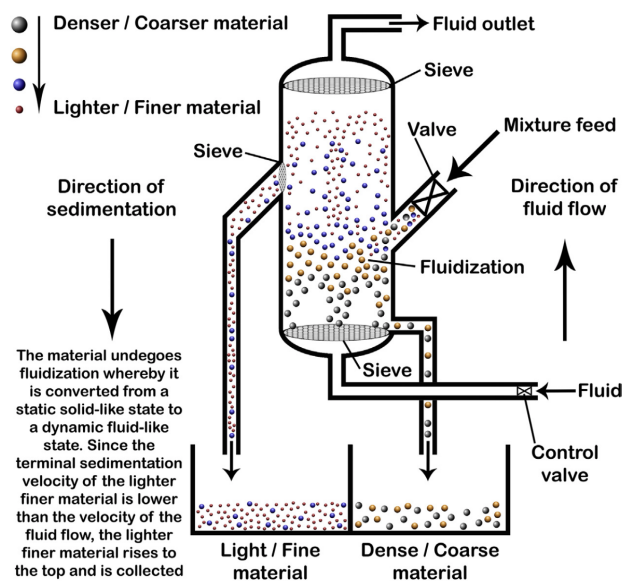

Figure 2.12: Representation of the process of elutriation to explicitly illustrate its separating mechanism (Crawford and Quinn, 2017).

High recovery rates exceeding 90 % are reported by using the analytical technique of elutriation. However, since many variations in design and setup of elutriation installations exist, optimisation and standardisation are essential.

2.3.7 Froth flotation

The foundation for effective separation by flotation is a difference in the surface chemical properties of the solids to be separated. Particles with nonpolar surfaces are typically hydrophobic or not readily wetted, while particles with polar surfaces react strongly with water and are hydrophilic or readily wetted. By introducing air bubbles in a solid-liquid mixture, particles with a high hydrophobicity will exhibit a high tendency to adhere the bubbles while particles with a low hydrophobicity (i.e. high wettability) will encounter little affinity to the air bubbles.

In general, flotation systems follow two main steps. The first one is a conditioning step with the aim to establish the fitting physical and chemical conditions to allow appropriate selectivity between the particles to be separated. The second step is the separation where air bubbles are introduced to the system to induce selective flotation by creating bubble-particle interactions. Subsequently, the floating hydrophobic particles are typically removed from the surface as a froth layer, which explains the commonly used term *froth flotation* in this context. In most applications, the froth overflow stream is termed concentrate while the slurry underflow is called the tailings. The conditioning and separation steps can be either combined in one processing unit or divided into separate units.

Froth flotation is applied analytically in microplastic research where both the conditioning and the separation step are typically combined in one unit. Considering that plastic materials are generally more hydrophobic than sediment particles, froth flotation presents a suitable microplastic separation technique. In particular, the microplastic particles that adhere air bubbles will rise to the surface where they are trapped in a froth layer and subsequently removed by overflow or mechanical action. A clarifying illustration is shown in Figure 2.13.
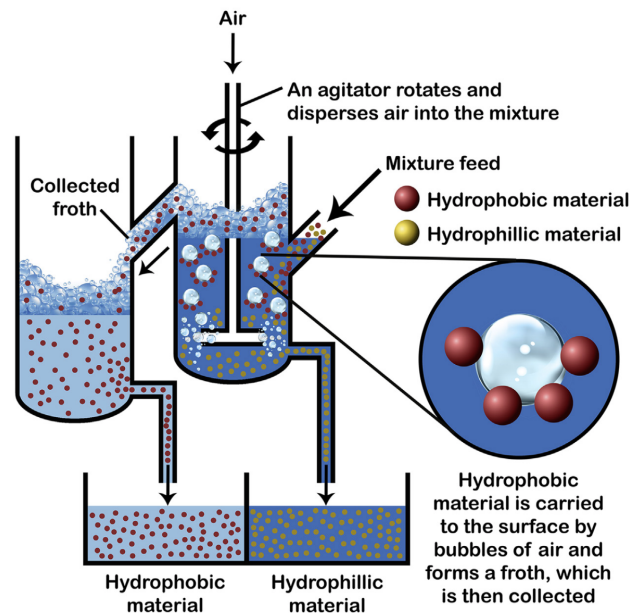
Figure 2.13: Representation of the technique of froth flotation to illustrate and summarize its separating mechanism (Crawford and Quinn, 2017).

Furthermore, flotation systems include many industrial applications as well. To illustrate, froth flotation is a rather old technique that was regularly used in the mining industry and still is to this day. In this regard, a classification exists to differentiate the large-scale mechanisms used for the generation and introduction of bubbles into the system. Six main types can be defined: electrolytic flotation units, dissolved-air flotation units, dispersed-air flotation units, mechanical cells, and flotation columns. A schematic representation of

a dissolved-air flotation unit (DAF) and a mechanical cell are depicted in Figure 2.14a and Figure 2.14b, respectively. For more information about the different types of flotation equipment, the reader is referred to Perry's Chemical Engineer's Handbook (1999).

(a) Dissolved-air flotation   **(b)** Mechanical cell flotation

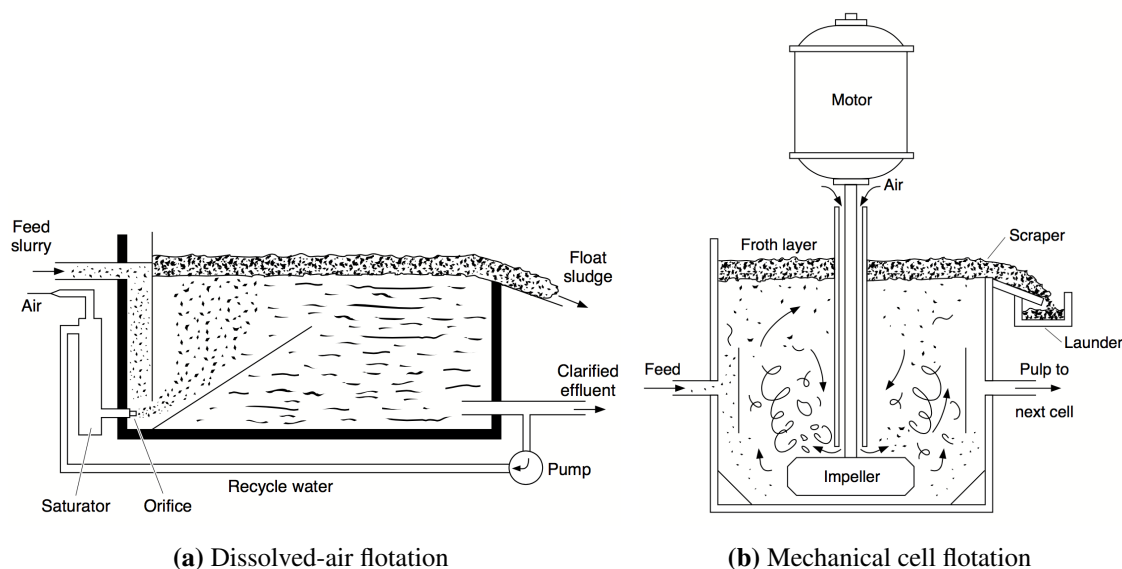**Figure 2.14:** Representation of two frequently applied industrial applications of froth flotation (Crawford and Quinn, 2017).

Regarding the conditioning step, certain modifiers such as wetting agents can be added to alter a material's wettability. In this way, different polymer types can be isolated from each other by selectively increasing wettability. A wetting agent (a.k.a. depressant) will act as a flotation suppressant by adsorbing to the surface of the corresponding material and inducing hydrophilic behaviour. In addition, other groups of modifiers are available such as activators, pH regulators, dispersants and flocculants. Next to modifiers, other types of surface-active compounds (a.k.a. surfactants) exist to regulate the froth flotation process. For instance, collectors selectively promote hydrophobic behaviour of exposed particles, while frothers contribute to stabilize the air bubbles for effective particle-bubble attachment, for a smooth particle-laden bubble carryover to the froth and for ease of froth removal.

Note that the term *flotation* is also used to describe the phenomenon of rising particles in density separation (Subsection 2.3.5) due to the elevated density of the separating liquid. However, in that case the separation occurs solely based on density differences. This is not true for froth flotation, so care is advised in using and interpreting the corresponding terminology.

2.3.8 Centrifuges

Attaining mechanical separation by means of centrifuges is a widely applied industrial technique. In general, two types of centrifuges exist for the separation of solid-liquid mixtures: sedimenting centrifuges and filtering centrifuges. Sedimenting centrifuges require a density difference between the particles to be separated, while filtering centrifuges retain solid particles by a filter medium based on their size. Both types operate under a centrifugal field generated by the rotational movement of the centrifuge along its central axis. This brings about a centrifugal acceleration directed radially outward from the axis of rotation to a body of mass moving along the curved trajectory. The magnitude of the outward acceleration depends on the angular velocity of the centrifuge and the radius from the axis of rotation. Figure 2.15 illustrates a schematic overview of a centrifuge and indicates its main components.
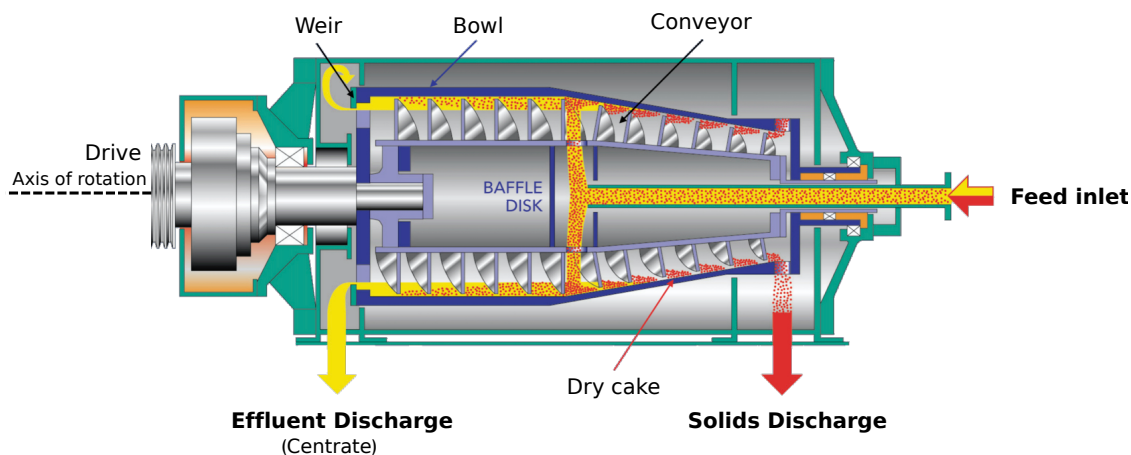
Figure 2.15: Representation of a sedimenting centrifuge, namely a decanter, to illustrate the fundamental elements in this solid-liquid separation technique (Adapted from Oil Sands Magazine, 2019.)

In a sedimenting centrifuge, the separation can be in the form of clarification, classification, thickening or dewatering. In clarification, the clarity of the liquid phase is the main objective, while in classification the separation of solids (typically fine particles) as centrate renders the product stream of the centrifugation process. In the latter, undesired large and dense particles can be captured in the cake as reject (Figure 2.15). The objective in thickening is to form a stream of concentrated solids. For dewatering, a dry cake with a high solids consistency is desired. Considering the nature of the objective, good separation or high settling velocity is achieved by high centrifuge speed, large particle size, large density difference between solid and liquid, large radius and small viscosity. In particular, centrifuge speed and particle size influence settling velocity significantly (i.e. varies as the square of both parameters). The following six types of sedimenting centrifuges are currently applied in industry: tubular-bowl, multichamber, knife-discharge, disc, decanter and screenbowl centrifuge. Only the last three allow continuous operation. For more information about the different types of sedimenting centrifuges, further reading in Perry's Chemical Engineer's Handbook (1999) is recommended.

In a filtering centrifuge, both solid and liquid phase move toward the bowl under the influence of the centrifugal field. There, sufficiently large solid particles are retained by the filter medium and form a cake layer similar to the one formed in sedimenting centrifuges. The liquid flows through the cake layer and the filter as illustrated in Figure 2.16. The solids treated by a filtering centrifuge are typically coarser than those treated by a sedimenting centrifuge. Furthermore, washing and subsequent dewatering are common in the operation of filtering centrifuges. Both batch, intermittent and continuous operations are available and also the manner in which the solids are removed from the basket differs between installation types. To illustrate, seven types of filtering centrifuges are listed with a decreasing minimum solids concentration of the feed stream: vibratory, tumbler, screen scroll, pusher, screen bowl, peeler and pendulum centrifuge.

2.3.9 Screening

The process of screening is nearly identical to the sieving separation technique described in Subsection 2.3.4. However, in this case the feed is typically a solids mixture and the scope is industry rather than analytically oriented. The latter suggesting a broader range of installation types answering the various needs of specific applications.

Analogous to sieving, the separation is achieved by means of one or multiple screening/sieving surfaces.
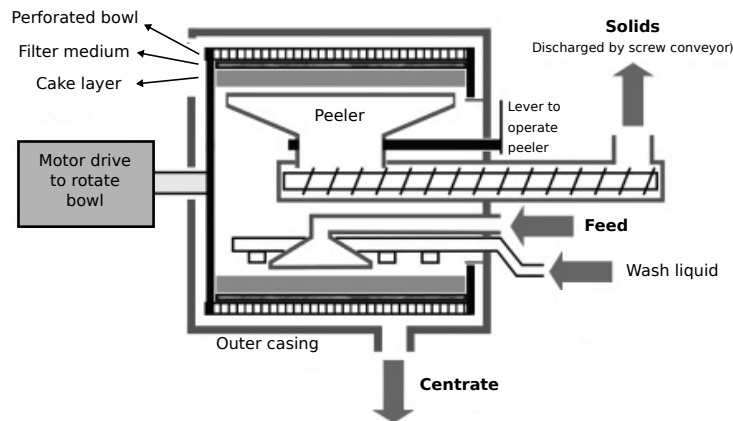
Figure 2.16: Representation of a filtering centrifuge, namely a horizontal axis peeler, to illustrate the filtering mechanism and the fundamental differences with a sedimenting centrifuge (Adapted from Tarleton and Wakeman, 2007).

Material retained on a given screening surface is defined as the oversize material, material passing through the screening surface is the undersize material, and the material passing one screening surface but retained by the subsequent is the intermediate material. The final fractions of material exhibit an increased uniformity in the particle size distribution in comparison with the initial feed mixture. In general, five main classes of screening installations can be defined: grizzlies, revolving screens, shaking screens, vibrating screens and oscillating screens. For large capacity and high efficiency operations, vibrating screens have become standard practise.

2.3.10   Jigging

During the industrial technique of jigging, separation occurs purely based on a difference in density. The pulsating movement of a liquid flow through a bed of solid materials causes heavy particles to settle to the bottom while carrying lighter particles to the top. Essentially, a jig is composed of an open tank filled with water, holding a perforated screen at the top, provided with a spigot in the hutch compartment to drain the concentrate. The jig screen is loaded with coarse, heavy particles (e.g. steel balls) known as the ragging material. The density of the ragging material should be intermediate to the densities of the particles to be separated. In the event of pulsation, the non-cohesive ragging material will aid to stratify the solid particles accordingly. Heavy particles are collected at the bottom of the hutch compartment and are removed via the spigot. Light particles overflow the hutch and are discarded at the top.

A basic jigging setup is illustrated in Figure 2.17 highlighting its main components. Several modifications in jigging installations are common with the main differences in the pulsating mechanism. For instance, the Harz jig is an early design utilizing a reciprocating plunger with differential piston action to bring about the pulsating movement. Other types are the Remer jig, Baum jig and Batac jig, with the last two using air pulsations to establish the desired separation.

2.3.11   Tabling

Tabling installations are characteristic of the traditional mining industry. Next to density, tabling separation techniques consider also shape and size of particles to effectuate a separation. Despite the complexity
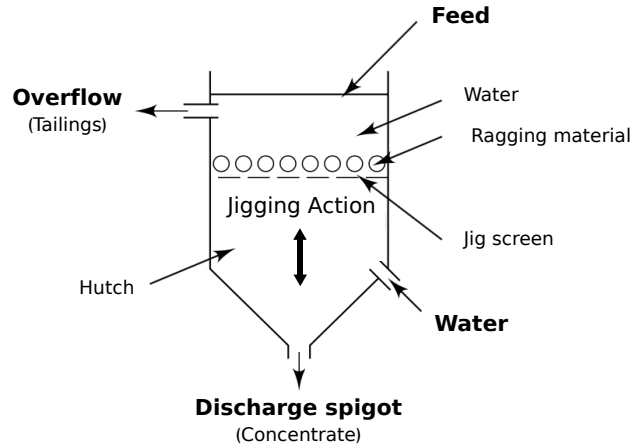
Figure 2.17: Representation of a conventional jig installation to illustrate its separation mechanism (Adapted from Wills and Finch, 2016).

of the mechanism, the setup is quite simple and economically attractive. In case of wet tabling, a solid-liquid mixture is introduced at the top corner of a rectangular riffled plane surface held at a horizontal (and transversal) inclination. The system is provided with a continuous flow of wash water and is differentially shaken in the direction of the long axis. From the feed, the heaviest particles are the least affected by the downward water flow. The riffles collect these heavy particles and guide them towards the concentrate side of the table. The lighter particles ride above the heavier ones and tend to wash over the riffles to the lower tailing side of the table. The material is subsequently collected in launders positioned at the lower edges of the table. Dividing equipment in the launders allows a clear separation of concentrate and tailings, and additionally permits a distinction between middlings and tailings as illustrated in Figure 2.18.
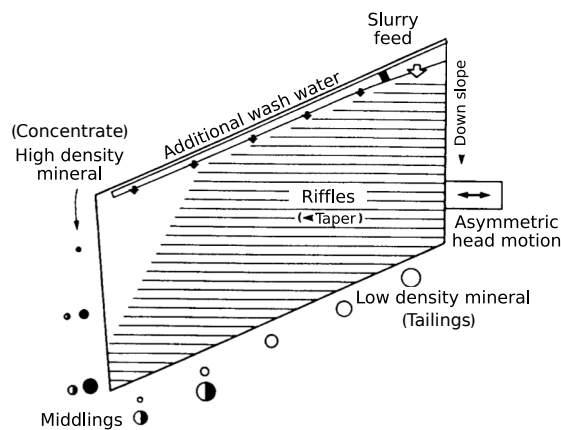
Figure 2.18: Representation of a conventional wet tabling installation to illustrate its separating mechanism (Adapted from Perry and Green, 1997).

Next to wet tabling, the technique of dry tabling is applied in industry. The working principle and equipment are very similar, although several important differences appear. The shaking motion is directed upwards from the horizontal and a stream of air flowing through a perforated deck behaves as the distributing medium instead of a uniform water flow. When water supply is limited or wetting the feed material is undesirable, dry tabling finds successful applications. Lastly, another type of tabling, commonly defined as agglomeration tabling, exists. In this case, selective flocculation or agglomeration is induced by the addition of an agglomerating agent. Afterwards, the mixture is introduced as feed on a water shaking table as described above, where the agglomerated large and feathery textured particles tend to ride with the water

flow over the riffles. The unflocculated particles are carried along the riffles to the concentrate side of the table rather than to the tailings side.

2.3.12   Spiral concentration

Separating solids by means of spiral concentration is primarily based on density differences, and the shape of the particles proves to be a second important separating factor. The most common industrial installation is called the Humphreys spiral and constitutes a spirally constructed channel with a modified semicircular cross-section, as schematically shown in Figure 2.19. Typically, the number of complete spiral turns equals 5 or less frequently 3, with a height drop of approximately 0.35 m per turn. As the feed mixture progresses from top to bottom in the spiral, the heavy particles sink to the bottom and manoeuvre towards the inside of the channel. The lighter particles move to the outside and are carried away by the more diluted, faster flowing pulp stream. Circular concentrate ports or openings are present in the bottom of the channel near the inside edge. Furthermore, wash water is provided along the entire inside edge of the channel to allow repeated washing stages as the mixture flows down the spiral. In general, the richest concentrate is attained from the concentrate ports near the top end of the system.
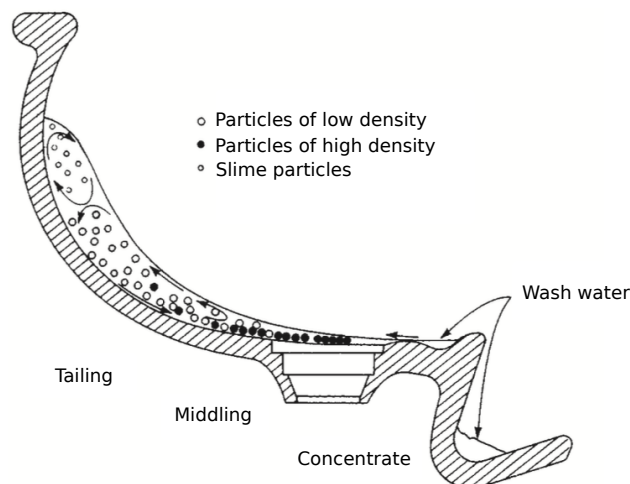
Figure 2.19: Representation of a Humpreys spiral concentrator to illustrate the separation technique of spiral concentration (Adapted from Perry and Green, 1997).

Mechanically, a spiral concentrator is -similar to tabling- a relatively simple and straightforward installation. However, the separating mechanism is quite complex as it involves a centrifugal field, friction action, gravity force and drag of the water.

2.3.13   Electrostatic separation

The electrostatic separation technique is based on the differential attraction or repulsion of charged particles under the influence of an externally applied electrical field. In order to attain charged particles, a charging mechanism is required. Three different techniques can be used for this purpose: contact electrification, conductive induction, and ion bombardment, the latter being the strongest method of charging particles for electrostatic separation. During ion bombardment, both conductor and non-conductor particles are struck by ions of atmospheric gas produced by an electrical corona discharge from a high-voltage electrode. When the bombardment ceases, conductor particles lose their acquired charge very rapidly and experience an opposite

electrostatic force repelling them from a present conducting surface. On the other hand, non-conductor particles are partly coated with ions of opposite charge in electrical polarity to that of the conducting surface. Therefore, these particles exhibit an electrostatic force holding them to the conducting surface. In case this force is greater than the force of gravity and any other force seeking to separate the nonconducting particle from the surface, the particle is said to be pinned on the conducting surface.

In practise, electrostatic separators that are using the charging technique of ion bombardment are by far the most widely applied, in particular the drum type separators. These consist of a conductive rotating drum at ground potential coupled with one or more high-voltage ionizing electrodes. The feeding mechanism is dependent on the range of particle sizes to be treated. However, solely dry mixtures can be processed by means of electrostatic separation. Common installations are fed by vibratory, belt, rotary spline or gravity methods. In addition, often a wiper is provided in the non-conductor product collection section. Essentially, the wiper is an alternating-current electrode system that aims to neutralize the charge on the pinned nonconducting particles. In doing so, the workload for mechanically operated brushing systems can be decreased. In other words, the objective of the brushes is to remove the nonconducting particles from the rotating drum. Splitters are used to create an effective collection mechanism for the separated streams. To illustrate, a schematic overview is given in Figure 2.20.
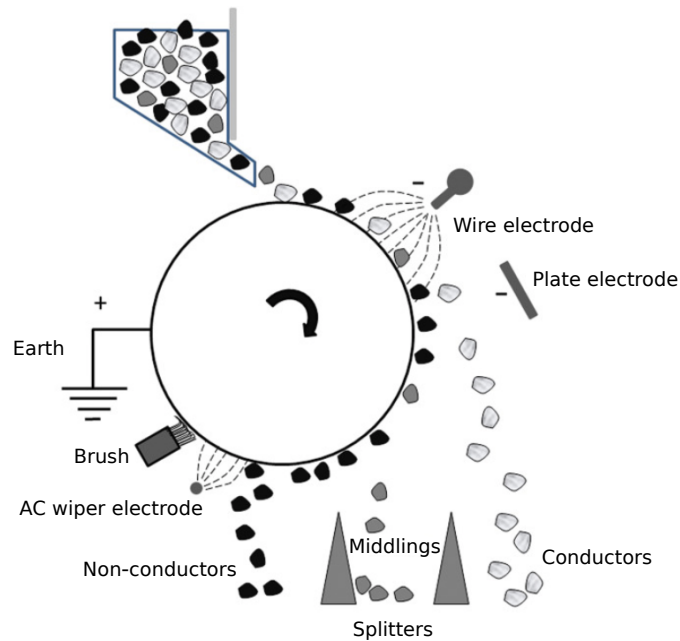
Figure 2.20: Representation of the technique of electrostatic separation to illustrate and summarize the separating mechanism and the various possible process units (Adapted from Gupta and Yan, 2016b).

2.3.14 Summary and preselection

To summarize the reviewed separation techniques, Table 2.3 was constructed. Various properties were independently attributed to the vertically tabulated techniques. Solely the most relevant features and characteristics were selected to maintain the conciseness of the table. Plus and minus signs were used to assign the properties to the corresponding separation techniques to create a visually meaningful representation.

In order to make an informed preselection as part of the overall objective stated in the following chapter (Chapter 3), Table 2.3 was used as the primary source of selection criteria. Considering that the size range of sediment and microplastic particles significantly overlap, it is assumed that techniques that are solely based

on a difference in size, such as filtration and sieving, are not suitable. The former statement is elaborated in Chapter 5 where a detailed feed characterization is provided. Furthermore, separation techniques that are unable to process sediment mixtures are determined as unsuitable. For instance, the technique of electrostatic separation requires exclusively dry mixtures as feed and is therefore not considered as promising for this context. Ultimately, the techniques that are applicable on a large scale and combine several relevant separation factors are favored above the others.

Taking this information into consideration, three distinctive separation techniques are defined as the most promising. Firstly, separation by means of centrifugal sedimentation is said to be a fundamental technique to examine when dealing with solid-liquid mixtures. In addition, it combines multiple separation factors namely the size, density and shape of solid particles. Secondly, froth flotation is selected as a promising separation technique given that it includes the polarity of particles, which proved to be an analytically effective separation property between sediment and microplastic particles. Lastly, wet tabling is recognized as a promising separation technique because it combines multiple, important separation factors and holds an elegant and economically appealing construction.

Table 2.3: Overview of the separation techniques discussed in Section 2.3 containing information about their most relevant characteristics to identify the most promising techniques for the remediation of microplastic particles from marine sediment mixtures. Plus signs (+) indicate that the separation technique holds the corresponding properties, while minus signs (−) indicate that the corresponding properties are absent or not appropriate for the separation technique.

Separation technique	Operation			Primary separation factors					Feed mixture
	Large-scale	Continuous	Low complexity	Size	Density	Polarity	Shape	Other	Sediment
Visual separation	-	-	+	-	-	-	+	+	+
Filtration	+/-	+/-	+	+	-	-	-	-	+
Sieving	+/-	+/-	+	+	-	-	-	-	+
Density separation	+/-	-	+	-	+	-	-	-	+
Elutriation	+/-	+	+/-	+	+	-	+	-	+
Froth flotation	+	+	-	-	+	+	-	-	+
Centrifuges	+	+	+	+	+	-	+	-	+
Screening	+	+	+	+	-	-	-	-	+
Jigging	+	+	-	-	+	-	-	-	+
Tabling	+	+	-	+	+	-	+	-	+
Spiral concentration	+	+	-	-	+	-	+	-	+
Electrostatic separation	+	+	-	-	-	-	-	+	-

3
Objective

At this point, a profound understanding of the different aspects associated with the research on microplastic particles is acquired. The literature review underlined relevant scientific findings and revealed a research gap in the remediation of microplastic particles. Furthermore, potential separation techniques to establish remediation of microplastic particles from sediment were presented and discussed. In addition, based on Table 2.3 presented at the end of the previous chapter and the feed characterisation provided in Section 5.1, three promising separation techniques were preselected, namely centrifugal sedimentation, froth flotation and wet tabling. Due to time restrictions together with the complexity and the limited understanding of the dynamics of the wet tabling process, it was decided to exclude the latter technique from the remainder of this thesis.

In general, the overall objective is to identify and optimize a separation technique that is able to isolate microplastic particles from marine sediments, while simultaneously aspiring a synergy with the dredging industry. To that end, three secondary objectives are defined. First, to establish a qualitative and quantitative feed characterisation. Second, to analyze the effect of marine biofouling and examine the sinking behaviour of the feed constituents, in particular of microplastic particles in solid-liquid systems. And third, to evaluate and optimize the selected separation technique(s).

4

Materials and methods

4.1 Feed characterisation

In order to evaluate the separation performance of a technique handling a particular feed mixture, the composition of that mixture needs to be characterized. The feed mixture considered in this research holds two main constituents, namely sediment and microplastic particles. The following subsections will describe the applied methodology to establish a more detailed characterization of these two constituents individually and to quantify their corresponding concentration in the feed mixture.

4.1.1 Sediment

Sediment composition is strongly dependent on the geographical location. In general, particle analysis of a sediment mixture typically quantifies three primary size fractions, namely the mud content (i.e. $d_p < 63$ μm), the sand content (i.e. 63 μm $< d_p < 2$ mm) and the gravel content (i.e. $d_p > 2$ mm), with d_p a measure of particle size. Table 4.1 illustrates the most commonly applied size fractions and subfractions. Aldridge *et al.* (2007) provide a descriptive summary of the available particle size data from 146 North Sea sediment samples. Data on river sediments were gathered from research performed on the Scheldt, Danube, Mississippi and Pearl River (Baeyens *et al.*, 1998; Toorman, 2009; Notebaert *et al.*, 2011; Baranya *et al.*, 2012; Liska, 2015; Remo *et al.*, 2016; Walstra *et al.*, 2011; Feng *et al.*, 2017). In addition, information about the particle size distribution (PSD) of dredged sediments worldwide was retrieved from the international dredging companies Jan De Nul and DEME.

The bulk mineralogy of North sea sediment mixtures was recently analyzed by Adriaens *et al.* (2018). Despite the strong spatial variation in sediment composition, the main constituents are typically identical for marine sediments worldwide. Therefore, information about the polarity of sediments can be obtained by analyzing the polarity of its most frequently occurring constituents. To that end, a summary was made of the available wettability data of the concerning constituents (Ethington, 1990; Shang *et al.*, 2008; Borysenko *et al.*, 2009; Ozdemir *et al.*, 2009; Kowalczuk *et al.*, 2017; Zheng and Zaoui, 2017; Deng *et al.*, 2018b,a).

Furthermore, the morphology of sediment particles plays an important role. The shape of sediment particles is typically correlated with its corresponding size fraction but varies significantly with the composition of the sediment. The work of Curray and Griffiths (1955); El Fishawi (1984) and Leggett (2012) was consulted to gain insight into the shape variation of sediment particles.

Table 4.1: Overview of the most commonly applied sediment classification according to particle size (Adapted from Huggett, 2011).

Particle fraction	Subfraction	Size range [mm]
Mud	Clay	< 0.002
	Silt	0.002 - 0.063
Sand	Very fine	0.063 - 0.125
	Fine	0.125 - 0.25
	Medium	0.25 - 0.5
	Coarse	0.5 - 1
	Very coarse	1 - 2
Gravel	Granules	2 - 4
	Pebbles	4 - 64
	Cobbles	64 - 256
	Boulders	> 256

4.1.2 Microplastic particles

The different types of polymers that make up microplastic particles were discussed in Section 2.1 and presented in Table 2.1 along with the corresponding density ranges. Information about the occurrence of these particular types of polymers in various sediments worldwide are presented in Appendix Table A.3. In addition, this table provides data about the most frequently observed microplastic particle size and shape. The entire size range of microplastic particles was defined in Subsection 2.2.1. Wettability properties of the polymer types are available in literature, among others Angu *et al.* (2000); Mittal (2001, 2003) and van Oss (2006). Furthermore, the mechanism of biofouling as a cause of density-modification was elaborated in Subsection 2.2.4. However, no experimental research is done about the effect of biofouling on the surface chemical properties, such as the polarity, of microplastic particles. Since these characteristics are of great importance for flotation techniques (Subsection 2.3.7), biofouling experiments were conducted with several polymer types. The applied approach and experimental setup are discussed below. In addition, the effect of biofilm formation on the sinking behaviour of floating microplastic particles is examined by predicting the biofouling conditions required to increase the average density of the bio-fouled microplastic above the density of seawater.

The aim of the biofouling experiments is to examine significant changes in contact angle due to the development of biofilms on the surface of various types of polymers. The contact angle is a measure of wettability of a solid surface, which will be elaborated during the analysis part. Therefore, by analyzing the effect of biofouling on the contact angle, the floatability of the corresponding polymer type in a froth flotation reactor can be predicted.

4.1.2.1 Sample collection

Six of the seven most produced non-fibre polymers (Subsection 2.1.2) were included in the experiments, namely polypropylene, low density polyethylene, high density polyethylene, polyvinylchloride, polyethylene terephthalate and polystyrene. For the remainder of this thesis, the commonly used abbreviations of the corresponding polymers will be adopted (Table 2.1). To obtain the polymers, long sheets were produced by means of extrusion, as explained in Subsection 2.1.1. Table 4.2 specifies the pellets used in the extruder.

However, PVC polymers are highly corrosive due to the production of hydrochloric acid (HCl) in the operating range of the extrusion process. Consequently, specialized corrosion-resistant materials are required for the extrusion of PVC pellets. The available extruder (i.e. Single Screw Extruder Brabender 19) was unable to generate sheets from PVC pellets. Therefore, post-processed PVC items were purchased and manipulated accordingly.

Table 4.2: Overview of the polymers used in the biofouling experiments containing information about the extruded pellets and the corresponding supplier.

Polymer type	Pellets	Supplier
LDPE	LD150AC	Exxon Mobil
HDPE	25055E	DOW
PP	6272NE1	Exxon Mobil
PS	158K	BASF
PET	Lighter C93	Prospector

In addition, six consumer products made from PP were added to the experiments. The aim is to explore the effect of additives on the contact angle of a polymer. Therefore, different colored items were chosen (Figure 4.1): Baybell cup (green), breakfast cereal clip (yellow), straw (black), M&M cup (multicolor), plastic fork (black) and a storage cup (black).
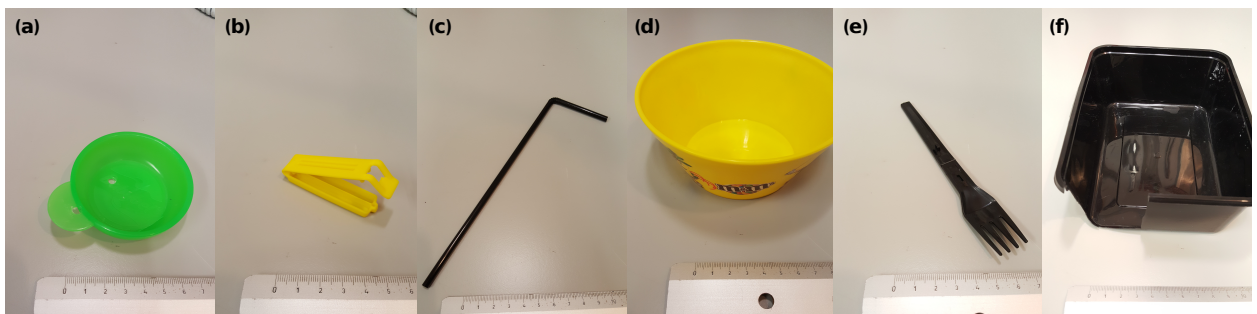

Figure 4.1: Images of the selected consumer products for the biofouling experiments: (a) Babybell cup, (b) breakfast cereal clip, (c) straw, (d) M&M cup, (e) plastic fork and (f) storage cup.

4.1.2.2 Sample preparation and incubation

The extruded polymer sheets were manually cut to form smaller sheets of approximately 2.5 by 5.0 cm. Similarly, the PVC items were sawn to form small sheets. A total of 12 tailored sheets per polymer were generated. To induce biofouling, these sheets were to be fixated in a tank filled with seawater. Therefore, the sheets were perforated with a soldering iron (ERSA Tip 260) of 3.15 mm in diameter. Afterwards, the polymer sheets with a density greater than the density of seawater were fixated at the top, while the polymer sheets with a smaller density were fixated at the bottom of the tank. This was realized by means of water-resistant ropes and sand-filled weights, as can be seen from Figure 4.2. The consumer products from PP were analogously perforated and held underwater.

The tank comprises an aquarium of 120 cm length, 50 cm height and 40 cm width. It was filled with seawater originating from the coast of Flanders and supplemented with biomass scraped from breakwaters nearby. In addition, a concentrated algae batch of 1 L was added. The latter was obtained by capturing algae with a plankton net dragged over surface water of the North Sea by means of the Belgian research vessel
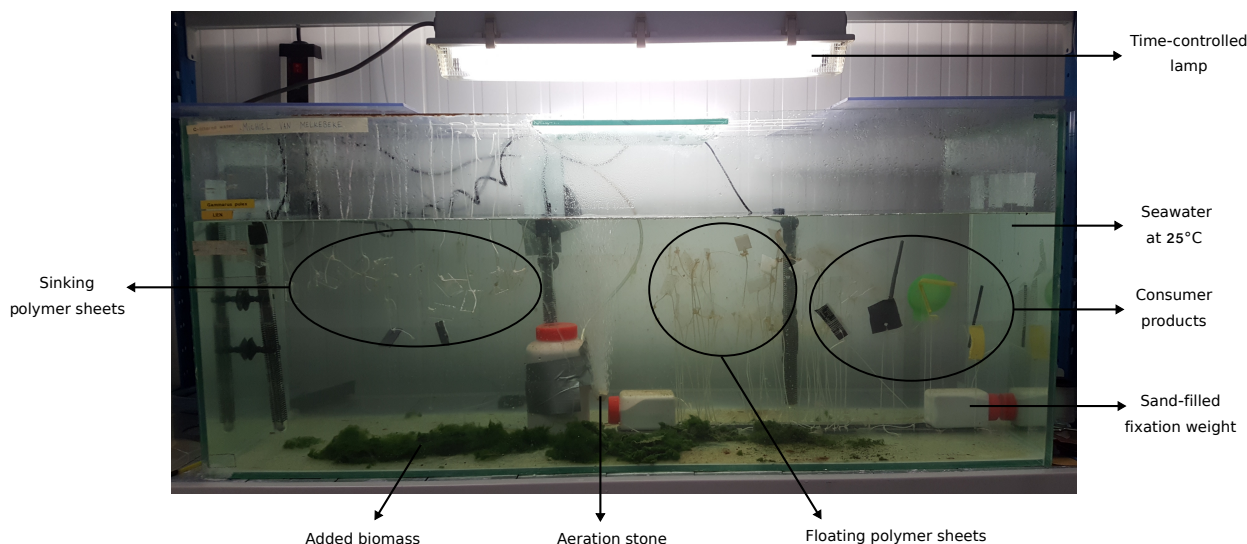
Figure 4.2: Image of the experimental biofouling setup added with clarifying information.

Simon Stevin. Salinity and temperature were kept constant in a control room at 25°C. Oxygen supply and circulation of the water were managed by means of an aeration stone. Time-controlled TL-lamps (OSRAM 36W/840) provided the system with sufficient light and simulated the day/night pattern of natural solar radiation. These conditions were managed to reach the point of adequate biofilm formation on the surface of the polymer sheets and consumer products.

4.1.2.3 Analysis of contact angle

The contact angle θ is the angle formed by the intersection of the liquid-solid interface and the liquid-vapour interface. The term *three-phase contact line* refers to the interface where solid, liquid and vapour co-exist. In case the contact angle is less than 90°, the solid surface is said to be hydrophilic, while a contact angle greater than 90° indicates a hydrophobic surface. In other words, small contact angles are observed when the liquid spreads on the surface, while large contact angles are observed when the liquid minimizes its contact with the surface and forms a compact droplet (Figure 4.3a).
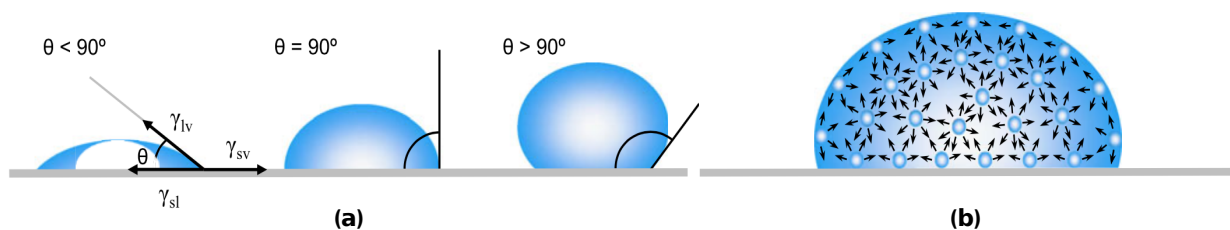
Figure 4.3: Illustration of (a) contact angles formed by a liquid droplet on a smooth homogeneous solid surface and (b) surface tension in a liquid droplet caused by the unbalanced forces of molecules at the surface (Yuan and Lee, 2013).

To explain the shape of a liquid droplet on a solid surface and the associated contact angle, understanding of surface tension is essential. When considering the molecules in the bulk of a pure liquid, each of them is pulled equally in every direction by neighbouring molecules. This results in a net force of zero. However, no balanced net force exists at the surface where molecules do not have neighbouring molecules in all directions. Therefore, the molecules are pulled inwards, which creates an internal pressure (Figure 4.3b). To maintain the lowest surface free energy, the droplet contracts its surface area explaining its spherical

shape. This intermolecular force to contract the surface is known as the surface tension. Since external forces, such as gravity, deform the shape of a droplet, the contact angle is determined by a combination of surface tension and external forces.

In 1805, Thomas Young was the first to describe the contact angle of a liquid droplet on an ideal surface. According to Young, it was defined by the mechanical equilibrium of the droplet under action of the three interfacial tensions, which can be deduced from the following equation:

$$\gamma_{lv} \, cos \, \theta_Y = \gamma_{sv} - \gamma_{sl} \tag{4.1}$$

where γ_{lv}, γ_{sv}, and γ_{sl} represent the liquid-vapor, solid-vapor, and solid-liquid interfacial tensions, respectively, and θ_Y is the Young's contact angle. Equation 4.1 is known as Young's equation. However, the three-phase contact line can be in motion, which renders the phenomenon of wetting to be dynamic rather than static. Therefore, advancing (θ_a) and receding (θ_r) contact angles are defined to indicate a maximum and minimum value, respectively. For the purpose of this research, it is assumed that the potential dynamic value of the measured contact angle θ is equal to Young's contact angle θ_Y and succeeds to appropriately characterize the wettability of the solid surface.

Prior to the contact angle measurement, 3 randomly selected sheets per polymer type were removed from the tank and subsequently dried in a laboratory oven at 60°C once the biofilm formation appeared to be sufficiently advanced. Afterwards, the sheets were individually mounted on a fixation bench to create a flat, horizontal surface. To measure the contact angle, a drop shape analyzer was used. More specifically, a Krüss Drop Shape Analyzer 10 Mk2, as depicted in Figure 4.4, using the sessile drop method where a single drop of distilled water is dosed on the surface of a solid sample. By means of an HD camera with a resolution of 1200 by 800 pixels at 200 fps, the integrated software is able to automatically fit an ellipsoid to the curvature of the sessile water droplet on the solid surface. From that, the value of the contact angle is calculated. By repeating this process 3 times for each sample, the average contact angles of both the bio-fouled polymers (including the consumer products) and the blanco polymer sheets were determined.
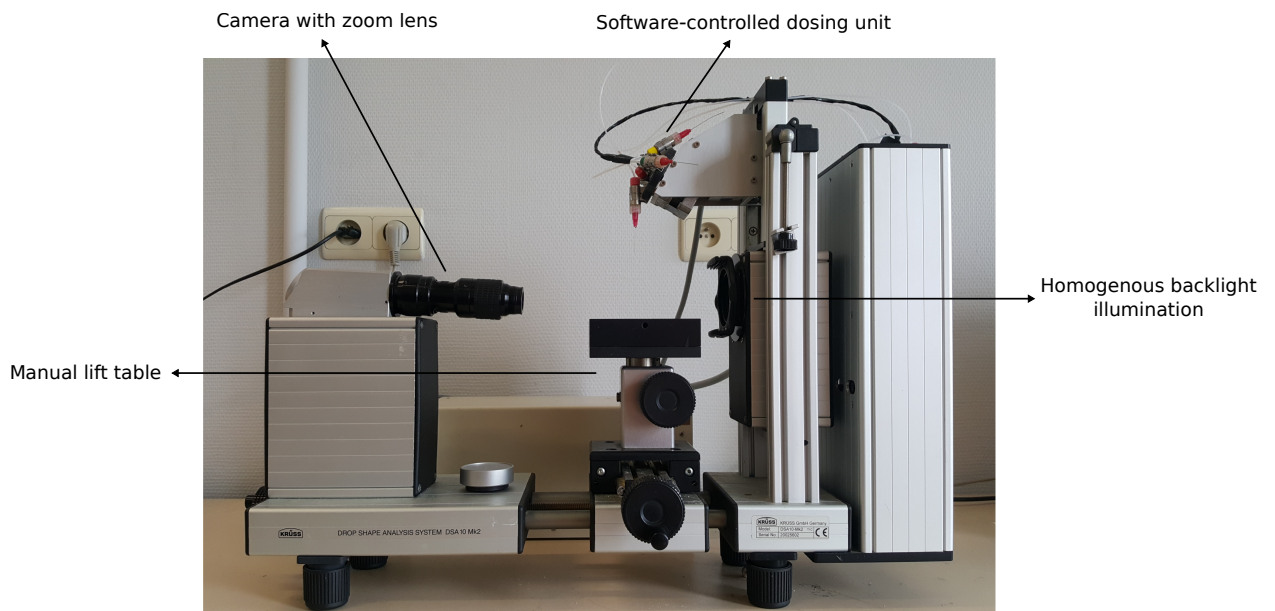

Figure 4.4: Image of the Krüss Drop Shape Analysis system DSA 10 Mk2 used during the contact angle measurements added with clarifying information.

4.1.2.4 Prediction of density-modification

To explore the significance of density-modification caused by biofouling on the sinking behaviour of microplastic particles in the marine environment, theoretical calculations were performed to predict the required biofilm thickness T_b on the surface of low-density microplastics (i.e. floating in seawater) to induce settling. To that end, two extreme shapes were considered, namely a perfect sphere and a thin foil. For the density ρ_p of the corresponding microplastic particles, a value of 925 kg/m^3 is assumed, which was derived by calculating the average density of the two most produced low-density polymer types, namely PE and PP (Subsection 2.1.2). Furthermore, a biofilm density ρ_b of 1100 ± 100 kg/m^3 is assumed (Ro and Neethling, 1991). The expression derived to describe the average density of the bio-fouled particle ρ_{bp} is given by:

$$\rho_{bp} = \frac{m_p + m_b}{V_p + V_b} \tag{4.2}$$

where m_p is the mass of the microplastic particle, m_b is the mass of the biofilm on the surface of the particle, V_p is the volume of the microplastic particle and V_b is the volume of the corresponding biofilm. Substitution of m_b by $V_b\,\rho_b$ yields the following equation:

$$\rho_{bp} = \frac{m_p + V_b\,\rho_b}{V_p + V_b} \tag{4.3}$$

Rearranging Equation 4.3 provides an expression for the volume of the biofilm V_b:

$$V_b = \frac{m_p - \rho_{bp}\,V_p}{\rho_{bp} - \rho_b} \tag{4.4}$$

Assuming that the density of seawater equals 1025 kg/m^3, the density of the bio-fouled particle ρ_{bp} is determined to be greater than or equal to 1025 kg/m^3 to induce settling in the marine environment as a result of biofouling.

For the case of a spherical microplastic particle, the values of V_p and m_p in Equation 4.4 can be calculated for a given diameter d_p. Therefore, the required biofilm volume V_b to induce settling behaviour can be determined. Afterwards, the thickness of the required biofilm T_b can be derived as follows:

$$2\,T_b = d_{bp} - d_p \tag{4.5}$$

where d_{bp} is the diameter of the bio-fouled particle. The factor 2 accounts for the fact that this diameter includes two times the thickness of the biofilm layer. Considering that the diameter of a sphere can be determined by six times the ratio of its volume over its surface area, substitution of d_{bp} in Equation 4.5 yields:

$$2\,T_b = \frac{V_{bp}}{A_{bp}}\,6 - d_p \tag{4.6}$$

where A_{bp} is the surface area of the bio-fouled particle. The volume of the bio-fouled particle V_{bp} is equal to the sum of V_p and V_b. The surface area of a sphere is determined by π times the diameter squared. However, by assuming that $A_{bp} = \pi\,d_p^2$ the surface area of the bio-fouled particle is considered to be independent of the biofilm thickness T_b. Given that the surface area of a sphere increases with the square of its diameter, this assumption would present a significant overestimation of the required biofilm thickness. Moreover, for a given biofilm thickness T_b, the sphere diameter d_p will increase with two times T_b. Therefore, the following expression is derived to approximate T_b:

$$2\,T_b = \frac{(V_p + V_b)}{\pi\,(d_p + 2\,T_b)^2}\,6 - d_p \tag{4.7}$$

This equation yields a third degree polynomial or cubic polynomial in T_b, where the real solution (as opposed to the complex solution) was approximated by using the extended mathematical Solve packages in Matlab R2018b.

For the case of a thin foil microplastic particle, a similar approach is suggested starting from Equation 4.4 that provides an expression for the required biofilm volume V_b. For simplification reasons, the foil particle is represented as a flattened cube with sides l_p and a fixed thickness h_p. Analogously, the corresponding bio-fouled particle is represented as a flattened cube with sides l_{bp} and thickness h_{bp}. Given a constant film thickness $h_p = 0.040$ mm, deduced from the results of the sinking experiments described in Section 4.2, and a value for l_p, the required biofilm volume V_b can be calculated. Furthermore, the thickness of the required biofilm T_b can be derived as follows:

$$2\,T_b = l_{bp} - l_p \tag{4.8}$$

where the factor 2 accounts for the fact that the side l_{bp} of the bio-fouled particle includes two times the thickness of the biofilm layer. Considering the volume and surface area of a flattend cube, the volume of the bio-fouled particle V_{bp} equals $l_{bp}^2\,h_{bp}$ and the corresponding surface area A_{bp} equals $2\,l_{bp}^2 + 4\,l_{bp}\,h_{bp}$. As a result, l_{bp} can be expressed as a function of V_{bp} and A_{bp}, namely $l_{bp} = \frac{4\,V_{bp}\,h_{bp}}{A_{bp}\,h_{bp}-2\,V_{bp}}$. Therefore, Equation 4.8 becomes:

$$2\,T_b = \frac{4\,V_{bp}\,h_{bp}}{A_{bp}\,h_{bp} - 2\,V_{bp}} - l_p \tag{4.9}$$

where V_{bp} can be substituted for the sum of V_p and V_b. Furthermore, h_{bp} is determined as $h_p + 2\,T_b$ and l_{bp} as $l_p + 2\,T_b$, analogous to the case of a spherical microplastic particle. Considering the expression for the surface area of a flattened cube described above, the equation for the required biofilm thickness on the surface of a thin foil particle is derived:

$$2\,T_b = \frac{4(V_p + V_b)\,(h_p + 2\,T_b)}{[2\,(l_p + 2\,T_b)^2 + 4(l_p + 2\,T_b)\,(h_p + 2\,T_b)]\,(h_p + 2\,T_b) - 2\,(V_p + V_b)} - l_p \tag{4.10}$$

This equation yields a fourth degree polynomial or quartic polynomial in T_b, where the physically meaningful solution was also calculated by using the extended mathematical Solve packages in Matlab R2018b.

By varying d_p and l_p for the case of a spherical and a foil microplastic particle respectively, two graphs were constructed that express the predicted biofilm thickness required to increase the density of the bio-fouled particle to a value of 1025 kg/m^3 (i.e. the assumed density of seawater) in function of a measure of particle size, in particular d_p or l_p.

4.1.3 Mixture

Information about the average concentration of microplastic particles in sediments worldwide, was discussed in Subsection 2.2.4. In addition, a review was provided about the scientific findings concerning the strong spatial variation in the concentrations of microplastic particles. Furthermore, Claessens *et al.* (2011) examined the Belgian coastal zone for the occurrence of microplastic particles including sediments in harbours. Van Cauwenberghe (2015) performed similar work and highlighted the importance of rivers, in particular the Belgian Scheldt River, in the distribution of microplastic particles. Both harbour and river sediments are frequently exposed to dredging operations, typically for maintenance purposes, which is of particular interest in the course of this thesis.

4.2 Sinking behaviour

Considering the aim to separate solid particles in a liquid medium from other solid material, a profound understanding of the behaviour of these solid particles in solid-liquid systems is essential. For decades scientists studied the sinking behaviour of sediment resulting in a wide range of empirical equations that estimate the settling velocity of a natural particle in a fluid. Yet very little research is performed on the sinking behaviour of (micro)plastic particles. This observation raises questions about the applicability of these empirical equations, which are based on naturally occurring particles, to microplastic particles which originate from artificially manufactured products. Given the variety of reported geometrical shapes of microplastic particles and its atypical and irregular appearance (Subsection 2.2.2), it is expected that shape will be a fundamental characteristic to consider.

In the interest of validating empirical equations for the settling velocity of particles (i.e. drag laws or drag models), the first subsection will provide a concise description of the fundamental aspects required to obtain an insightful understanding of the dynamics of the presented formulae. This was put together by consulting the work of Albertson (1953); Stringham *et al.* (1969); Graf (1971); Dietrich (1982); Goossens (1987); Gregory (1996); Rhodes (2008) and Dioguardi *et al.* (2018). Afterwards, the following subsection will elaborate on the conducted experiments that were performed to examine the sinking behaviour of microplastic particles and to evaluate the drag models formulated in the first subsection.

4.2.1 Theories

4.2.1.1 Foundation of drag laws

In general, three distinct forces act on a particle falling from rest in a fluid, namely gravity, buoyancy and drag. These forces determine the acceleration force that the particle experiences:

$$gravity - buoyancy - drag = acceleration\ force \tag{4.11}$$

The drag force, F_D, is an important component controlling the settling behaviour of solid particles in static and moving fluids. It is defined as:

$$F_D = \frac{1}{2}\,\rho_f\,A\,u_t^2\,C_D \tag{4.12}$$

where ρ_f is the fluid density, A the cross-sectional area of the particle, u_t the terminal velocity and C_D the particle drag coefficient. The cross-sectional area of the particle A is defined as the projected area of the particle on a plane normal to the direction of flow. For spherical particles A is apparent and equals $\frac{\pi d_p^2}{4}$ where d_p is the corresponding particle diameter. The terminal velocity u_t is reached when driving force and frictional force compensate each other. At this point, the particle reaches a constant velocity (i.e. no acceleration). Considering that the gravitational force, which combines the effect of gravity and buoyancy, is proportional to the volume of the dispersed particle, the gravitational acceleration g and the absolute value of the density difference between particle and fluid, Equation 4.11 becomes:

$$\frac{\pi\,d_p^3}{6}\,g\,|\rho_p - \rho_f| - \frac{1}{2}\,\rho_f\,\frac{\pi\,d_p^2}{4}\,u_t^2\,C_D = 0 \tag{4.13}$$

where ρ_p is the particle density. Furthermore, the following expression for the drag coefficient under terminal velocity conditions can be formulated:

$$C_D = \frac{4}{3}\,\frac{d_p\,g}{u_t^2}\,\frac{|\rho_p - \rho_f|}{\rho_f} \tag{4.14}$$

Rearranging Equation 4.14 gives Newton's impact formula expressing the terminal velocity of a particle falling in a static fluid:

$$u_t = \sqrt{\frac{4}{3}\frac{d_p\,g}{C_D}\frac{|\rho_p - \rho_f|}{\rho_f}} \tag{4.15}$$

The value of C_D is determined by the type of flow conditions, which may be derived from the Reynolds number for particles Re_p:

$$Re_p = \frac{\rho_f\,u_t\,d_p}{\mu} \tag{4.16}$$

where μ is the dynamic viscosity of the fluid. For $Re_p \leq 1$ the flow regime is called laminar and is often referred to as creeping flow or the Stokes' law region. This occurs at very slow relative velocities, which is the case for relatively small particles (i.e. typically ≤ 50 µm in water) according to Equation 4.16. For spherical particles, these conditions effect a linear correlation between the drag coefficient and the particle Reynolds number, namely:

$$C_D = \frac{24}{Re_p} \tag{4.17}$$

The combination of Equation 4.15 and 4.17 yields **Stokes' law** for the terminal velocity or the steady rate of fall:

$$u_t = \frac{d_p^2\,g\,|\rho_p - \rho_f|}{18\mu} \tag{4.18}$$

At higher Reynolds numbers, for instance due to higher relative velocities, the inertia of the fluid starts to dominate and the regime is no longer laminar. A transient regime is defined where $1 < Re_p \leq 400$ and a turbulent regime corresponds to $400 < Re_p \leq 2 \times 10^5$. In the transient regime, the correlation between the drag coefficient and the particle Reynolds number can be approximated by $C_d = \frac{24}{Re_p^{0.646}}$ for spherical particles. Therefore, the corresponding terminal velocity is approximately equal to:

$$u_t = \sqrt[1.354]{\frac{d_p^{1.646}\,g\,|\rho_p - \rho_f|}{18\,\rho_f^{0.354}\,\mu^{0.646}}} \tag{4.19}$$

The turbulent regime, also known as the Newtons' law region, is characterized by a constant drag coefficient for spherical particles, namely $C_D = 0.44$. Together with Equation 4.15, the terminal velocity in the Newton's law region can be derived:

$$u_t = 1.74\sqrt{\frac{d_p\,g\,|\rho_p - \rho_f|}{\rho_f}} \tag{4.20}$$

Figure 4.5 illustrates the different flow regions in the form of the so-called standard drag curve, which gives the relationship between the drag coefficient and the particle Reynolds number.

Generally, when calculating the terminal velocity of a given particle, the flow regime dictates which equation is relevant. However, in order to obtain the flow regime, the Reynolds number must be calculated. Since the latter depends on both the terminal velocity as the equivalent particle diameter, this seems problematic. One way around this is to determine the following dimensionless group:

$$C_D\,Re_p^2 = \frac{4}{3}\frac{d_p^3\,g\,\rho_f\,|\rho_p - \rho_f|}{\mu_2} \tag{4.21}$$

which is independent of u_t. For given particle and fluid properties, the dimensionless group $C_D\,Re_p^2$ is a constant and will therefore generate a straight line of slope -2 if plotted on the logarithmic coordinates of the standard drag curve depicted in Figure 4.5. Subsequently, the value of the particle Reynolds number can be derived from the intersection of this straight line with the drag curve. Therefore, the flow regime can be determined from which the terminal velocity can be calculated.
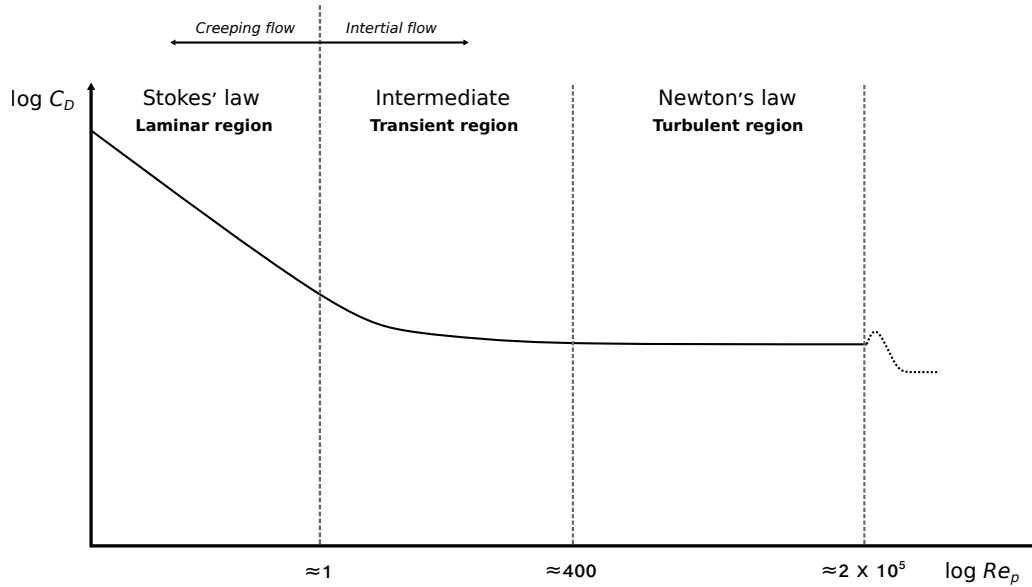
Figure 4.5: Hypothetical standard drag curve for the motion of a perfect sphere in a fluid to illustrate the different flow regions (Adapted from Rhodes, 2008).

4.2.1.2   Shape-dependent drag laws

For non-spherical particles, the drag coefficient is dependent on both the particle Reynolds number and the shape. As a consequence, the correlations between C_D and Re_p suggested above and visually summarized in Figure 4.5 are no longer valid. Furthermore, shape affects the drag coefficient significantly more in the transient and turbulent region than in the laminar region. The particle Reynolds number determines the flow conditions analogously to the approach explained above. However, for non-spherical particles Equation 4.16 is based on the volume-equivalent sphere diameter given by:

$$d_p = \sqrt[3]{\frac{6}{\pi} V_p} \tag{4.22}$$

where V_p is the particle volume. For spheres, Equation 4.22 simply returns the particle's diameter.

The difficulties engineers and scientists experienced over history to account for the effect of shape on the drag coefficient is primarily due to the complexity of describing the particle shape for irregular particles. Drag laws that empirically attempt to include the effect of shape are a function of different shape descriptors, among which sphericity Φ is the most widely applied:

$$\Phi = \frac{surface\ area\ of\ a\ sphere\ whose\ volume\ equals\ the\ particle\ volume}{surface\ area\ of\ the\ particle} = \frac{A_{sph}}{A_p} \tag{4.23}$$

where Φ is a value between 0 and 1 with $\Phi = 1$ indicating a perfect sphere. Another commonly used shape descriptor is the circularity χ, which is a value greater than 1 with $\chi = 1$ indicating a perfect circular contour:

$$\chi = \frac{projected\ area\ of\ the\ particle}{projected\ area\ of\ a\ sphere\ with\ perimeter\ equal\ to\ particle\ perimeter} \tag{4.24}$$

Since measuring the parameters in Equation 4.23 and 4.24 of irregular particles is not straightforward in practice, several shape descriptors are based on the principal axes of the best-fit triaxial ellipsoid to approximate particle shape. These axes are illustrated in Figure 4.6 where a is the longest principal axis, b the intermediate principal axis and c the shortest principal axis. They can be measured by means of the most commonly used image particle analysis techniques, such as ImageJ and SPIP.
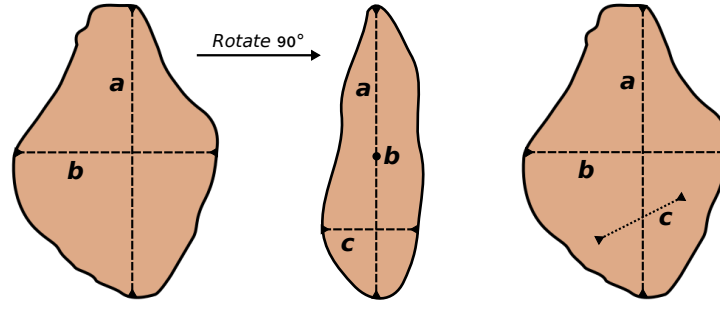
Figure 4.6: Illustration of the three principal axes concept used to approximate the shape of an irregular particle (Adapted from Pettijohn, 1975).

A first empirical equation for the settling velocity of both spherical and non-spherical particles is proposed by **Dietrich (1982)** and involves a particularly well-known shape factor, namely the Corey Shape Factor (CSF):

$$u_t = \sqrt[3]{\frac{(\rho_p - \rho_f)}{\rho_f} \, g \, \nu \, R_3 \, 10^{R_1 + R_2}} \tag{4.25}$$

where

$$R_1 = -3.76715 + 1.92944 \, log \, d_* - 0.09815 \, (log \, d_*)^2 - 0.00575 \, (log \, d_*)^3 + 0.00056 \, (log \, d_*)^4$$

$$R_2 = log\left(1 - \frac{1 - \text{CSF}}{0.85}\right) - (1 - \text{CSF})^{2.3} \, tanh(log \, d_* - 4.6) + 0.3(0.5 - \text{CSF}) \, (1 - \text{CSF})^2 \, (log \, d_* - 4.6)$$

$$R_3 = \left[0.65 - \frac{\text{CSF}}{2.83} \, tanh(log \, d_* - 4.6)\right]^{1 + \frac{3.5 - \text{P}}{2.5}}$$

$$d_* = \frac{(\rho_p - \rho_f)}{\rho_f \, \nu^2} \, g \, d_p^3$$

where ν is the kinematic viscosity of the fluid and d_* is the dimensionless nominal diameter according to Dietrich (1982). Furthermore, CSF is derived by means of the three principal axes characterizing the best-fit ellipsoid of an irregular particle:

$$\text{CSF} = \frac{c}{\sqrt{a \, b}} \tag{4.26}$$

and P representing the Powers Index, which is a measure of roundness and obtained by comparing the particle with a set of 12 predefined images (Figure 4.7) and subsequently assigning it a score from 0 to 6 in the corresponding numerical scale of Folk (1955). Perfectly rounded particles correspond to P = 6. The shape descriptor CSF varies from 0 to 1 with CSF = 0 resembling an infinitely flat particle.

Seven years later, **Haider and Levenspiel (1989)** derived a general shape-dependent drag law based on sphericity:

$$C_D = \frac{24}{Re_p} \, (1 + A \, Re_p^B) + \frac{C}{1 + \frac{D}{Re_p}} \tag{4.27}$$

where

$$A = exp(2.3288 - 6.4581 \, \Phi + 2.4486 \, \Phi^2)$$
$$B = 0.0964 + 0.5565 \, \Phi$$
$$C = exp(4.905 - 13.8944 \, \Phi + 18.4222 \, \Phi^2 - 10.2599 \, \Phi^3)$$
$$D = exp(1.4681 + 12.2584 \, \Phi - 20.7322 \, \Phi^2 + 15.8855 \, \Phi^3)$$

Roundness classes	Very Angular	Angular	Sub-angular	Sub-rounded	Rounded	Well rounded
High Sphericity						
Low Sphericity						
Roundness indices = *Powers Index*	1.02 - 0.72	1.50 - 1.02	2.10 - 1.50	2.94 - 2.10	4.20 - 2.94	6.00 - 4.20

Figure 4.7: Representation of the chart proposed by Powers (1953) to quantitatively estimate the roundness of an irregular particle (Adapted from Powers, 1953).

Swamee and Ojha (1991) suggest the use of CSF to predict the effect of shape on the terminal settling velocity of crushed particles:

$$C_D = \left[\frac{48.5}{(1 + 4.5\,\beta^{0.35})^{0.8}\,Re_p^{0.64}} + \left(\frac{Re_p}{Re_p + 100 + 1000\,\beta} \right)^{0.32} \frac{1}{(\beta^{18} + 1.05\,\beta^{0.8})} \right]^{1.25} \tag{4.28}$$

where β is the shape factor proposed by Swamee and Ojha (1991) yet identical to the Corey Shape Factor (CSF) defined by Equation 4.26.

The drag law proposed by **Ganser (1993)** introduces two shape factors, namely a Stokes shape factor K_1 and a Newton shape factor K_2:

$$C_D = K_2 \left[\frac{24}{K_1\,K_2\,Re_p} \left(1 + 0.1118\,(K_1\,K_2\,Re_p)^{0.6567} \right) + \frac{0.4305}{1 + \frac{3305}{K_1\,K_2\,Re_p}} \right] \tag{4.29}$$

where

$$K_1 = \left(\frac{1}{3} + \frac{2}{3\,\sqrt{\Phi}} \right)^{-1}$$
$$K_2 = 10^{1.8148\,(-log\,\Phi)^{0.5743}}$$

The work of **Dellino *et al.* (2005)** led to a relatively simple expression for the drag coefficient of irregular particles, but suggests the use of a different shape factor Ψ:

$$C_D = \frac{0.9297}{\Psi^{1.6}\,Re_p^{0.0799}} \tag{4.30}$$

where

$$\Psi = \frac{\Phi}{\chi} \tag{4.31}$$

In addition, Dellino *et al.* (2005) derived an equation for the particle surface area A_p, which is in turn used to calculate the sphericity Φ in Equation 4.23. The proposed expression is a function of the three principal axes that allow to conveniently approximate a particle's irregular shape (Figure 4.6):

$$A_p = 4\,\pi \left[\frac{\left(\frac{a}{2}\right)^z \left(\frac{b}{2}\right)^z + \left(\frac{a}{2}\right)^z \left(\frac{c}{2}\right)^z + \left(\frac{b}{2}\right)^z \left(\frac{c}{2}\right)^z}{3} \right]^{\frac{1}{z}} \tag{4.32}$$

where $z = 1.6075$.

The shape-dependent drag law proposed by **Pfeiffer *et al.* (2005)** is a modification of the original expression derived by Walker *et al.* (1971) and Wilson and Huang (1979). It differentiates different flow regions based on the value of the particle Reynolds number and presents a particle aspect ratio φ to describe the shape:

$$C_D = \begin{cases} \dfrac{24}{Re_p}\,\varphi^{-0.828} + 2\,\sqrt{1-\varphi} & Re_p \leq 10^2 \\[2ex] 1 - \dfrac{1 - C_D(Re_p = 100)}{900}\,(10^3 - Re_p) & 10^2 < Re_p \leq 10^3 \\[2ex] 1 & Re_p > 10^3 \end{cases} \tag{4.33}$$

where

$$\varphi = \frac{b+c}{2\,a} \tag{4.34}$$

Starting from the work of Dietrich (1982) and Cheng (1997), a general formula for the settling velocity of a particle is presented by **Camenen (2007)**. The same shape descriptors as applied by Dietrich (1982) are suggested, namely the Corey Shape Factor and the Powers Index:

$$u_t = \frac{\nu}{d_p}\left[\sqrt{\frac{1}{4}\left(\frac{A}{B}\right)^{\frac{2}{m}} + \left(\frac{4}{3}\frac{d_{**}^3}{B}\right)^{\frac{1}{m}}} - \frac{1}{2}\left(\frac{A}{B}\right)^{\frac{1}{m}}\right]^m \tag{4.35}$$

where

$$A = 24 + 100\left[1 - sin\left(\frac{\pi}{2}\,\text{CSF}\right)\right]^{2.1+0.06\,\text{P}}$$

$$B = 0.39 + 0.22\,(6 - \text{P}) + 20\left[1 - sin\left(\frac{\pi}{2}\,\text{CSF}\right)\right]^{1.75+0.35\,\text{P}}$$

$$m = 1.2 + 0.12\,\text{P}\,sin^{0.47}\left(\frac{\pi}{2}\,\text{CSF}\right)$$

$$d_{**} = \sqrt[3]{\left(\frac{\left(\frac{\rho_p}{\rho_f} - 1\right)g}{\nu^2}\right)}\,d_p$$

where d_{**} is the dimensionless nominal diameter according to Camenen (2007).

The next shape-dependent drag law proposed by **Dioguardi and Mele (2015)** makes use of the shape descriptor Ψ defined by Dellino *et al.* (2005) in Equation 4.31:

$$C_D = \begin{cases} \dfrac{C_{D,sphere}}{Re_p^2\,\Psi^{Re_p^{-0.23}}}\left(\dfrac{Re_p}{1.1883}\right)^{\frac{1}{0.4826}} & Re_p \leq 50 \\[3ex] \dfrac{C_{D,sphere}}{Re_p^2\,\Psi^{Re_p^{0.05}}}\left(\dfrac{Re_p}{1.1883}\right)^{\frac{1}{0.4826}} & Re_p > 50 \end{cases} \tag{4.36}$$

where $C_{D,sphere}$ is calculated by means of the drag law of Clift and Gauvin (1971):

$$C_{D,sphere} = \frac{24}{Re_p}[1 + 0.15\,Re_p^{0.687}] + \frac{0.42}{1 + \frac{42500}{Re_p^{1.16}}}$$

Bagheri and Bonadonna (2016) constructed a general drag law by using two other shape descriptors, namely the particle flatness $\mathcal{F}$ and elongation e, based on the three principal axes a, b and c of an irregular particle:

$$C_D = \frac{24\,K_S}{Re_p}\left[1 + 0.125\left(Re_p\,\frac{K_N}{K_S}\right)^{\frac{2}{3}}\right] + \frac{0.46\,K_N}{1 + \frac{5330}{Re_p\frac{K_N}{K_S}}} \tag{4.37}$$

where

$$K_S = \frac{F_S^{\frac{1}{3}} + F_S^{\frac{-1}{3}}}{2} \qquad\qquad \alpha_2 = 0.45 + \frac{10}{exp(2.5\,log\rho' + 30)}$$

$$K_N = 10^{\alpha_2\,(-log\,F_N)^{\beta_2}} \qquad\qquad \beta_2 = 1 - \frac{37}{exp(3\,log\rho' + 100)}$$

$$F_S = \mathcal{F}\,e^{1.3}\left(\frac{d_{sph}^3}{a\,b\,c}\right) \qquad\qquad \mathcal{F} = \frac{c}{b}$$

$$F_N = \mathcal{F}^2\,e\left(\frac{d_{sph}^3}{a\,b\,c}\right) \qquad\qquad e = \frac{b}{a}$$

with ρ' the particle to fluid density ratio $\frac{\rho_p}{\rho_f}$ and d_{sph} the diameter of the volume-equivalent sphere, which equals d_p in this context according to Equation 4.22.

The most recent developed expression for the drag coefficient is the one by **Dioguardi *et al.* (2018)**. The proposed empirical drag law is claimed to hold an unmatched, wide range of applicability and uses the shape descriptor Ψ by Dellino *et al.* (2005) that accounts for both the sphericity and the circularity of a particle (Equation 4.31):

$$C_D = \frac{24}{Re_p}\left(\frac{1-\Psi}{Re_p} + 1\right)^{0.25} + \frac{24}{Re_p}\left(0.1806\,Re_p^{0.6459}\right)\Psi^{-Re_p^{0.08}} + \frac{0.4251}{1 + \frac{6880.95}{Re_p}\Psi^{5.05}} \qquad (4.38)$$

To summarize, a table is constructed listing the authors of the discussed drag laws or drag models with the corresponding applied shape descriptors. In addition, Table 4.3 indicates the examined experimental particle Reynolds number range to derive the corresponding equations. The latter provides information about the applicability-range of the expressions.

Table 4.3: Overview of the different shape descriptors used to derive the discussed drag laws (or drag models) along with the reported corresponding particle Reynolds number range for which the equations are theoretically intended.

Author(s) drag law	Shape descriptor(s)	Experimental Re_p range
Dietrich (1982)	CSF, P	$0.07 < Re_p < 5 \times 10^4$
Haider and Levenspiel (1989)	Φ	$Re_p < 2.6 \times 10^5$
Swamee and Ojha (1991)	$\beta = f(\text{CSF})$	$Re_p < 1.5 \times 10^5$
Ganser (1993)	$K1 = f(\Phi), K2 = f(\Phi)$	$Re_p < 2.5 \times 10^4$
Dellino *et al.* (2005)	$\Psi = f(\Phi, \chi)$	$Re_p > 60$
Pfeiffer *et al.* (2005)	φ	$0.1 < Re_p < 10^4$
Camenen (2007)	CSF, P	$Re_p < 10^5$
Dioguardi and Mele (2015)	$\Psi = f(\Phi, \chi)$	$0.01 < Re_p < 10^4$
Bagheri and Bonadonna (2016)	$\mathcal{F}, e$	$Re_p < 3 \times 10^5$
Dioguardi *et al.* (2018)	$\Psi = f(\Phi, \chi)$	$0.03 < Re_p < 10^4$

Finally, it needs to be mentioned that the collection of shape descriptors discussed above does not represent an exhaustive overview. Over the past century, an excessive amount of possible shape descriptors emerged due to the availability of digital image analyzers. A critical review of the most popular particle shape statistics is provided by Smart (2013). To illustrate, Equation 4.32 can be used to derive an approximation of a particle's sphericity Φ, which is generally defined by Equation 4.23. However, many other approximations of sphericity exist among which sphericity Φ_K proposed by Krumbein (1941), $\Phi_{S\&F}$ by

Sneed and Folk (1958) and Φ_R by Riley (1941) are the most favored:

$$\Phi_K = \sqrt[3]{\frac{b\,c}{a^2}} \qquad\qquad \Phi_{S\&F} = \sqrt[3]{\frac{c^2}{a\,b}} \qquad\qquad \Phi_R = \sqrt{\frac{d_i}{d_c}} \qquad (4.39)$$

where d_i is the largest inscribed circle and d_c is the smallest circumscribed circle of an irregular particle.

4.2.1.3 Orientation

The effect of a particle's orientation on its terminal velocity u_t was a topic of interest for many scientists studying the sinking behaviour of irregular particles, among which several are referred above. Interestingly, in the laminar region particles fall predominantly with their longest surface parallel to the direction of motion, while in the turbulent region particles present their maximum area to the oncoming fluid. Therefore, an important distinction appears between the laminar and turbulent region concerning the effect of orientation. In the case of turbulent conditions, a restricted number of particle orientations will be stable. In practice, the orientation where the maximal cross-section of the particle is set perpendicular to the flow direction, is accepted as the only stable position. Merely at extremely high turbulent flow (i.e. $Re_p > 10^4$), the development of a vortex trail behind the settling particle will induce an oscillating motion, yet the average orientation will be identical to the one described before. However, in the case of laminar conditions every initial orientation is theoretically stable. Therefore, a particle will retain its original orientation during settling in the laminar region.

4.2.1.4 Boundaries

In case a particle settles in a fluid in the presence of a solid boundary, its terminal velocity u_t will be lower compared to the terminal velocity reached by a particle falling in an infinite fluid. Typically, the effect of boundaries is solely considered when using the falling sphere method to measure the viscosity of a fluid. When a particle is settling along the axis of a vertical pipe, the boundary effect can be described by means of a wall factor f_w. A common expression for the wall factor is derived by Francis (1933):

$$f_w = \left(1 - \frac{d_p}{D}\right)^{2.25} \quad \text{for} \ \ Re_p \le 0.3 \ \text{and} \ \frac{d_p}{D} \le 0.97 \qquad (4.40)$$

where D is the diameter of the vertical pipe. For the purpose of this thesis, the boundary effect will not be considered further.

4.2.2 Experiments

The aim of the sinking experiments described below is to gain insight into the sinking behaviour of microplastic particles. In particular, the effect of shape on the settling velocity is explored. Afterwards, this knowledge is used to select the most appropriate expression to theoretically predict the terminal velocity of microplastic particles among the discussed drag models presented in Subsection 4.2.1.

4.2.2.1 Sample collection

To make the results more representative, the experiments were conducted on common plastic waste products that potentially find their way to the marine environment where they contribute to the formation of

microplastic particles. Therefore, six of the seven considered products were retrieved at waste management company IVAGO from the collected municipal waste. This was done in collaboration with the project *Matter* that aims to provide sustainable recycling solutions for mixed plastic waste streams in Belgium. Furthermore, PVC-pipes purchased from a local hardware store were added as a final plastic product to include in the experiments. Table 4.4 specifies all the plastic products used in the sinking experiments.

Table 4.4: Overview of the plastic (waste) products used in the sinking experiments containing information about the selected product parts, the corresponding polymer type and the number (#) of selected particles.

Product	Product part	Polymer type	# selected particles
Coca Cola 1.5 L	Bottle	PET	20
Dash stralend wit 195 cL	Bottle	HDPE	20
Flowerpot brown	Tray	PP	20
Mushroom container 500 g	Tray	PS	20
Jupiler 15 cans shrink wrap	Foil	PE	20
Lotus Speculoos package 12.5 g	Foil	PE + PVDC	20
PVC-pipe	Pipe	PVC	20

4.2.2.2   Sample preparation

Once the different plastic products were acquired, each item was subjected to a washing cycle of three consecutive stages with deionized water. Afterwards, the items were dried at room temperature to allow further processing. The non-foil products, with the exception of the PVC-pipes, were individually fragmented by means of a Shini SG-16N/20N Granulator. The two foil products required specialized equipment executed by a Hellweg 340/150 Granulator. Prior to this fragmentation, the foil items were submerged in liquid nitrogen to reduce the flexibility of the foil and therefore facilitate the shredding process. Lastly, the PVP-pipes were manipulated with a miter saw to produce fibres.

The generated irregular particles were collected per plastic product and divided into two size ranges, namely smaller than 2 mm and between 2 and 5 mm. This was done by means of an Endecott Sieve Shaker. Subsequently, 10 particles were randomly selected from each size category with small tweezers to ensure incorporating various particle sizes comprised within the microplastic range. The individual particles were separately contained in 1.5 mL tubes and given a unique identification label. In total, 140 different particles (i.e. 20 particles per product) were considered in the sinking experiments.

4.2.2.3   Sample characterization

The mass m of each individual particle was measured with an accuracy of 0.01 mg by means of a Mettler Toledo AX105 laboratory balance. To determine the density ρ_p, a Precisa Density Kit 350 was used in combination with ethanol (100 % HPLC grade) as liquid medium. By successively measuring the mass of an object exposed to the ambient air and submerged in a liquid medium, the integrated software of the Precisa Density Kit is able to determine the density of the object based on the difference in mass. However, given the restricted precision of this measurement for particles with a mass lower than 0.1 g and the assumption that the density of a plastic item is uniformly distributed over its surface, particles larger than 5 mm were used to derive the density. More specifically, 10 different particles that were unable to pass the 5 mm sieve plate of the Endecott Sieve Shaker per plastic product were subjected to the density analysis. Afterwards, the average value together with the standard deviation were assigned to all 20 different particles of the

corresponding product. By combining the data of particle mass and density, the volume of each particle V_p was determined. Subsequently, the volume-equivalent sphere diameter d_p and the volume-equivalent sphere surface area A_{sph} were calculated by means of Equation 4.22 and by considering that $A_{sph} = \pi \, d_p^2$.

To quantify the shape of the irregular particles, a combination of different analysis techniques was applied. A Keyence VHX-500FE Digital Microscope (Figure 4.8) was used to generate high resolution 2D-images. Afterwards, by means of the image analysis software *ImageJ* several shape descriptors such as the circularity χ were derived. However, caution is advised when interpreting the predefined shape descriptors in the ImageJ interface. For instance, the circularity generated by ImageJ is equal to the inverse of the traditional circularity χ defined in Equation 4.24. To calculate the sphericity Φ, the numerator and denominator of Equation 4.23 were determined separately. The numerator represents A_{sph}, which was calculated as described in the previous paragraph. Furthermore, Equation 4.32 provides an expression for the denominator A_p, which is a function of the three principal axes a, b, and c of the best-fit ellipsoid of a particle. These axes were obtained by combining the measurements of a Mitutoyo Digimatic Indicator with the data gathered from the 2D-image analysis. Hence, the sphericity Φ of each particle was determined. Consequently, the shape factor Ψ could be calculated via Equation 4.31. The other applied shape descriptors CSF, φ, $\mathcal{F}$ and e are calculated as described in Subsection 4.2.2 since they are merely functions of a, b and c. Lastly, the Powers Index P was derived by visually comparing each particle with the 12 images proposed by Powers (1953) (Figure 4.7).

Figure 4.8: Image of the Keyence VHX-500FE Digital Microscope used for the shape characterization of the microplastic particles considered during this research.

4.2.2.4   Analysis of sinking velocity

To experimentally determine the terminal velocity u_t of the characterized particles, the expected time for a particular particle to reach its terminal velocity is to be estimated. To that end, Zaichik *et al.* (1997) among others derived an equation for the relaxation time τ, which indicates the time required to reach a velocity that is 63 % of the terminal velocity:

$$\tau = \frac{d_p^2 \, \rho_p}{18 \, \mu} \tag{4.41}$$

Moreover, a particle will reach 95 % of the terminal velocity after three times the relaxation time τ. Considering the acquired physical properties of the 140 particles, a conservative estimation of $\tau = 0.5$ s was found. By consulting the work of Kowalski *et al.* (2016), a conservative prediction for the maximum terminal velocity of the considered microplastic particles of approximately 0.1 m/s was made. Therefore, it was assumed that every particle would reach their terminal velocity before a distance of 20 cm was travelled in water or ethanol as medium.

To measure the terminal velocity of a particle, a traditional cylindrical settling column of 45 cm height and 10 cm in diameter was used. Based on the particle density, deionized water ($\rho_f = 1000$ kg/m^3) was used as the medium for the particles derived from the Cola bottles, mushroom trays and PVC-pipes, while disolol (i.e. ethanol denatured with eurodenaturant; $\rho_f = 790$ kg/m^3) acted as the medium for the particles derived from the Dash bottles, flowerpots, Jupiler shrink foil and Lotus Speculoos packages. Prior to the sinking measurements, the plastic particles were submerged in a beaker filled with the corresponding medium at the same temperature to avoid electrostatic discharge at the surface of the particles. The latter phenomenon might affect the sinking behaviour of plastic particles, which is undesirable during the experiments. After submersion, the particles were individually transferred to the top of the settling column and gently released in the fluid by using tweezers. Time recording started 20 cm below the surface of the medium to ensure that the particle reached its terminal velocity. More specifically, the time a particle needed to cross a distance of two times 10 cm was measured by means of an HDR-CX160 Camera at 100 frames per second. Given the measured sinking time and the predefined travelled distance, the terminal velocity of each individual particle was calculated.

Furthermore, the sinking experiments were conducted in a temperature-controlled room to avoid fluctuations in viscosity of the medium between measurements. The relation between viscosity and temperature is most commonly described by the Vogel–Fulcher–Tammann–Hesse equation:

$$log\, \mu = A + \frac{B}{T - T_0} \tag{4.42}$$

where A, B and T_0 are constants dependent on the fluid under consideration, and T is the absolute temperature. Despite the fact that this equation dates back to the early 1900s, Luis *et al.* (2007) demonstrated its validity more recently. Based on Equation 4.42, the Dortmund Data Bank (DDB) provides a list with the required parameters to calculate the viscosity at a specific temperature for 30 different fluids among which water and ethanol. These values were used to derive the viscosity of water and disolol.

4.2.2.5 Validation

To validate the measured sinking velocities, two different types of perfectly round references spheres were used. Polypropylene spheres (PPS Cospheric) with a certified mean diameter of 2.45 mm $\pm$ 0.05 mm and a density of 900 kg/m^3 were used in combination with disolol, while polystyrene spheres (PSS Cospheric) with a certified mean diameter of 1.94 mm $\pm$ 0.05 mm and a density of 1050 kg/m^3 were used in water as the operating medium. The two average values of 10 successive sinking velocity measurements for both polymer types were compared to theoretical sinking velocities $u_{t,calc}$ calculated by using the reference law for spheres formulated by Dietrich (1982):

$$u_{t,calc} = \sqrt[3]{\frac{(\rho_p - \rho_f)}{\rho_f}\, g\, \nu\, u_*} \tag{4.43}$$

where u_* is the dimensionless nominal settling velocity, which is correlated to the dimensionless nominal diameter d_* previously defined in Equation 4.23 as follows:

$$log\, u_* = -3.76715 + 1.92944\, log\, d_* - 0.09815\, (log\, d_*)^2 - 0.00575\, (log\, d_*)^3 + 0.00056\, (log\, d_*)^4 \tag{4.44}$$

The presented formula was chosen to calculate $u_{t,calc}$ instead of the popular Stokes' law (Equation 4.18), primarily because the latter is assuming a very low particle Reynolds number. As a consequence, Stokes' law solely applies to low settling rates and typically overestimates the terminal velocity of low-density spheres with a diameter bigger than 200 µm in an aqueous medium. To illustrate, Gregory (2006) demonstrated that Stokes' law significantly overestimates the terminal velocity of particles larger than 1 mm by a factor of 10 or higher. Therefore, it is stated that Stokes' law does not apply to particles settling at a rate higher than a few mm/s in water. The formula of Dietrich (1982) presented above (Equation 4.43) is considerably more complex, yet proven to be valid over a broader and more appropriate range of particle Reynolds numbers (i.e. from 0.07 to 5×10^4).

4.2.2.6 Determination of best drag model

Once the terminal settling velocities of the 140 different irregular microplastic particles were experimentally determined, the results were compared with the shape-dependent drag laws discussed in Subsection 4.2.1. Since all these drag models depend directly or indirectly on the particle Reynolds number Re_p, which is given by Equation 4.16, the viscosity μ of the medium was derived. Considering that the viscosity depends on the operating temperature, the Vogel–Fulcher–Tammann–Hesse Equation 4.42 was used. Therefore, the particle Reynolds number of each particle was calculated. Subsequently, by using the fundamental Equation 4.14, the drag laws were rearranged to provide a theoretical expression for the terminal velocity u_t. Afterwards, the following formulae for the average error and the root mean squared error (RMSE) were calculated for each drag law individually:

$$\text{average error } [\%] = \frac{\sum\limits_{i=1}^{N} \frac{u_{t,calc,i}-u_{t,meas,i}}{u_{t,meas,i}} \times 100}{N} \tag{4.45}$$

$$\text{RMSE} = \sqrt{\frac{\sum\limits_{i=1}^{N} \left(\frac{u_{t,calc,i}-u_{t,meas,i}}{u_{t,meas,i}}\right)^2 \times 100}{N}} \tag{4.46}$$

where $N = 140$ is the number of performed terminal velocity experiments, $u_{t,meas,i}$ is the measured terminal velocity of particle i and $u_{t,calc,i}$ is the corresponding terminal velocity calculated by the drag law under consideration. Therefore, the drag law with the smallest error for the dataset could be identified and selected for further anaylsis. In addition, standard drag curves and scatter plots of $u_{t,calc}$ as a function of $u_{t,meas}$ were generated to visualize the measure of fit and the effect of irregular particle shapes.

4.3 Separation by centrifugal sedimentation

An insightful evaluation of centrifugal sedimentation as a potential separation technique of microplastic particles was performed. To that end, the fundamental aspects of centrifuge engineering were considered and briefly presented in the first part of the following subsection, based on the work of Perry and Green (1997); Records and Sutherland (2001); Yang (2003) and Bell (2013). Afterwards, indicative theoretical calculations were carried out applied to an appropriate centrifuge design. The objective is to predict the applicability of centrifugal sedimentation as potential remediation technique for microplastics from marine sediments in a quantitative fashion to avoid unnecessary, time-consuming experiments. Given the availability of proven and reliable formulae describing the process of centrifugal sedimentation, this was assumed to be a valid approach.

4.3.1 Centrifuge engineering

4.3.1.1 Centrifugation

A centrifugal force F_c is generated by introducing a mixture in a rotating vessel. For a particle moving along a curve trajectory with the radius of curvature r and at tangential velocity v_θ, the centrifugal force is given by:

$$F_c = \frac{m\,v_\theta^2}{r} \tag{4.47}$$

where $v_\theta = \Omega\,r$ and Ω the angular velocity of the rotational motion given by:

$$\Omega = 2\,\pi\,n \tag{4.48}$$

where n denotes the speed in revolutions per second. The force F_c acts perpendicular to the direction of motion and is directed radially inward. The kinematic relationship that describes the centrifugal acceleration a_c corresponds to:

$$a_c = \Omega^2\,r \tag{4.49}$$

where a_c is directed radially outward from the axis of rotation and therefore follows the opposite direction as the centrifugal force F_c. Equation 4.49 holds for a non-inertial, rotating reference frame, which is the case when considering centrifuges. Furthermore, centrifugal gravity is commonly expressed in terms of Earth gravity g by means of the so-called *relative centrifugal force* (RC):

$$RC = \frac{\Omega^2\,r}{g} \tag{4.50}$$

From Equation 4.49 it appears that the acceleration increases proportionally to the distance r from the centre of rotation. Therefore, the acceleration of a particle moving outwards will increase so that the particle never reaches a steady state. To account for this relative centrifugal force, Stokes' law for the terminal velocity (Equation 4.18) is adjusted as follows:

$$u_c = u_t \times RC = \frac{d_p^2\,|\rho_p - \rho_f|\,g}{18\mu}\,RC = \frac{d_p^2\,|\rho_p - \rho_f|\,g}{18\mu}\,\frac{\Omega^2\,r}{g} = \frac{d_p^2\,|\rho_p - \rho_f|\,\Omega^2\,r}{18\mu} \tag{4.51}$$

Equation 4.51 represents the generally applied formula to describe the settling velocity u_c of spherical particles in a fluid mixture induced by means of a centrifuge rotating at angular velocity Ω.

4.3.1.2 Grade efficiency

The grade efficiency quantifies the separation probability related to the particle size and is commonly used to predict centrifuge performance. Typically, a grade efficiency curve is constructed to represent the efficiency of the separation process as a function of the particle size. In addition, the diameter of the smallest particles that are completely isolated from the feed mixture during the separation process $d_{p,100}$ and/or the diameter of the particles which are retained at 50 % efficiency $d_{p,50}$ (i.e. critical diameter or cut-size) are identified to characterize centrifuge performance. In general, the efficiency of a centrifuge depends on the residence time t_a of the fluid and on the time required for the desired particle separation.

To illustrate, a rotating drum centrifuge is considered (Figure 4.9). The corresponding grade efficiency for a given particle size E_{d_p} is based on Equation 4.51 and determined by:

$$E_{d_p} = \frac{R^2}{R^2 - r_i^2}\left[1 - exp\left(-\frac{(\rho_p - \rho_f)\,\Omega^2\,t_a}{9\,\mu}\,d_p\right)\right] \leq 1 \tag{4.52}$$

where R is the radius of the cylindrical drum and r_i is the radius from the axis of rotation to the point where the mixture is located against the wall of the centrifuge. Furthermore, $d_{p,100}$ as described above for a rotating drum centrifuge is given by:

$$d_{p,100} = \sqrt{\frac{18\,\mu\,Q\,ln\left(\frac{R}{r_i}\right)}{(\rho_p - \rho_f)\,\Omega^2\,V_{eff}}} \tag{4.53}$$

where Q is the flow rate and V_{eff} is the effective volume of the drum centrifuge.
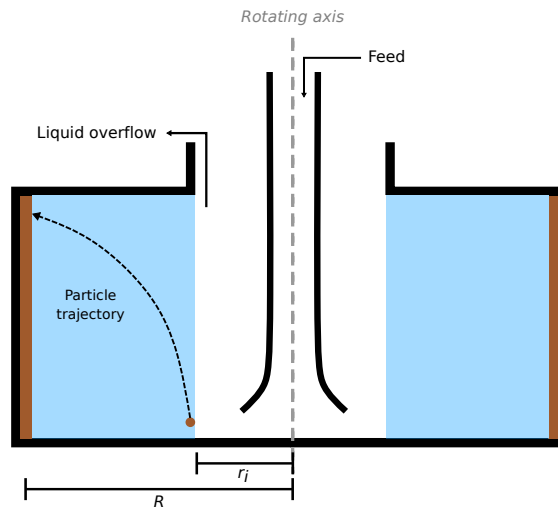

Figure 4.9: Representation of a rotating drum centrifuge to illustrate the separation process and clarify the parameters of Equation 4.52 (Adapted from Geankoplis, 1993).

4.3.1.3   Decanter case study

With respect to the feed mixture defined in Section 5.1, it was concluded that a decanter centrifuge best aligns with the separation requirements for this research. A decanter or solid-bowl centrifuge consist of a rotating solid bowl with both a cylindrical and conical section. In the centre of the centrifuge, a screw conveyor is present that also rotates at a high yet differential speed relative to the solid bowl. The latter is responsible for conveying the sediment from the cylindrical to the conical discharge end. The feed mixture is typically introduced via a stationary feed tube into the feed chamber equipped with a hub accelerator positioned at the transition zone of cylindrical to conical section where the material is rotationally accelerated before it enters the separation pool in the solid bowl. In the separation pool, heavy solid particles settle as a cake towards the bowl wall under centrifugal gravity while the clarified liquid moves radially towards the pool surface. Ultimately, the liquid is discharged through adjustable weirs, while the cake is transported to the conical section, commonly known as the beach, by means of the screw conveyor.

The objective is to calculate the grade efficiency curve for a representative decanter centrifuge operating on the feed mixture defined in Section 5.1. To that end, a particular decanter configuration is chosen based on commercially available models of global decanter suppliers such as GEA, Andritz, Flottweg, HAUS and Siebtechnik Tema. An industrial size bowl diameter of 470 mm was selected, which will be explained in more detail at the end of this section. Typically, the total bowl length to bowl diameter ratio varies from 2 to 4 (Minaker, 1995). Hence, a bowl length of 1410 mm was obtained. Furthermore, the ratio of the length of the cylindrical section to the conical section is assumed to be 3. Therefore, the length of the cylindrical section is said to be 1058 mm. The ratio of the weir diameter to the bowl diameter is assigned a value of
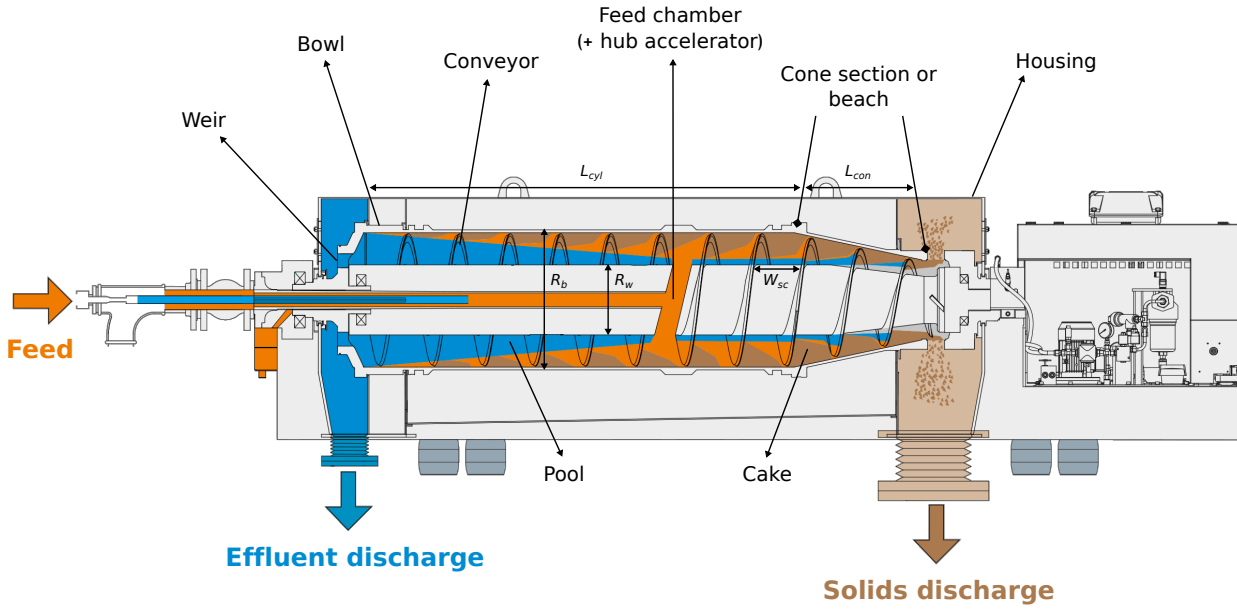
Figure 4.10: Representation of a decanter centrifuge used as case study for the calculations of the grade efficiency curve (Adapted from Hiller, 2019).

0.55, which sets the weir diameter to 259 mm. Lastly, the screw pitch is assumed to be 25 mm. An overview of the dimensions of the proposed decanter centrifuge are listed in Table 4.5.

Table 4.5: Overview of the dimensions of a hypothetical decanter centrifuge in order to appropriately calculate the corresponding grade efficiency curve.

Parameter	Symbol	Value	Unit
Bowl diameter	D_b	470	mm
Bowl radius	R_b	235	mm
Weir diameter	D_w	259	mm
Weir radius	R_w	129	mm
Total bowl length	L_b	1410	mm
Cylindrical length	L_{cyl}	1058	mm
Screw Pitch	W_{sc}	25	mm

Predicting the grade efficiency curve of a decanter centrifuge is more complex compared to the expression for a rotating drum centrifuge presented in Equation 4.52. This is primarily due to the fact that a decanter makes use of an internal screw conveyor for the continuous discharge of the moist cake, which significantly complicates the associated theoretical models. Nonetheless, Gleiss (2018) appeared to be successful in the development of a dynamic process model for the mechanical fluid separation in decanter centrifuges. The following expression was derived for the grade efficiency curve of a decanter centrifuge, which shows noticeable similarities with Equation 4.52:

$$E_{d_p} = \frac{R_b}{R_b - R_w} \left[1 - exp \left(-\frac{(\rho_p - \rho_f) \, R_H \, d_p^2 \, \Omega^2}{18 \, \mu} \, \frac{(R_b - R_w) \, W_{sc} \, L_{cyl}}{Q_{in}} \right) \right] \leq 1 \qquad (4.54)$$

where Q_{in} is the inlet flow rate and R_H is the hindered settling function, which depends on the solids content of the feed mixture. The latter variable describes the phenomenon of hindered settling, which occurs when falling particles influence each other's settling behaviour. Depending on the particle concentration,

the hindered terminal velocity will generally be lower than the terminal velocity of a single particle in an identical medium. For the purpose of this thesis, the hindered settling function will not be further elaborated and the following expression proposed by Richardson and Zaki (1954) is assumed to hold true for R_H when needed:

$$R_H = (1 - \epsilon)^{4.65} \tag{4.55}$$

where ϵ is the solids volume fraction. Despite the efforts by Gleiss (2018) to include every parameter that affects the separation probability of a decanter centrifuge, Equation 4.54 assumes spherical particles and consequently does not account for the effect of particle shape. Considering that it was previously stated that the shape of microplastic particles play a fundamental role in its sinking behaviour, Equation 4.54 requires further modification.

From the results of Subsection 4.2.2, it appears that the shape-dependent drag law proposed by Dioguardi *et al.* (2018) and given by Equation 4.38 best fits the experimental data. To account for this shape-dependent drag coefficient in the calculations of the grade efficiency curve, the structure of Equation 4.54 was analyzed in detail. From this analysis and comparison with the grade efficiency Equation 4.52 for a rotating drum centrifuge, it is clear that the expression for the centrifugal settling velocity of a (spherical) particle u_c given by Equation 4.51 plays a crucial role in the determination of the grade efficiency curve of a centrifuge. Moreover, Equation 4.51 is nearly identically formulated in the decanter grade efficiency Equation 4.54. In particular, the section of this formula highlighted below provides an expression for $\frac{u_c}{r}$:

$$E_{d_p} = \frac{R_b}{R_b - R_w} \left[1 - exp \left(- \frac{(\rho_p - \rho_f) \, \mathbf{d_p^2} \, \Omega^2}{18 \, \mu} R_H \frac{(R_b - R_w) \, W_{sc} \, L_{cyl}}{Q_{in}} \right) \right] \leq 1 \tag{4.56}$$

Furthermore, in order to include the effect of particle shape in the expression for u_c, the fundamental equation for the terminal velocity of a falling particle u_t given by Newton's impact formula in Equation 4.15 was adapted to hold for centrifugal sedimentation:

$$u_c = \sqrt{\frac{4}{3} \frac{d_p \, \Omega^2 \, r}{C_D} \frac{|\rho_p - \rho_f|}{\rho_f}} \tag{4.57}$$

Therefore, the expression for $\frac{u_c}{r}$ becomes:

$$\frac{u_c}{r} = \sqrt{\frac{4}{3} \frac{d_p \, \Omega^2}{C_D \, r} \frac{|\rho_p - \rho_f|}{\rho_f}} \tag{4.58}$$

Consequently, the shape-dependent drag law proposed by Dioguardi *et al.* (2018) and given by Equation 4.38 can be substituted in Equation 4.58, which can be in turn substituted in the highlighted section of Equation 4.56 to account for the irregular shape of (microplastic) particles. For simplification, r was set equal to R_w, which is a reasonable assumption considering the objective to examine the relative differences in grade efficiency between sediment and microplastic particles. Hence, the proposed shape-dependent grade efficiency curve for a decanter centrifuge is given by:

$$E_{d_p} = \frac{R_b}{R_b - R_w} \left[1 - exp \left(- \sqrt{\frac{4}{3} \frac{d_p \, \Omega^2}{C_D \, R_w} \frac{|\rho_p - \rho_f|}{\rho_f}} R_H \frac{(R_b - R_w) \, W_{sc} \, L_{cyl}}{Q_{in}} \right) \right] \leq 1 \tag{4.59}$$

where C_D depends on the shape descriptor Ψ, but additionally on the particle Reynolds number Re_p, which is in turn function of the settling velocity, as can be seen from Equation 4.16. Therefore, the alternative approach suggested in Subsection 4.2.1 using the dimensionless group given by Equation 4.21 was followed. However, considering the vast amount of data points required to construct the grade efficiency curve for each

constituent of the feed mixture at varying values for Ψ, a Matlab function (Matlab R2018b) was constructed that returns the approximated value for the particle Reynolds number from input values for d_p, ρ_p, ρ_f, μ, Ψ and an initial prediction for Re_p. Moreover, the Matlab function was coded in such fashion that d_p is allowed to be a numerical array so that the generated output resembles an array of corresponding Re_p values. Therefore, in combination with a predefined value of Ψ, the drag coefficient C_D associated with a particular particle size d_p can be calculated. Hence, the corresponding grade efficiency can be obtained by means of Equation 4.59. The code for the iterative algorithm is included in Appendix Table A.4.

In order to construct the grade efficiency curves based on the decanter dimensions provided in Table 4.5, the characteristics of the two main feed constituents were retrieved from Section 5.1. An average sediment density of 2650 kg/m^3 was assumed for both sediment scenarios 1 and 2 defined in Section 5.1. For scenario 1 and 2 a shape factor Ψ of 0.8 and 0.6, respectively, was assumed for the sediment particles, with $\Psi = 1$ as best-case scenario (BCS) and $\Psi = 0.3$ as worst-case scenario (WCS) considering the aim to discharge sediment as solids near the cone section, while separating microplastic particles as part of the effluent. To that end, microplastic particles with a density lower than the density of seawater (i.e. the operating medium) are assumed to be isolated in the effluent with a 100 % probability. On the other hand, microplastic particles with a higher density are assumed to be more difficult to separate with the effluent, hence PVC, PET and PC with an average density of 1450, 1350 and 1200 kg/m^3, respectively (Table 5.1), are predicted to be the most troublesome. In addition, microplastic particles with an original density lower than the surrounding seawater that were subjected to marine biofouling were considered. The latter particles were assumed to hold a bio-fouled microplastic density of 1100 kg/m^3 (i.e. the density of a biofilm), which represents the maximum density of a floating, bio-fouled microplastic particle. An average shape factor Ψ of 0.5 was assumed for microplastic particles based on the results of the shape characterization performed as part of the sinking experiments (Section 5.3) and on Table 5.1 provided in Section 5.1, with $\Psi = 0.01$ as BCS and $\Psi = 1$ as WCS. Consequently, by implementing the constructed iterative algorithm (Appendix Table A.4), the drag coefficients C_D of the grade efficiency Equation 4.59 were calculated for each of the discussed feed constituents over a d_p range from 1 µm to maximum 5 mm.

For the operational parameters, common values of industrial decanters were considered. For instance, global technology supplier HAUS offers decanter centrifuges with a bowl diameter D_b ranging from 238 to 820 mm with a maximum angular velocity Ω of 5400 to 2600 rpm, respectively. Furthermore, typical flow rates vary from 1 to 250 m^3/h. Via trial and error, the most desirable and feasible combination of decanter dimensions and angular velocity considering both sediment scenarios defined in Section 5.1 was selected, namely a bowl diameter of 470 mm that is capable of rotating at 5400 rpm. For both sediment scenarios 1 and 2 the corresponding optimal operational conditions were derived for a minimum sediment critical diameter $d_{p,50} = 2$ and 63 µm, respectively, where $d_p = 63$ µm represents the shifting point between the two sediment scenarios. The optimal conditions were determined by using an algorithm that maximizes the distance between the critical diameters of sediment and microplastic particles by varying both the angular velocity Ω and the inlet flow rate Q_{in}, while maintaining the predefined minimum sediment critical diameter of the corresponding scenario. In case the solution violates the preset boundary conditions of the operational parameters (i.e. $\Omega \in [825, 5400]$ rpm and $Q_{in} \in [1, 250]$ m^3/h), the predefined minimum sediment critical diameter of the corresponding scenario is increased automatically until the boundary conditions are met. In addition, a secondary applied boundary condition stated that the minimum distance between the critical diameters of the two main feed constituents must be 30 µm to facilitate graphical interpretation of the results. By assuming the expected values (i.e. not the BCS or WCS values) for the shape factor Ψ for the optimization algorithm, $\Omega = 3500$ rpm and $Q_{in} = 30$ m^3/h was found for sediment scenario 2 with $d_{p,50} = 63$ µm, while $\Omega = 5400$ rpm and $Q_{in} = 10$ m^3/h was derived for sediment scenario 1 with $d_{p,50} = 39$ µm.

Note that every equal multiple of Ω and Q_{in} will result in identical grade efficiency curves according to Equation 4.59 (i.e. Ω and Q_{in} are inversely proportional). Therefore, to obtain the two presented optimal combinations of operational parameters, it was additionally assumed that the inlet flow rate is to be maximized as opposed to minimizing the angular velocity, which is common practice in industry, and that given the opportunity (i.e. more than one solution is available that reached the predefined minimum sediment critical diameter) an angular velocity of 3500 rpm is favored for the decanter design, as recommended by global technology suppliers, such as HAUS and Andritz. The former assumption explains why the potential optimal combination of Ω = 825 rpm and Q_{in} = 1.5 m³/h was not selected for sediment scenario 1, and the latter assumption explains why the potential optimal combination of Ω = 5400 rpm and Q_{in} = 46.3 m³/h was not selected for sediment scenario 2. Lastly, the solids volume fraction ϵ = 0.2 required to calculate the hindered settling function R_H in Equation 4.55 was based on typical values of dredged sediment mixtures provided by dredging company Jan De Nul.

4.4 Separation by froth flotation

The second explored separation technique is froth flotation. In a first part, relevant theoretical aspects that were not included in the fundamental description of froth flotation in Subsection 2.3.7 are briefly discussed. This was done based on the work of Zisman (1964); Weber and Paddock (1983); Fraunholcz (1997); Dai *et al.* (2000); Shen *et al.* (2001); Emerson (2007); Goel and Jameson (2012); Wang *et al.* (2015); Pita and Castilho (2017) and Prakash *et al.* (2018). Afterwards, the applied methodology to examine the applicability of froth flotation as potential remediation technique for microplastics from marine sediments by means of different experimental setups is provided. The final part concludes with a novel design proposal of a tailor-made froth flotation installation to separate microplastic particles from sediment mixtures.

4.4.1 Bubble-particle interaction

The interaction between air bubbles and the particles to be separated is of paramount importance for the flotation process. It dictates both the selectivity as the efficiency of the separation technique. In general, bubble-particle interaction consists of three major sub-processes, which can be divided into collision, attachment and detachment. Hence, the probability of particle collection P is given by:

$$P = P_c \, P_a \, (1 - P_d) \tag{4.60}$$

where P_c is the probability of collision between bubbles and particles, P_a the probability of adhesion after collision and P_d the probability of subsequent detachment. Among the three successive sub-processes, collision has been the most extensively researched and various models have been developed for the prediction of the collision efficiency. A critical review of these models is provided by Dai *et al.* (2000). All models suggest an increase in collision efficiency for increasing particle size and highlight the significance of hydrodynamic interactions. The second sub-process, attachment, involves three distinct steps. Firstly, thinning of the intervening water film between bubble and particle occurs until the film ruptures. Secondly, a three-phase contact nucleus develops after the rupture of the intervening film. And thirdly, expansion and relaxation of the three-phase contact line (Subsection 4.1.2) from the critical radius establishes a stable wetting perimeter. It is stated that interfacial forces rather than hydrodynamic interactions play a dominant role in the attachment efficiency. The stability of the bubble-particle aggregate, hence the detachment probability, depends on both hydrodynamics and interfacial forces.

The reputable model proposed by Emerson (2007) to describe the collision probability P_c made use of numerical solutions of the Navier-Stokes equations to derive the following equation:

$$P_c = A \left(\frac{d_p}{d_{bu}} \right)^n \tag{4.61}$$

where d_{bu} is the bubble diameter and both A and n are parameters which depend on the Reynolds number. From this equation, it is clear that the functional relationship between the collision probability P_c and the ratio of particle to bubble diameter $\frac{d_p}{d_{bu}}$ represents a power law. Furthermore, it indicates that P_c depends on the flow regime. In particular, the bubble Reynolds number Re_{bu} is commonly used to express the parameters A and n, as proposed by Weber and Paddock (1983):

$$A = \frac{3}{2} \left(1 + \frac{0.1875 \, Re_{bu}}{1 + 0.29 \, Re_{bu}^{0.56}} \right) \tag{4.62}$$

where $n = 2$ and Re_{bu} is given by:

$$Re_{bu} = \frac{u_{bu} \, d_{bu}}{\nu} \tag{4.63}$$

where u_{bu} is the terminal bubble rising velocity. Therefore, by substitution of Equation 4.62 in Equation 4.61 the probability of collision P_c becomes:

$$P_c = \frac{3}{2} \left(1 + \frac{0.1875 \, Re_{bu}}{1 + 0.29 \, Re_{bu}^{0.56}} \right) \left(\frac{d_p}{d_{bu}} \right)^2 \tag{4.64}$$

To derive an expression for the probability of attachment P_a, the particle surface properties are essential. Given the event of bubble-particle collision, the particle will slide over the surface of the bubble for a finite period of time commonly defined as the sliding time. It is stated that bubble-attachment occurs when sliding time is longer than induction time, where induction time represents the time required for the previously described film thinning process. In that regard, the process of bubble-attachment is generally treated as a chemical reaction. Solely when the particle holds a sufficient amount of kinetic energy to overcome the energy barrier created by the interfacial forces, bubble-collision results in bubble-attachment. Therefore, the functional relationship to describe P_a is similar to the Arrhenius equation that expresses the rate constant in function of the activation energy for a chemical reaction:

$$P_a = exp \left(-\frac{E_1}{E_k} \right) \tag{4.65}$$

where E_1 is the energy barrier for bubble-particle attachment and E_k is the kinetic energy of collision.

The probability of detachment P_d is a function of the combined effect of gravitational forces, turbulent forces and bubble oscillations. It increases with particle size due to the increase in inertia. Hence, the probability of detachment determines the upper limit of floating particle size. Goel and Jameson (2012) defined the dimensionless Bond number Bo as the ratio of forces of detachment to forces of attachment. Consequently, they derived the following expression for the probability of detachment:

$$P_d = exp \left(1 - \frac{1}{Bo} \right) \tag{4.66}$$

where Bo is a function of g, Re_p, Re_{bu} and ρ_p among others.

The equations presented above are experimentally derived for the case of mineral flotation. In these ore flotation processes, the particle size range of the solids to be separated varies between 30 μm and 1 mm, while the air bubbles are typically up to 1.5 mm in diameter. Therefore, a single bubble is capable of carrying

multiple (hydrophobic) solid particles during flotation. However, considering the size range of microplastic particles (i.e. 1 μm – 5 mm), the bubble-particle configurations will deviate from the traditionally observed aggregates in ore flotation. In particular, multiple bubbles will attach to a single plastic particle of sufficient size. In addition, the occurrence of bubble-particle aggregates where multiple plastic particles are clustered together is frequently reported. Figure 4.11 illustrates the differences in the configuration of bubble-particle aggregates in ore flotation versus plastic flotation.
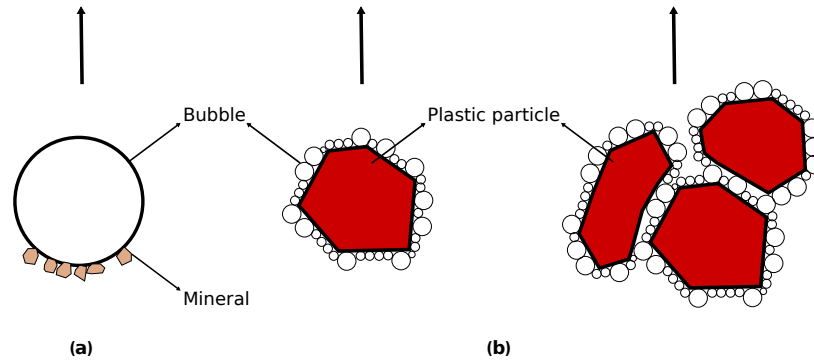

Figure 4.11: Representation of the typical configurations of bubble-particle aggregates in (a) ore flotation and (b) plastic flotation (Adapted from Fraunholcz, 1997).

Furthermore, considering that most plastic particles have a low density compared to minerals, such as quartz (ρ_p = 2650 kg/m^3), the particle size limit for flotation lies at higher values for plastic flotation. Ultimately, it is the density of the bubble-particle aggregate ρ_a that determines whether the solid particle will be floated. In general, the bubble-particle aggregate will float given that ρ_a is strictly lower than the flotation medium. The density of the bubble-particle aggregate ρ_a depends on the size distribution of the attaching bubbles, the fraction of the particle surface covered by bubbles, the specific surface area of the particle, the particle density and the particle size. Assuming that the bubbles are uniform in volume, the density of the bubble-particle aggregate is determined by:

$$\rho_a = \frac{\rho_p \, V_p}{V_p + N \, V_{bu}} \tag{4.67}$$

where V_{bu} is the bubble volume and N is the number of bubbles attached to the particle surface given by:

$$N = K \, \frac{A_p}{A_o} \tag{4.68}$$

where K is the bubble coverage percentage of the particle surface, A_p the surface area of the particle and A_o the surface area of the particle occupied by a single bubble. The coverage percentage K is related to the surface chemical properties of the particle. More specifically, K will increase with the contact angle θ of the particle or in other words with the hydrophobicity of the particle. Note that the surface area of the particle A_p strongly depends on its shape. Therefore, Equation 4.23 for the sphericity Φ of a particle can be rearranged to derive an expression for A_p:

$$A_p = \frac{\pi \, d_p^2}{\Phi} \tag{4.69}$$

where d_p is defined by Equation 4.22 and represents the volume-equivalent sphere diameter. From the assumption that a bubble forms a hemisphere of equal volume when attached to a particle, the occupied area of the particle surface by a bubble is given by:

$$A_o = \frac{\pi}{4} \, d_o^2 = \frac{\pi}{4} \left(\sqrt[3]{2} d_{bu} \right)^2 \tag{4.70}$$

where d_o is the hemisphere diameter and d_{bu} the bubble diameter. Substitution of Equation 4.69 and 4.70 into Equation 4.68 yields:

$$N = \frac{4\,K\,d_p^2}{\Phi\,\left(\sqrt[3]{2}d_{bu}\right)^2} \tag{4.71}$$

Considering that the volume of sphere can be determined by $\frac{1}{6}\,\pi\,d^3$, substituting Equation 4.71 into Equation 4.67 results in:

$$\rho_a = \frac{1.59\,\Phi\,\rho_p\,d_p}{1.59\,\Phi\,d_p + 4\,K\,d_{bu}} \tag{4.72}$$

Interestingly, Equation 4.72 predicts that irregular particles (i.e. $\Phi < 1$) will exhibit a higher floatability than spherical particles. In addition, it can be deduced that floatability will decrease with particle size and that a decrease in bubble coverage percentage K, for instance by applying wetting agents, will lower the floatability as a consequence to the increase in ρ_a. These findings were experimentally confirmed by Fraunholcz (1997); Shen *et al.* (2001) and Pita and Castilho (2017).

4.4.2 Gamma flotation

Adding to the description of (Young's) contact angle θ in Subsection 4.1.2 by means of Equation 4.1, the definition of the critical surface tension γ_c is introduced. Given that the relation between $cos\,\theta$ and γ_{lv} is approximately linear, the critical surface tension for wetting γ_c is defined by the intercept of the horizontal line $cos\,\theta = 1$ with the extrapolated line that describes the relation of $cos\,\theta$ versus γ_{lv}. Furthermore, if a sufficient difference in γ_c exists between two hydrophobic materials, selective wetting can be realised by reducing γ_{lv}. In particular, at appropriate values of γ_{lv}, bubble-particle attachment will occur for the solids with the lowest γ_c, while the other particles will be sufficiently wetted to suppress bubble attachment during flotation. This method is called *gamma flotation*.

Another interpretation of gamma flotation states that it is the only method of flotation that does not involve chemical or physical conditioning. In that regard, gamma flotation is solely applicable when the intrinsic floatability of the materials to be separated are significantly different and appropriate for the desired separation. The remainder of this section describes the used methodology to explore and develop gamma flotation techniques that -by definition- do not require a conditioning step to effectuate the separation of microplastic particles from a sediment mixture.

4.4.3 Explorative experiments

In a first stage, three different types of flotation installations were explored to gain insight into the behaviour of microplastic particles in a sediment mixture when exposed to different bubble generation systems. In addition, the techniques were evaluated on their microplastic recovery rate and their ability to process feed mixtures of sediment and microplastic particles. The conducted preliminary experiments involved colored, virgin PET and LDPE pellets of approximately 2 mm in diameter (Table 4.6). Commercial sand was acquired from a local construction firm with a particle size distribution between 2 µm and 2 mm.

4.4.3.1 Mechanical flotation cell

A mechanically agitated flotation cell as depicted in Figure 4.12 introduces air bubbles to the system from the base of its agitator by the shearing action of the impellers. These impellers rotate at high speed and cause mechanical mixing of the feed material, which is typically introduced near the top of the flotation cell.

Table 4.6: Overview of the polymers used in the explorative experiments containing information about the purchased pellets and the corresponding supplier.

Polymer type	Pellets	Supplier
PET	Lighter C93	Prospector
LDPE	310E	Dow

Floated particles accumulate in a froth layer at the surface of the fluid and leave the system as concentrate by means of overflow or mechanical action.
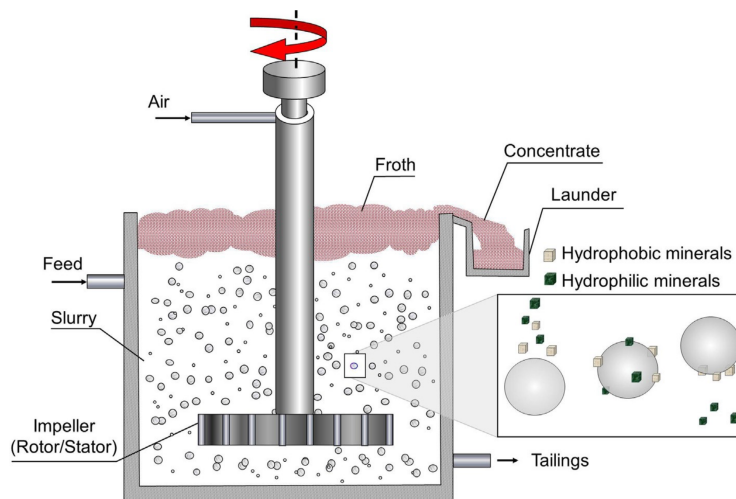

Figure 4.12: Representation of a mechanical flotation cell used in the mineral industry as common froth flotation technique (Wills and Finch, 2016).

Firstly, 50 microplastic particles (i.e. 25 PET and 25 LDPE particles) were added to a cylindrical container of 10 L. After filling the container with tap water, the mechanical agitator was set in position and the flotation process was initiated. Observations related to the flotation behaviour of the plastic particles and to the overall separation performance were documented for a time period of 10 minutes. Secondly, 50 g of sediment was added to a similar microplastic mixture of 50 particles before being fed to the system in a subsequent iteration. Similarly, observations were reported for 10 minutes and additionally analyzed for the behaviour of sediment particles. Both iterations were repeated 3 times.

4.4.3.2 Pneumatic flotation column

A pneumatic flotation column makes use of an air sparger, such as the disc diffuser applied here, to generate bubbles at the bottom of the column. The feed is added at the top, which creates a counter-current flow of the feed moving towards the bottom and the bubbles moving upwards. Consequently, mixing action is provided and bubble-particle contact is promoted. The floated particles are collected from the surface as a froth, similar to the mechanism in flotation cells. A schematic representation of a pneumatic flotation column is given in Figure 4.13.

The experiments were performed analogously to those described for the mechanical flotation cell. However, in this case the air flow rate to the sparger could be controlled manually. Therefore, each iteration included three repetitions at low, intermediate and high air flow rate, respectively.
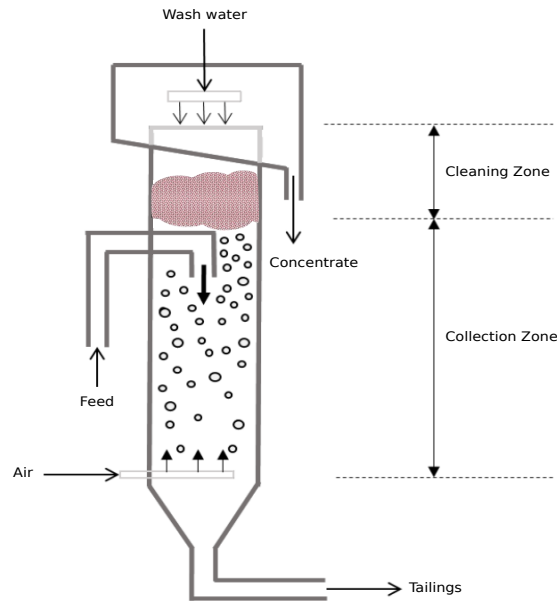
Figure 4.13: Representation of a pneumatic flotation column commonly used for industrial applications (Adapted from Coterio *et al.*, 2016).

4.4.3.3   Dissolved air flotation

Dissolved air flotation or DAF uses saturated water to introduce micro-bubbles into the system. More specifically, air is pressurized to dissolve into water until saturation is reached. Afterwards, the water is pumped through a depressurizing valve, which leads to the generation of micro-sized air bubbles, typically between 20 and 100 μm in diameter. Similar to the two previously discussed flotation techniques, the particles to be separated accumulate in a froth layer at the surface, which is mechanically removed or collected by means of overflow.

The explorative experiments regarding the DAF installation did not include the introduction of sediment. This was primarily due to the unsatisfying results from the iterations with solely microplastic particles. Moreover, two additional iterations that evaluated the separation performance of the two types of plastic separately were conducted. The operated DAF installation holds three small tanks with a volume of 2 L each. This allowed to perform multiple experiments simultaneously.

4.4.4   Design proposal of a flotation column

Based on the results of the explorative experiments and the encountered difficulties, a novel design of a flotation column is proposed with the aim to develop an efficient and versatile separation technique for the removal of microplastic particles from sediment mixtures. In particular, dredged sediment mixtures are considered as target feed. First, the general concept of the design and the main source of inspiration is presented. Afterwards, the used methodology to derive graphical simulations in order to predict the flow behaviour and adjust the flotation design is explained. Subsequently, the experimental setup is discussed and illustrated, followed by a description of the performed experiments.

4.4.4.1   Concept

The conceptual design of the novel flotation column proposed in this thesis is primarily based on a recent innovation realized in the mineral industry, namely the development of the cyclonic-static microbubble

flotation column (FCSMC) (Liu, 2002). This type of flotation includes a column flotation section, a cyclone separation section and a micro-bubble generator. In the column flotation section, particles with a high floatability are immediately captured by rising bubbles and leave the system at the top as concentrate. The particles that reach the cyclone separation section are subjected to a strong and intense swirling current where the most hydrophilic and dense particles are forced out the system under the influence of a centrifugal field. The middlings are subsequently pumped into a pipe section where the micro-bubble generator is located. Strong turbulent regime in the pipe section increases the probability of collision P_c (Equation 4.64) and improves the separation of hydrophobic particles with poor floatability, which are afterwards recycled to the system. The latter three-phase flow enters the system tangentially at the transition of the column flotation section to the cyclone separation section and is responsible for the generation of the cyclone vortex. At this intersection an inverted cone is provided to further increase the development of the vortex. This FCSMC-concept is illustrated in Figure 4.14 and shapes the main idea behind the proposed design. The latter with the objective to capture all microplastic particles in the overflow, while removing sediment particles via the discharge at the bottom of the installation.
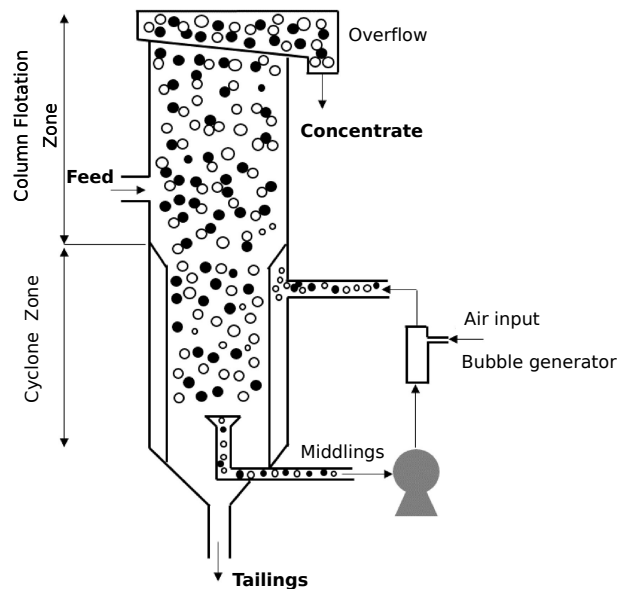
Figure 4.14: Representation of a traditional FCSMC installation used in the mineral industry. In -and outlet streams are highlighted in bold (Adapted from Li *et al.*, 2016).

In order to achieve this objective, several adjustments to a traditional FCSMC installation have been implemented, which will be discussed in more detail during the description of the experimental setup. The most prominent adaptation involves the option to add sieve plates in the column section in combination with two venturi spargers that provide bubbles to the system. The selected venturi system is able to provide air bubbles over a broader size range and particularly of larger bubble diameter in comparison with traditional micro-bubble generators. This is required to separate the larger sized microplastic particles compared to the minerals considered in the design of the original FCSMC. The selected configuration of the sieve plates allows to homogenously distribute the rising bubbles over the cross-section of the column and to make a secondary selection in the operating bubble size. Furthermore, the vertical position of the suction point of the recycle flow is made adjustable to increase flexibility and to experimentally determine the most favorable conditions.

4.4.4.2 Simulations

To gain insight into the flow behaviour of the multiple considered flotation designs, various computer simulations were made. This was done by means of the graphical tools integrated in the software package of Siemens NX. An important aspect concerning the design of the flotation column involved the tangential inlet of the recycled stream at the intersection of the column flotation section to the cyclone separation section. Simulations were performed to examine the effect of different inlet configurations, in particular the number of tangential inlet flows, by considering water as medium with a corresponding inlet flow rate of 1.2 m³/h. Furthermore, changes in the height of the column flotation section were virtually analyzed regarding the flow behaviour. Therefore, a rudimental blueprint for the construction of the first prototype of the novel flotation installation was created by means of Siemens NX.

4.4.4.3 Experimental setup

After three rudimental evaluations during the construction process of the installation, the finished prototype of the novel flotation column was obtained. The result is depicted in Figure 4.15. The body of the installation is composed of transparent polymethylmethacrylate (PMMA), typically known by the trade name Plexiglas. Despite the risk of microplastic contamination, it holds the essential ability to observe the behaviour of the flotation process in operation and allows relatively flexible manipulations during the construction phase compared to transparent glass. The circulation pipes are made from stainless steel AISI 316 and hold two venturi spargers. The venturis act as hydrodynamic cavitation devices to generate bubbles with good control of bubble size. In general, a venturi contains a convergent zone that increases the velocity of the passing stream due to the decrease in cross-sectional diameter, which reduces the pressure according to Bernoulli's principle. Therefore, air is drawn into the venturi via the gas inlet. After passage through the divergent zone of a venturi, the corresponding increase in pressure causes hydrodynamic cavitation, which results in instantaneous mixing and the supply of cavitation bubbles. This bubble generation mechanism can be controlled by adjusting the air pressure, the flow velocity of the passing stream and the geometry of the venturi sparger. The circulation pump that regulates the velocity of the recycled stream is a Maxima 180 PX (TIP) submersible pump capable of processing mixtures of water, plastic and sediment. The inlet of the recycle flow is realized by means of a reversed cone, whose vertical position is adjustable in the cyclone separation section. Further downstream, the recycled flow is split into two pipes that carry the venturi spargers before re-entering the flotation column tangentially at opposite side of each other. The air inlet of the venturis is provided with an LZB-6 Chenfeng flowmeter that measures and controls the air flow rate that enters the venturi. At present, the prototype installation does not contain a continuous feed system. Instead, the feed mixtures are dosed batchwise in the middle of the column flotation section. An overflow collects the floated particles from the top and an outlet valve at the bottom allows the discharge of settled particles.

Furthermore, the total height of the flotation column is 100 cm with a diameter of 10 cm. The column flotation section and the cyclone separation section are 80 and 20 cm, respectively. The feed mixture enters the system from a tube of 15 mm in diameter at 40 cm from the top. Both tangential inlets have a diameter of 28 mm and enter the flotation column at 40 cm from its bottom. In addition, the flotation column holds an iron bar at its centre to fixate the sieve plate mentioned above. The configuration of the corresponding sieve plate (Figure 4.16) was created with the AutoCAD 2019 software package and costructed from a 5 mm thick PMMA sheet by means of laser cutting. It contains pore sizes of 4 to 8 mm. The entire installation is anchored to a wall to ensure sufficient stability during operation and a hoisting mechanism is set up to facilitate maintenance and structural adjustments.

Figure 4.15: Images of the constructed flotation installation with clarifying information about the different components (left), and illustration of the different flows (right).

4.4.4.4 Analysis of separation efficiency

To evaluate the separation performance of the novel flotation design, six commonly produced polymer types (Table 2.1) were considered. Three polymer types with an average density lower than the density of seawater ($\pm$ 1025 kg/m^3) were selected (PP, LDPE and HDPE) and three polymer types with an average density strictly higher than the density of seawater (PET, PC and PS). The experiments were performed on spherical microplastic particles, which is assumed to be a conservative approach considering that the shape of microplastic particles can significantly deviate from spheres (Subsection 2.2.2) and that an increase in floatability is expected for non-spherical particles (Equation 4.72). More information about the used spherical pellets is provided in Table 4.7. The corresponding densities of the pellets were determined by means of the Precisa Density Kit 350. Furthermore, natural sand with a particle diameter ranging between 2 µm and 5 mm was obtained from a specialized construction firm and in combination with water used as representative of marine sediment during the experiments. Therefore, the natural sand was sieved in two fractions by means of an Endecott Sieve Shaker, namely a fraction smaller than 63 µm (i.e. sediment scenario 1) and a fraction between 63 µm and 2 mm (i.e. sediment scenario 2).

A first experimental phase involved the exploration of operational variables with the aim to pinpoint the most optimal conditions. The considered variables were the position of the recycle inlet $H_{recycle}$, the addition of a sieve plate and its corresponding position H_{sieve}, the number of active venturi spargers $N_{venturi}$ and the air flow rate Q_{air} at the gas inlet of the venturi. All possible combinations were visually evaluated based on the characteristics of the corresponding liquid-air medium in the flotation column, such as bubble concentration, bubble size, bubble dispersion, vortex behaviour and stability of flow. In addition, the visually most promising configurations were subjected to further analysis by adding microplastic particles to the
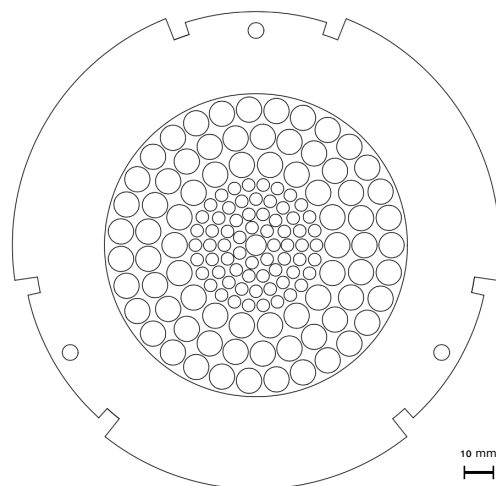
Figure 4.16: Representation of the sieve plate model created in the AutoCAD 2019 software environment. The corresponding sieve plate was constructed and implemented in the flotation installation proposed in this research.

Table 4.7: Overview of the polymers used in the experiments performed on the novel flotation installation containing information about the purchased pellets and the corresponding density, size range and supplier.

Polymer type	Pellets	ρ_p [kg/m^3]	d_p [mm]	Supplier
PP	6272NE1	898.6 ± 3.2	3.563 ± 0.200	Exxon Mobil
LDPE	LD150AC	920.4 ± 4.2	3.756 ± 0.231	Exxon Mobil
HDPE	25055E	935.2 ± 3.7	4.145 ± 0.028	Dow
PET	Lighter C93	1420.2 ± 15.2	2.661 ± 0.087	Prospector
PS	158K	1048.6 ± 6.9	3.471 ± 0.137	BASF
PC	Lexan PD3969	1181.2 ± 11.8	2.642 ± 0.185	Sabic

system. The PET particles (Table 4.7) were chosen considering their theoretically most difficult floatability potential (i.e. relatively lowest density and contact angle). The operational conditions that were associated with the highest microplastic recovery were selected as the optimal conditions of the flotation installation. These optimal conditions were kept constant for the following four experimental phases.

In a second phase, the recovery rates of the six polymer types described in Table 4.7 were determined separately and without the addition of sediment. To that end, 50 microplastic particles of the concerning polymer type were selected and subsequently introduced into the system. After 10 minutes of operation, the overflow was collected and sieved by means of a filter with 0.5 mm pore size. Afterwards, the retrieved microplastic particles were manually counted to determine the recovery rate. Each iteration was repeated five times and an average recovery rate per polymer type was calculated.

In a third phase, 25 g of sediment was added to 25 microplastic particles for sediment scenario 1, while 50 g of sediment was added to 50 microplastic particles for sediment scenario 2. Therefore, each iteration of a particular polymer type included two different runs to cover both sediment scenarios. Considering the expected results from the second phase with respect to the three polymer types with a density lower than the density of seawater (i.e. low-density microplastics), it was decided to only consider the polymer types with a density higher than the density of seawater (i.e. high-density microplastics) in the subsequent experimental phases, namely PET, PS and PC. After 10 minutes of operation, the overflow was collected and the microplastic particles were manually removed and counted. Subsequently, vacuum filtration was

performed on the residual overflow to quantify the mass of the entrained sediment. The applied cellulose filters (pore size = 5 µm) were dried in an oven at 100°C for 4 hours. Therefore, the recovery rate of microplastic particles and the mass percentage of sediment that escapes the system through the overflow instead of via the discharge at the bottom was determined. Each iteration was repeated three times and the corresponding averages were calculated.

In a fourth phase, the three polymer types PET, PS and PC were combined and equally added to form a feed mixture composed of 75 microplastic particles and 75 g of sediment for scenario 1, while the feed mixture of scenario 2 contained 150 microplastic particles and 150 g of sediment. Once the mixture was fed into the system, the flotation process was maintained in operation for 10 minutes. Afterwards, the overflow was collected and analogously analyzed for the recovery rate and sediment entrainment as explained in phase three. Similarly, the iteration was repeated three times for each scenario.

In a fifth and final phase, PET, PS and PC microplastic particles were analogously combined to form a feed mixture of different polymer types. However, these iterations involved a significantly lower microplastic concentration in the feed mixture to evaluate the applicability of the installation towards average microplastic concentrations of marine sediments worldwide. To that end, 10 microplastic particles of each polymer type were added to 300 g of sediment for scenario 1, while 20 microplastic particles of each polymer type were added to 600 g of sediment for scenario 2. This represents the global average concentration of microplastic particles in marine sediment (Subsection 2.2.4). Similarly, after 10 minutes of operation, the overflow was analyzed for the recovery rate and sediment entrainment. The iteration was repeated three times.

The operational variables applied during each phase are listed in Table 4.8. This table provides a concise overview of the performed experiments and highlights the differences between each iteration.

Table 4.8: Overview of the different experimental phases performed on the novel flotation installation with the microplastic recovery rate and/or the sediment entrainment as dependent variables, containing information about the involved polymer types, the addition of sediment, the number of performed iterations, the constant variables and the variables under consideration.

	Polymer type	Sediment	Iterations	Constant variables[a]	Considered variables
Phase 1	PET	N/A	N/A	N/A	$H_{recycle}$, H_{sieve}, Q_{air}, $N_{venturi}$
Phase 2	PP, LDPE, HDPE, PET, PS, PC	N/A	5 x 6	$H_{recycle}$ = -15 cm, H_{sieve} = 10 cm, Q_{air} = 0.3 m³/h, $N_{venturi}$ = 1	Polymer type
Phase 3	PET, PS, PC	2 scenarios	3 x 6	$H_{recycle}$ = -15 cm, H_{sieve} = 10 cm, Q_{air} = 0.3 m³/h, $N_{venturi}$ = 1	Polymer type, sediment scenarios
Phase 4	PET, PS, PC	2 scenarios	3 x 2	$H_{recycle}$ = -15 cm, H_{sieve} = 10 cm, Q_{air} = 0.3 m³/h, $N_{venturi}$ = 1	Polymer type interaction, sediment scenarios
Phase 5	PET, PS, PC	2 scenarios	3 x 2	$H_{recycle}$ = -15 cm, H_{sieve} = 10 cm, Q_{air} = 0.3 m³/h, $N_{venturi}$ = 1	Polymer concentration, sediment scenarios

[a] $H_{recycle}$ and H_{sieve} are expressed relative to the fixed horizontal plain where the recycle flow enters the flotation column

5

Results and discussion

5.1 Identification and characterisation of feed scenarios

5.1.1 Identification of feed scenarios

Analysis of North Sea sediments performed in 2000 revealed dominating sand size fractions, with 90 % of the samples containing less than 10 % mud (Table 4.1), and an overall mean particle size $d_p = 0.192$ mm $\pm$ 1.725 mm. The large standard deviation confirms the strong spatial variation in particle size distribution of sediments. Findings on river sediments indicated smaller size fractions. Sediment particles of the Scheldt were confined between 0.002 and 0.3 mm, with 90 % having a particle size smaller than 0.063 mm among the analyzed samples. Research on the Austrian section of the Danube revealed a mean particle size distribution of 15 % clay fraction, 70 % silt fraction and 15 % fine sand fraction. The particle size distribution of a particular section of the upper Mississippi was situated within the range 0.08 mm – 0.60 mm, where the upper end of the interval was associated with the most upstream section. For the Pearl River in China, the median particle size of the analyzed sediment samples also indicated small size fractions, namely between 0.0030 and 0.0344 mm. However, the sediment distribution in river estuaries is particularly complex. Gravel deposits are typically found upstream, sand fractions are dominant near the mouth of the river and mud fractions are often prominent in between. For the purpose of this thesis, the assumption is made that river sediments are generally characterized by prevailing mud fractions, while marine sediments are typically composed of mainly sand fractions.

Results of the analysis of dredged sediments worldwide suggest similar conclusions as deduced above. It appears that, in general, dredging operations can be divided into maintenance works and beach nourishments. The former is typically performed in harbours and rivers to ensure accessible transportation routes for maritime vessels. This involves deepening of important access channels and stabilization of dikes. Beach nourishments consist of sand suppletion along coastlines and on recreational beaches, where erosion causes a continuous loss of sand. To that end, sand is typically collected by a trailing suction hopper dredger (TSHD) from a donor site, preferably located near the suppletion site. The particle size distributions obtained from Jan De Nul and DEME indicate that dredged sediments extracted for maintenance works primarily consist of particles from the mud fraction, while the dredged sediments associated with beach nourishments mostly contain particles from the sand fraction.

Therefore, it was decided to consider two different feed mixtures regarding the particle size distribution of sediment. The first feed scenario contains sediment particles within the mud fraction (i.e. sediment

scenario 1), while the second feed scenario contains sediment particles related to the sand fraction (i.e. sediment scenario 2) (Table 4.1). No other differences concerning the feed composition are assumed between the scenarios.

5.1.2 Qualitative and quantitative characterisation of feed scenarios

Table 5.1 was constructed summarizing the physicochemical properties of the considered feed constituents. This information was used to make an informed selection with respect to the most promising separation techniques at the end of Chapter 2. The values of sphericity Φ provided in the table give an indication of the possible range associated with sediment and microplastic particles. It needs to be mentioned that the sphericity of sediment is correlated with its corresponding size fraction, as defined in Table 4.1, and with the time period over which the particles have been transported. For instance, the silt fraction in the North Sea primarily consists of quartz minerals that have been transported over a long distance, which increases the sphericity under the influence of erosion. Therefore, values of Φ are generally larger than 0.9. However, the clay fraction in the North Sea consists of clay minerals such as kaolinite, illite and montmorillonite, which are typically characterized by non-spherical shapes such as flakes. Consequently, Φ is mostly smaller than 0.7, with $\Phi = 0.3$ as a lower bound. When considering the sand fraction (as is the case in sediment scenario 2), average sphericities larger than 0.8 are common depending on the composition of the sediment. The sphericity range of microplastic particles provided in Table 5.1 is drawn from the performed sinking experiments described in Subsection 4.2.2.

Furthermore, it is clear that the density of sediment is generally greater than the density of (micro)plastic particles. Quartz is typically the most dominant natural mineral and therefore largely determines the average density of marine sediments, which as a consequence varies around 2650 kg/m^3. With respect to microplastics, PVC and PET particles appear to have the relatively largest density with a maximum value of 1700 and 1400 kg/m^3, respectively. The significant difference in density between the two main feed constituents explains why density is considered as an important separation factor in the selection of the most promising sediment remediation techniques for microplastics. From the contact angles presented in Table 5.1, it is stated that the average contact angle of marine sediment does not exceed 90°, considering that all discussed corresponding constituents hold a contact angle smaller than 60°. Consequently, marine sediment is determined as hydrophilic. Microplastics, on the other hand, show contact angles strictly greater than 60° with the maximum values of the individual polymer types mostly exceeding 90°. However, the range of possible contact angles of PET particles lies significantly below the value of 90°. Therefore, microplastic particles are considered as hydrophobic or at least less hydrophilic compared to sediment particles.

5.1.3 Conclusion

Four interesting conclusions regarding the physicochemical characteristics of the considered feed mixture can be derived from Table 5.1. Firstly, the particle size ranges of sediment and microplastic particles significantly overlap. Secondly, the average density of sediment is considerably greater than the different types of (micro)plastic particles. Thirdly, sediment is said to be hydrophilic, while microplastic particles appear to be hydrophobic or at least less hydrophilic compared to sediment. And lastly, it may be concluded that the average sphericity of sediment particles is typically greater in comparison to microplastic particles, although the latter particularly depends on the composition of the mixture.

Table 5.1: Overview of the feed constituents containing information about particle size, density, contact angle and sphericity. Characterization of the two different sediment scenarios considered in this research is included.

Feed constituent	Size range d_p [mm]		Density ρ_p [kg/m³]	Contact angle θ [°]	Sphericity Φ
	Scenario 1	Scenario 2			
SEDIMENT[a]					
Quartz			2650 – 2660	27 – 50	
Feldspar			2550 – 2760	20 – 40	
Calcite			2710 – 2711	27 – 53	
Aragonite			2940 – 2950	27 – 53	
Mica			2800 – 3100	17 – 46	
Kaolinite	< 0.063	0.063 – 2	2160 – 2680	17 – 28	0.3 – 1
Illite			2600 – 2900	29 – 43	
Montmorillonite			1700 – 2000	21 – 56	
Vermiculite			2400 – 2700	21 – 56	
Chlorite			2600 – 3300	20 – 50	
Organic matter			1100 ± 100	N/A	N/A
MICROPLASTICS[b]					
PP			890 – 920	90 – 117	
LDPE			910 – 930	78 – 104	
HDPE			930 – 970	78 – 104	
PVC			1200 – 1700	80 – 94	
PET	0.001 – 5	0.001 – 5	1300 – 1400	63 – 83	0.01 – 1
PS			1040 – 1100	73 – 91	
PA			1020 – 1150	61 – 96	
PC			1150 – 1250	73 – 88	
PUR			870 – 1420	67 – 89	

[a]Gathered from Curray and Griffiths (1955); El Fishawi (1984); Ethington (1990); Ro and Neethling (1991); Gaines *et al.* (1998); Shang *et al.* (2008); Borysenko *et al.* (2009); Ozdemir *et al.* (2009); Leggett (2012); Kowalczuk *et al.* (2017); Zheng and Zaoui (2017); Adriaens *et al.* (2018) and Deng *et al.* (2018a,b)

[b]Gathered from Angu *et al.* (2000); Mittal (2001, 2003); van Oss (2006); Andrady (2011) and Edmondson and Gilbert (2017)

5.2 Formation and effect of biofouling on plastics

5.2.1 Biofilm formation

Initially, no additional biomass was added to the biofouling tank holding the plastic sheets. However, after two months incubation it appeared that the volume of seawater in a controlled environment under the specified conditions was unable to induce biofilm formation. Therefore, extra biomass was added as described in Subsection 4.1.2. In one week, partial biofouling was observed and after another two months a mature biofilm developed on the surface of the plastic sheets and consumer products.

5.2.2 Effect on contact angle

Results of the contact angle measurements are summarized in Table 5.2. The values of the blanco polymer sheets are within the corresponding range suggested in literature and presented in Table 5.1, except for the blanco consumer products. Despite the fact that the consumer products are composed of PP, the contact angle measurements deviate from the expected PP interval. In general, the average contact angle of the consumer products is lower than the average contact angle of the extruded PP sheets. This observation is most likely due to the additives incorporated in the production of plastic products or to the post-production surface printing with different types of ink. For instance, to create the bright colours of the considered consumer products, colorants are added in the manufacturing process, which seem to affect the contact angle of the product. Other commonly used additives are mentioned in Subsection 2.1.1.

Table 5.2: Summary of the results of the bio-fouling experiments conducted in this research.

| Polymer type | Contact angle θ [°] | |
↳ *Consumer product*	**Blanco**	**Bio-fouled**
LDPE	90.0 ± 2.6	32.3 ± 2.3
HDPE	81.3 ± 2.7	31.8 ± 2.2
PVC	71.5 ± 2.7	31.2 ± 1.8
PET	73.3 ± 1.0	32.4 ± 2.9
PS	83.3 ± 1.1	33.3 ± 2.5
PP	96.1 ± 1.2	35.4 ± 2.7
↳ *Babybell cup*	84.8 ± 1.2	31.7 ± 2.3
↳ *Breakfast cereal clip*	73.0 ± 1.7	37.2 ± 3.9
↳ *Straw*	80.1 ± 2.4	33.5 ± 2.4
↳ *M&M cup*	83.3 ± 2.0	32.9 ± 1.6
↳ *Fork*	82.7 ± 1.0	35.5 ± 2.3
↳ *Storage cup*	81.5 ± 3.5	36.6 ± 3.1

Measurements of the bio-fouled plastic surfaces imply a consistent and significant drop in contact angle towards values of θ between 30 and 40°. It appears that the contact angle of bio-fouled plastic sheets is independent of the polymer type. Furthermore, addition of additives such as colorants seems to have little effect on the contact angle of bio-fouled consumer products. The uniform increase in standard deviation of the measurements for the bio-fouled samples is due to the increase in surface roughness as a consequence of biofilm formation. Elevated surface roughness is known to complicate measurements by means of a Drop Shape Analyzer 10 Mk2. In addition, it has been derived that increasing surface roughness will enhance wettability (Wenzel, 1936). Therefore, a hydrophilic surface will become more hydrophilic when surface roughness is added. Similarly, a hydrophobic surface becomes more hydrophobic with increasing surface roughness.

5.2.3 Effect on density

Figure 5.1 graphically summarizes the calculated predictions regarding the required thickness of a biofilm T_b on the surface of a floating microplastic particle to increase its density to where it matches the density of the surrounding seawater, which is assumed to be 1025 kg/m^3. As elaborated in Subsection 4.1.2, a distinction was made between two extreme shapes, namely a perfectly spherical microplastic particle and

a flattened cube with a fixed thickness of 40 μm. It appears that for spherical microplastic particles, the required biofilm thickness T_b increases linearly with the spherical diameter d_p. As can be seen from the left graph of Figure 5.1, this linear relation is approximated by $T_b = 0.88\,d_p$ with $R^2 > 0.99$. Therefore, a spherical microplastic particle with $\rho_p = 925$ kg/m^3 and $d_p = 20$ μm would require a biofilm thickness T_b of at least 18 μm to induce settling behaviour in seawater, while a similar particle with $d_p = 2.0$ mm would require a biofilm thickness T_b of at least 1.8 mm.
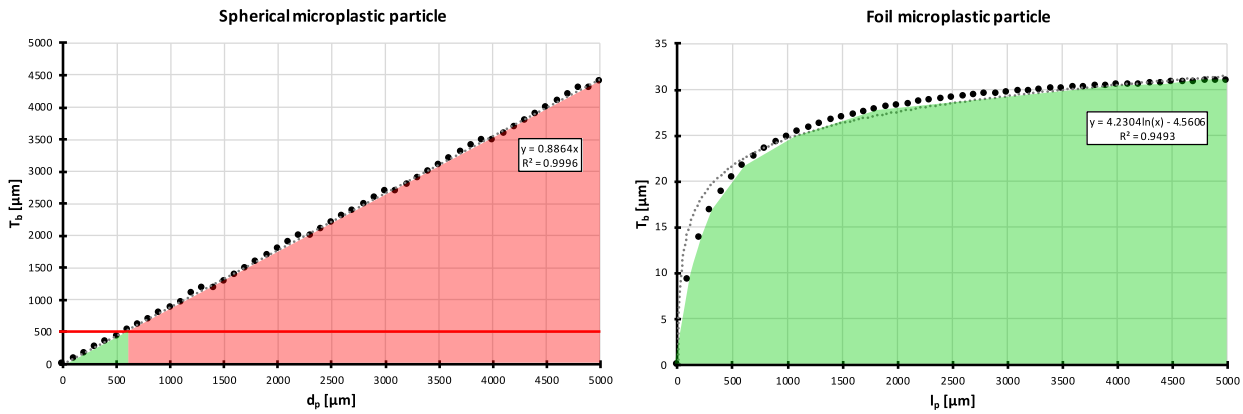

Figure 5.1: Graphical representation of the predicted biofilm thickness T_b required to increase the density of a microplastic particle with $\rho_p = 925$ kg/m^3 to match the density of seawater (i.e. 1025 kg/m^3). Two plots are provided with T_b versus d_p (i.e. particle diameter) for a spherical microplastic particle (left) and T_b versus l_p (i.e. flattened cube side) for a thin foil microplastic particle with a fixed thickness $h_p = 40$ μm (right). Biofilm thickness values that are assumed to be realistic are highlighted in green, while biofilm thickness values that are assumed to be unlikely to occur in the marine environment are highlighted in red.

From the right graph of Figure 5.1, it appears that for a thin foil particle with $h_p = 40$ μm and $\rho_p = 925$ kg/m^3, the required biofilm thickness T_b increases logarithmically with the side l_p of the flattened cube. In particular, considering the microplastic size range, it can be stated that a biofilm thickness $T_b = 35$ μm will induce settling behaviour of a foil microplastic particle, irrespective of the length of its sides l_p.

Furthermore, the average thickness of a marine biofilm is difficult to predict considering that it depends, among others, on medium composition, substrate nature, the present microbial strains and the physico-chemical properties of the surrounding seawater (Lehaitre *et al.*, 2008). For instance, the rate of biofouling is typically higher close to the shore and decreases with increasing depth, while temperature and seasonal changes significantly affect the composition of the corresponding biofilm. Moreover, the biofilm thickness is generally not homogenous. However, it is assumed that an average marine biofilm has a thickness ranging from roughly 1 to 500 μm, based on the findings of Lehaitre *et al.* (2008); Salta *et al.* (2013); Doghri *et al.* (2015); Li *et al.* (2015) and Inaba *et al.* (2017). This suggests that spherical microplastic particles with $\rho_p = 925$ kg/m^3 and a diameter d_p larger than approximately 600 μm are unlikely to reach an average bio-fouled density of 1025 kg/m^3 as a result of marine biofouling, which is illustrated by the red zone in Figure 5.1. On the other hand, it seems reasonable to assume that biofouling is able to increase the average bio-fouled density of floating foil microplastic particles to where it reaches the density of the surrounding seawater. The latter partly explains why more than 90 % of marine plastic litter accumulates on the seabed (Subsection 2.2.4) despite the fact that approximately 60 % of the total worldwide non-fibre plastic production is associated with polymer types having a density smaller than 1025 kg/m^3 (Subsection 2.1.2).

It needs to be mentioned that the predictions discussed above solely consider biofouling as possible cause to induce settling behaviour of floating microplastic particles. However, other processes such as the phenomenon of marine snow (Subsection 2.2.4) can explain the presence of microplastic particles with a density smaller than 1025 kg/m^3 on the bottom of the ocean. In addition, note that the green zone highlighted

in the left graph of Figure 5.1 seems nearly negligible relative to the red zone. However, considering that small microplastics (i.e. < 1 mm) are much more abundant than large microplastics in the marine environment, as elaborated in Subsection 2.2.4, the predicted amount of (perfectly) spherical microplastic particles that reach an average bio-fouled density of 1025 kg/m^3 due to biofouling is substantial.

5.2.4 Conclusion

The experimental observations suggest that the contact angle of materials vulnerable to bio-fouling in the marine environment will migrate from their initial value towards θ values between 30 and 40°. Furthermore, given biofilm formation on the surface of the object, this trend seems to be independent of material properties. Translated to (micro)plastic particles, this implies a shift from their generally hydrophobic state towards increasing hydrophilic behaviour. Thus, it closes the gap in polarity as well as in floatability differences between sediment and (micro)plastic particles highlighted in Table 5.1.

In addition, it may be concluded that biofouling is able to induce settling behaviour of common floating microplastic particles in the marine environment. In particular, thin foil microplastic particles, such as the ones originating from plastic bags, seem more likely to end up on the seabed given appropriate biofouling conditions compared to spherical microplastic particles. These spherical microplastic particles are unlikely to hold an average bio-fouled density greater than the density of seawater for diameters larger than approximately 600 μm.

5.3 Sinking behaviour of microplastic particles

5.3.1 Characterisation and impact of shape

A total of 140 microplastic particles, i.e. 20 particles for each of the 7 considered products, were physically characterized by mass m, density ρ_p, volume V_p, volume-equivalent spherical diameter d_p, volume-equivalent spherical surface area A_{sph}, particle surface area A_p, the three principal axes a, b and c, as well as by the shape descriptors Φ, χ, P, CSF, Ψ, φ, $\mathcal{F}$ and e. The precision of the laboratory balance was sufficient to measure the mass of the microplastic particles appropriately. However, the used Precisa Density Kit 350 required particles with greater mass, as described in Subsection 4.2.2. To illustrate, the standard deviation of the average density of the Dash bottle was 5.81 % for microplastic particles and 0.09 % for particles larger than 5 mm. Interestingly, the average density appeared nearly identical, which suggests a good accuracy of the measurements. Furthermore, by means of the determined terminal velocities $u_{t,meas}$ and Equation 4.14, the corresponding drag coefficients $C_{D,meas}$ were calculated. The latter allows a more meaningful comparison between the products considering that the sinking experiments were performed in different media. Table 5.3 provides a concise overview of the general results of the experiments, while Table 5.4 summarizes the shape characterization of the considered microplastic particles by means of the discussed shape descriptors. The post-processed 2D-images captured by means of the Keyence VHX-500FE Digital Microscope are depicted in Appendix Figure A.1 to Figure A.7.

From Table 5.3, it is clear that the standard deviations of the densities associated with the two foil products (i.e. Jupiler shrink wrap and Lotus Speculoos package) are significantly higher in comparison with the other products. This is most likely due to two main reasons. Firstly, stretching of packaging foil is common practice, which alters the density of the foil at certain areas. Secondly, the precision of the density measurements was lower for the foil products. The latter is a consequence of the relatively low mass of the

Table 5.3: Summary of the results of the sinking experiments conducted in this research containing information about the characterization of the considered microplastic particles. Intervals indicate the minimum and maximum observed values, respectively, of the particles associated with a particular plastic product.

Product	m [mg]	ρ_p [kg/m^3]	d_p [mm]	$u_{t,meas}$ [mm/s]	$C_{D,meas}$ [-]
Coca Cola	$0.71 - 15.67$	1370 ± 1.51	$1.00 - 2.80$	$18.4 - 104.7$	$1.20 - 14.19$
Dash stralend wit	$1.94 - 21.05$	952 ± 0.85	$1.57 - 3.48$	$23.6 - 47.8$	$3.08 - 7.60$
Flowerpot brown	$2.12 - 8.92$	953 ± 1.18	$1.62 - 2.61$	$26.1 - 44.3$	$3.10 - 7.88$
Mushroom container	$1.09 - 5.30$	1054 ± 1.81	$1.25 - 2.13$	$5.1 - 16.4$	$4.61 - 35.27$
Jupiler shrink wrap	$0.21 - 3.76$	950 ± 20.18	$0.76 - 1.98$	$7.0 - 19.9$	$12.56 - 45.05$
Lotus Speculoos package	$0.13 - 1.63$	1013 ± 15.70	$0.63 - 1.45$	$4.5 - 9.1$	$54.89 - 117.62$
PVC-pipe	$0.20 - 3.11$	1432 ± 0.63	$0.64 - 1.61$	$8.0 - 24.8$	$10.51 - 75.08$

foil particles used for the density measurements due to practical considerations. For instance, a thin foil such as Jupiler shrink wrap or Lotus Speculoos package with a mass of 0.1 g (i.e. the recommended lower boundary; Subsection 4.2.2) occupies a volume that is too large to appropriately process with the Precisa Density Kit 350.

Furthermore, from Table 5.4 it is apparent that the microplastic fibres (i.e. PVC-pipe particles) considered in the dataset are characterized by a particularly high value of the circularity χ (namely 85 % of the fibres have $\chi > 3$), while the corresponding values of the common shape descriptor sphericity Φ are comparable to the intervals of the non-fibre microplastic particles. The Powers Index P and the elongation e seem to successfully account for the prominent shape of fibres as well, yet considerably less profound compared to the circularity χ. Therefore, it is concluded that a measure of circularity seems an added value to differentiate and quantify the shapes of microplastic particles adequately.

Table 5.4: Summary of the shape characterization of the considered microplastic particles by means of the dimensionless shape descriptors discussed in this research. Intervals indicate the minimum and maximum observed values, respectively, of the particles associated with a particular plastic product.

Product[a]	CSF	P	Φ	χ	φ	$\mathcal{F}$	e
CC	$0.071 - 0.832$	$1.32 - 3.00$	$0.22 - 0.97$	$1.130 - 1.890$	$0.21 - 0.89$	$0.092 - 0.879$	$0.336 - 0.961$
DSW	$0.110 - 0.364$	$1.26 - 2.28$	$0.43 - 0.87$	$1.274 - 1.815$	$0.18 - 0.54$	$0.155 - 0.621$	$0.284 - 0.939$
FPB	$0.120 - 0.271$	$1.20 - 4.68$	$0.43 - 0.90$	$1.227 - 1.852$	$0.22 - 0.55$	$0.144 - 0.477$	$0.311 - 0.897$
MC	$0.042 - 0.113$	$1.14 - 2.88$	$0.23 - 0.47$	$1.130 - 2.222$	$0.17 - 0.46$	$0.052 - 0.179$	$0.290 - 0.870$
JSW	$0.012 - 0.048$	$1.08 - 2.10$	$0.10 - 0.28$	$1.250 - 2.146$	$0.12 - 0.45$	$0.015 - 0.069$	$0.233 - 0.0872$
LSP	$0.004 - 0.061$	$1.08 - 2.82$	$0.04 - 0.14$	$1.163 - 2.174$	$0.14 - 0.41$	$0.006 - 0.120$	$0.261 - 0.818$
PVC-P	$0.021 - 0.162$	$0.42 - 1.38$	$0.16 - 0.58$	$1.761 - 14.286$	$0.02 - 0.20$	$0.075 - 0.733$	$0.030 - 0.341$

[a]CC = Coca Cola; DSW = Dash stralend wit; FPB = Flowerpot brown; MC = Mushroom container; JSW = Jupiler shrink wrap; LSP = Lotus Speculoos package; PVC-P = PVC pipe

From the standard drag curve given in Figure 5.2 it appears that the drag coefficient C_D is larger for irregular particles than for spherical particles at all considered values of Re_p. This in turn translates to a higher drag force F_D (Equation 4.12) and a decrease in terminal velocity u_t (Equation 4.15). To illustrate, the shape descriptors for the Lotus Speculoos package particles indicate a strong deviation from perfect spherical shapes, in particularly the values of the most frequently applied shape descriptor Φ ($0.04 - 0.14$;

Table 5.4), while these particles are associated with the highest measured values of the drag coefficient. These observations align with the intuitive perception that non-spherical particles experience an elevated resistance in comparison with spherical particles when falling in an identical medium. In addition, the results suggest that foil particles carry the highest drag coefficient of all considered microplastic particles, namely 80 % of the Jupiler shrink wrap and Lotus Speculoos package particles have a drag coefficient $C_{D,meas} > 30.00$, while 97 % of the non-foil particles have a $C_{D,meas} < 30.00$ over a particle Reynolds number range from 1 to 300. However, it needs to be recognized that a comparison of the drag coefficients of different particle shapes is generally only meaningful for identical values of the particle Reynolds number, considering that C_D is a function of Re_p. For that reason, particle Reynolds numbers greater than 10^4 are typically chosen for this type of comparison, considering that the drag coefficient takes on a constant value that is characteristic of a particular particle shape for high values of Re_p, as can be seen from Figure 4.5 in Subsection 4.2.1.
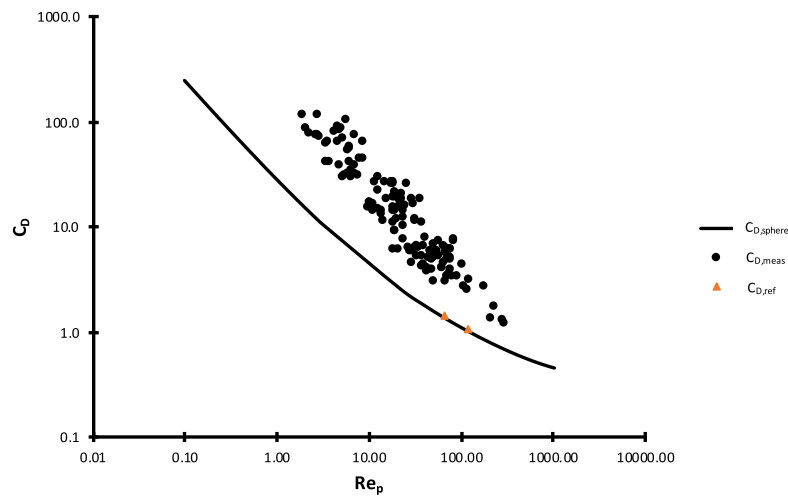

Figure 5.2: Log-log plot of C_D versus Re_p to illustrate the measured drag coefficients of the dataset established in this research $C_{D,meas}$ (black dots) in comparison to the standard drag curve for a sphere $C_{D,sphere}$ defined by Haider and Levenspiel (1989) (solid black line). In addition, the drag coefficient of the reference spheres used for validation $C_{D,ref}$ are depicted (orange triangles).

5.3.2 Validation of sinking experiments

The average measured sinking velocity of the reference PS spheres in water was 31.0 ± 3 mm/s and of the reference PP spheres in disolol 68 ± 8 mm/s. By means of the chosen reference law for spheres derived by Dietrich (1982) and given by Equation 4.43, theoretical sinking velocities of 29.7 and 63.7 mm/s, respectively, were calculated. The theoretical values do not deviate more than 1 times the standard deviation of the average measured sinking velocity. Therefore, it is concluded that the applied methodology to measure the sinking velocity is valid and that the results obtained during the sinking experiments are reliable. In addition, from the values of the drag coefficient for the reference spheres $C_{D,ref}$ illustrated in Figure 5.2, it is further verified that the drag coefficient increases for non-spherical particles.

Furthermore, the more popular reference law for spheres, namely Stokes' law (Equation 4.18), was calculated to validate the findings by Gregory (2006), elaborated at the end of Subsection 4.2.2, who stated that Stokes' law does not apply to particles larger than 200 μm in an aqueous medium. Results show that Stokes' law overestimates the measured settling velocity of the reference PS spheres by a factor of 4 and of the reference PP spheres by a factor of 5. This partly confirms the work by Gregory (2006) who claimed that an overestimation by a factor of 10 or more was to be expected.

5.3.3 Evaluation of drag models

The drag coefficients given by each of the shape-dependent drag laws presented in Subsection 4.2.1 were calculated for the 140 different irregular microplastic particles. Therefore, the applied shape descriptors summarized in Table 4.3 and the particle Reynolds number were determined beforehand. The measured particle Reynolds number Re_p of the established dataset ranged from 1 to 300, which corresponds to the non-laminar flow region. The latter is important considering that particle shape affects the terminal settling velocity in the laminar region only marginally (Subsection 4.2.1). This statement explains the similar trend of standard drag curves in the laminar region when comparing different drag models. In addition, the initial particle orientation is expected to significantly affect the terminal settling velocity of particles in the laminar region, while in the non-laminar region only one orientation is assumed to be stable, as elaborated at the end of Subsection 4.2.1. As a result, the initial orientation of a microplastic particle during the sinking experiments is assumed to have no effect on the terminal settling velocity. Thus, it is generally more appropriate to evaluate shape-dependent drag laws for $Re_p > 1$ compared to $Re_p \leq 1$. Once the theoretical terminal settling velocities $u_{t,calc}$ of all microplastic particles were derived from their corresponding calculated drag coefficients for each drag model separately by means of Equation 4.15, Table 5.5 was constructed in order to compare the average error and the RMSE given by Equation 4.45 and 4.46, respectively.

Table 5.5: Summary of the results used to compare the shape-dependent drag laws discussed in this research.

Author(s) drag law	Average error [%][a]	RMSE
Dietrich (1982)[b]	19.43	28.46
Haider and Levenspiel (1989)	60.53	67.41
Swamee and Ojha (1991)	34.08	46.28
Ganser (1993)	20.11	25.75
Dellino *et al.* (2005)	23.88	30.61
Pfeiffer *et al.* (2005)	48.46	59.78
Camenen (2007)	29.09	33.04
Dioguardi and Mele (2015)	46.90	50.93
Bagheri and Bonadonna (2016)	21.89	27.35
Dioguardi *et al.* (2018)	13.20	19.09

[a]All averages are statistically different from each other (df = 139, p < 0.001)
[b]The corresponding drag model was merely applicable to 30 % of the data

A first remark regarding Table 5.5 concerns the shape-dependent drag law proposed by Dietrich (1982) and given by Equation 4.25. Considering that the parameter R_2 in that particular equation only yields a real value (as opposed to an imaginary or complex value) for CSF values larger than 0.15 and that 98 from the 140 microplastic particles in the dataset hold a CSF value smaller than 0.15, the drag law of Dietrich (1982) fails to adequately describe the sinking behaviour of the considered particles. It is stated that the expression of Dietrich (1982) predicts the drag coefficient of particles appropriately given a CSF value ≥ 0.30, hence not for extreme flattening.

Secondly, it can be seen that the drag law proposed by Dioguardi *et al.* (2018) best fits the data. The average error of 13.20 % indicates that on average the deviation of the theoretical settling velocity predicted by the drag model equals 13.20 % of the measured settling velocity. The RMSE is an absolute measure of fit of the corresponding model to the applied dataset that indicates the standard deviation of the unexplained variance. As a consequence, a low value of RMSE corresponds to a good fit. Therefore, it can be concluded

that the drag model of Dioguardi *et al.* (2018) describes the sinking behaviour of the considered microplastic particles better than the other evaluated drag models. Consequently, the corresponding applied shape factor Ψ defined by Equation 4.31 that takes into account both the sphericity Φ and the circularity χ appears to be an interesting measure to quantify the shape of microplastic particles. The latter statement aligns with the conclusions of Subsection 5.3.1.

To illustrate, the stepwise calculation process to derive the calculated settling velocity $u_{t,calc}$ proposed by Dioguardi *et al.* (2018) of two different microplastic particles is provided. A first considered particle originates from a Dash bottle and holds a mass of 3.02 mg and a density of 952 kg/m^3, which dictates a volume of 3.17 mm^3. Applying Equation 4.22 results in a volume-equivalent spherical diameter d_p of 1.82 mm. Consequently, the surface area of the volume-equivalent sphere A_{sph} equals 10.4 mm^2. The corresponding post-processed 2D-image captured by means of a digital microscope and analyzed by means of the image analysis software ImageJ is given by Figure 5.3 on the left-hand side. From this 2D-analysis and a measure of the third dimension provided by means of a digimatic indicator as described in Subsection 4.2.2, the three principal axes of the particle are obtained, namely $a = 3.533$ mm, $b = 2.361$ mm and $c = 0.832$ mm. These parameters are used to estimate the surface area of the microplastic particle A_p by applying Equation 4.32 derived by Dellino *et al.* (2005):

$$A_p = 4\,\pi \left[\frac{\left(\frac{3.533}{2}\right)^{1.6075} \left(\frac{2.361}{2}\right)^{1.6075} + \left(\frac{3.533}{2}\right)^{1.6075} \left(\frac{0.832}{2}\right)^{1.6075} + \left(\frac{2.361}{2}\right)^{1.6075} \left(\frac{0.832}{2}\right)^{1.6075}}{3} \right]^{\frac{1}{1.6075}}$$

which equals 15.5 mm^2. Dividing A_{sph} by A_p yields an approximation for the sphericity Φ according to Equation 4.23. Thus, the sphericity Φ for the considered microplastic particle equals $\frac{10.4}{15.5} = 0.67$. Based on the 2D-analysis with ImageJ, a measure of circularity is provided. However, as explained in Subsection 4.2.2, this measure is equal to the inverse of the commonly applied definition of circularity given by Equation 4.24. Therefore, the circularity χ of the microplastic particle becomes $0.701^{-1} = 1.427$. Afterwards, the shape descriptor Ψ applied by Dioguardi *et al.* (2018) in the corresponding drag model can be calculated by Equation 4.31 as follows:

$$\Psi = \frac{\Phi}{\chi} = \frac{0.67}{1.427}$$

which equals 0.47. Subsequently, the particle Reynolds number is calculated by means of the iterative algorithm provided in Appendix Table A.4 for the input values of $d_p = 1.82$ mm, $\rho_p = 952$ kg/m^3, $\Psi = 0.47$, $\rho_f = 790$ kg/m^3, $\mu = 1.223 \times 10^{-3}$ Pa s and $Re_{start} = 1$, considering that all microplastic particles originating from Dash bottles were used in combination with disolol as operating medium. As a result, the particle Reynolds number is determined as 42.36. Consequently, the drag model proposed by Dioguardi *et al.* (2018) and given by Equation 4.38 can be calculated as follows:

$$C_{D,calc} = \frac{24}{42.36} \left(\frac{1 - 0.47}{42.36} + 1 \right)^{0.25} + \frac{24}{42.36} \left(0.1806\,42.36^{0.6459} \right) 0.47^{-42.36^{0.08}} + \frac{0.4251}{1 + \frac{6880.95}{42.36}\,0.47^{5.05}}$$

which equals a drag coefficient of 3.81. By applying Equation 4.15, the corresponding value of the terminal settling velocity $u_{t,calc}$ can be derived:

$$u_{t,calc} = \sqrt{\frac{4}{3} \frac{d_p\,g}{C_D} \frac{|\rho_p - \rho_f|}{\rho_f}} = \sqrt{\frac{4}{3} \frac{1.82 \times 9.81}{3.81} \frac{|952 - 790|}{790}}$$

which equals 35.8 mm/s. Considering that the measured terminal settling velocity $u_{t,meas}$ of this microplastic particle appeared to be 36.0 mm/s, the corresponding drag model seems to perform very well for this particular particle.
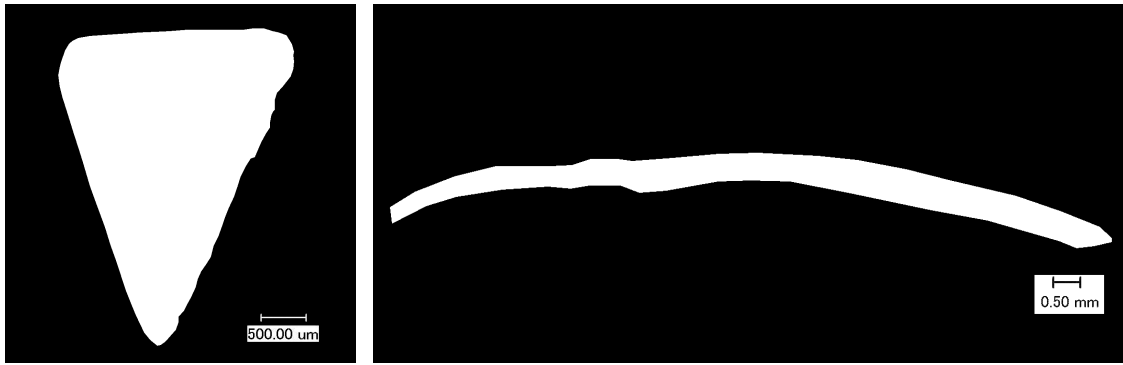
Figure 5.3: Post-processed 2D-images captured by means of the Keyence VHX-500FE Digital Microscope and edited by the image analysis software ImageJ of a microplastic particle originating from a Dash bottle (left) and a microplastic particle originating from a PVP-pipe (right).

A second considered microplastic particle is depicted on the right-hand side of Figure 5.3 and concerns a fibre originating from a PVC-pipe holding a particle mass of 0.94 mg and a density of 1432 kg/m^3. Analogous to the previously described calculations, the following variables are derived: d_p = 1.08 mm, a = 13.34 mm, b = 0.64 mm, c = 0.132 mm, A_{sph} = 3.65 mm^2, A_p = 14.2 mm^2, Φ = 0.26 , χ = 8.333 and Ψ = 0.03. Similarly, the particle Reynolds number is derived by means of the constructed Matlab function for the corresponding input values with ρ_f = 1000 kg/m^3 and μ = 9.780 × 10^{-4} Pa s, considering that all microplastic particles originating from PVC-pipes were used in combination with deionized water as operating medium. As a result, a particle Reynolds number of 19.60 is obtained. Thus, by applying Equation 4.38 accordingly, a drag coefficient of 126.38 is calculated, which translates to a terminal settling velocity $u_{t,calc}$ equal to 6.9 mm/s by using Equation 4.15. However, the measured terminal settling velocity appeared to be 17.8 mm/s, which indicates that the corresponding drag law significantly underestimates (i.e. by a factor of 2.6) the terminal velocity of this particular particle.

By applying this approach, the terminal settling velocities of all 140 considered microplastic particles were calculated for each drag model presented in Table 5.5 separately, including the corresponding average error and RMSE values elaborated above. In addition, scatterplots of $u_{t,calc}$ versus $u_{t,meas}$ of the discussed drag models were generated. To illustrate, the scatterplots of the two drag laws that best fit the entire dataset according to Table 5.5 are given in Figure 5.4. Note that the depicted trendlines are constructed by means of linear regression and are forced through the origin by specifying the point where x = 0 and y = 0 as intersection. As a consequence, the corresponding equations are of the type $y = ax$. Therefore, the performance of the drag model can be evaluated based on the ability to reproduce the measured terminal velocities, rather than solely from the correlation coefficient R^2. In that regard, the best possible fit is associated with R^2 approximating a value of 1 and a trendline equation given by $y = x$. From Figure 5.4, the drag law by Dioguardi *et al.* (2018) shows a high correlation coefficient (R^2 = 0.96) with $y = 0.99\,x$, which indicates an excellent model performance for the considered dataset with a slight tendency to underestimate the measured terminal velocities. The drag law proposed by Ganser (1993) holds a correlation coefficient R^2 of approximately 0.95 with $y = 1.17\,x$, both suggesting a less favorable fit of the model, which additionally seems to carry a tendency to overestimate the measured terminal velocity of microplastic particles. The scatterplots of the other eight discussed drag models, supplemented with two scatterplots corresponding to the drag models for spherical particles as proposed by Stokes (1851) and by Dietrich (1982), are provided in Appendix Figure A.8 and Figure A.9, respectively.

Interestingly, the average error and RMSE of the drag model derived by Dioguardi *et al.* (2018) drops to 9.27 % and 10.93, respectively, in case the fibres (i.e. PVC-pipe particles), as illustrated above by the calculation discussion of the second microplastic particle, are excluded from the dataset. This significant
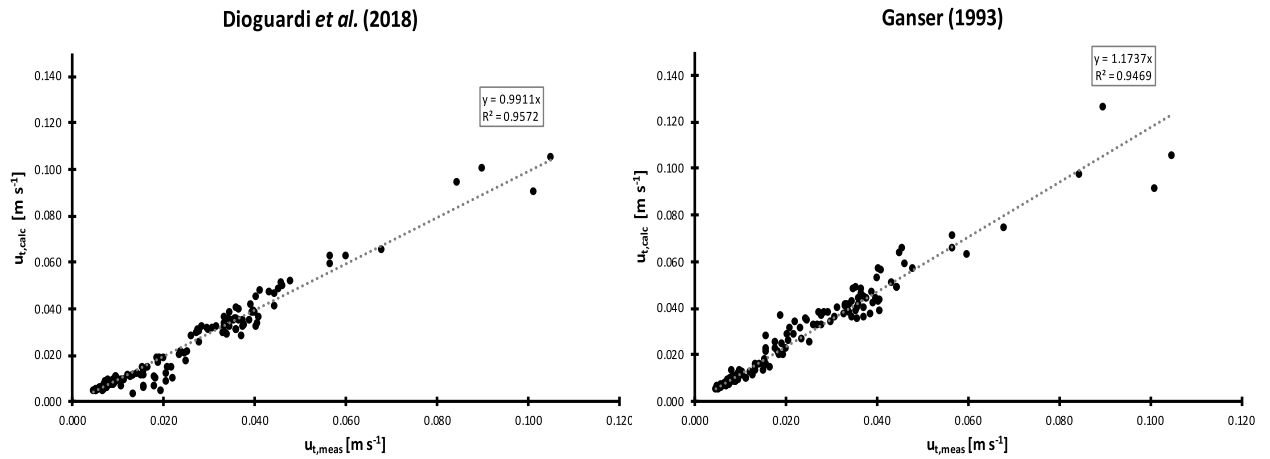
Figure 5.4: Scatter plots of $u_{t,calc}$ versus $u_{t,meas}$ comparing the theoretical terminal velocity calculated by the shape-dependent drag laws proposed by Dioguardi *et al.* (2018) (left) and Ganser (1993) (right). Dotted grey lines represent the linear regression lines of the type $y = ax$ with R^2 the corresponding correlation coefficient.

increase in model performance is, in proportion to the initial error values, the highest compared to all other examined drag models. The performance of the drag models proposed by Pfeiffer *et al.* (2005) and Camenen (2007) even worsened after excluding fibrous particles. This underlines the complexity to derive a single empirical equation that describes the sinking behaviour of (microplastic) particles with both spherical and extremely irregular shapes such as fibres. In addition, it indicates that the shape-dependent drag law by Dioguardi *et al.* (2018) performs particularly well for non-fibre microplastic particles. This might be explained by the particles that were originally used by Dioguardi *et al.* (2018) to derive their drag model with the main objective to reduce the error of commonly applied drag models in multiphase flow engineering. It appears that the shape descriptor values Ψ of these particles covered a range from 0.335 to 1, with 1 indicating a perfect sphere. However, all the Ψ values of the PVC fibres used in this research are smaller than 0.200, which implies that the drag model of Dioguardi *et al.* (2018) is not appropriately designed to account for the shape of fibrous particles.

5.3.4 Conclusion

As a general conclusion of this section, the considered dataset verified that the drag coefficient C_D of non-spherical particles is greater in comparison with spherical particles of equal density and size. In addition, it is found that the drag coefficients of foil particles are particularly elevated compared to the other microplastic particles. Furthermore, it appeared that the circularity χ is the most appropriate shape descriptor to adequately describe the shape of fibrous microplastic particles. Therefore, it is recommended to include a measure of circularity in the model to predict the sinking behaviour of microplastic particles. To that end, the shape-dependent drag law derived by Dioguardi *et al.* (2018) was identified as the model that best fits the dataset with a particle Reynolds number range of 1 to 300. From the evaluation of 10 different commonly used drag models, the model derived by Dioguardi *et al.* (2018) seems to predict the terminal settling velocity u_t of microplastic particles with the lowest error. The corresponding applied shape factor Ψ that takes both the circularity χ and the sphericity Φ into account is said to be the most appropriate shape descriptor to geometrically describe the considered dataset. However, the sinking behaviour of fibrous particles seems to remain troublesome to accurately predict by the currently available empirical drag models.

5.4   Separation performance of a decanter centrifuge

5.4.1   Grade efficiency curves

Figure 5.5 illustrates the grade efficiency curves for both sediment scenarios of the considered feed constituents, namely the corresponding sediment particles, high-density microplastic particles (PVC, PET and PC) and low-density bio-fouled microplastic particles, supplemented with the grade efficiency curves of the corresponding worst- and best-case scenarios. All grade efficiency curves assumed the optimal operational conditions derived in the last paragraph of Section 4.3, which appeared to be Ω = 5400 rpm and Q_{in} = 10 m^3/h for sediment scenario 1, and Ω = 3500 rpm and Q_{in} = 30 m^3/h for sediment scenario 2. Considering the sediment particles associated with scenario 2 (i.e. bottom left corner of Figure 5.5), $d_{p,50}$ and $d_{p,100}$ are given by 63 μm and 113 μm, respectively, meaning that sediment particles with d_p = 63 μm have a 50 % probability to be separated in the solids discharge of the decanter centrifuge, while sediment particles with $d_p \geq$ 113 μm have a 100 % probability to be separated in the solids discharge according to Equation 4.59. However, the corresponding $d_{p,50}$ values of PVC, PET and PC microplastic particles are given by 150, 169 and 233 μm. Since microplastic particles are meant to escape with the effluent outlet and span a size range of 1 μm to 5 mm, the separation process appears to be ineffective for expected feed mixtures associated with sediment scenario 2 and polluted with high-density microplastic particles. The corresponding WCS grade efficiency curves (i.e. bottom right corner of Figure 5.5) suggest a similar conclusion. The BCS grade efficiency curves indicate that $d_{p,50}$ of PVC, PET and PC increases to 1251, 1667 and 3277 μm, respectively, while $d_{p,100}$ of sediment drops to 109 μm. Despite the improvement of these results in comparison with the expected scenario, it seems that a decanter centrifuge is unable to successfully isolate all high-density microplastic particles in its effluent outlet for feed mixtures associated with sediment scenario 2 or the sand size fraction.

Regarding sediment scenario 1, $d_{p,50}$ and $d_{p,100}$ of the sediment particles for the expected scenario (i.e. top left corner of Figure 5.5) equal 39 and 54 μm, respectively. For PVC, PET and PC the $d_{p,50}$ values are equal to 69, 86 and 114 μm, respectively, which is unfavorable for the desired separation. Notice the difference in x-as range between sediment scenario 1 and 2 of the graphs illustrated in Figure 5.5. Considering the WCS (i.e. top right corner of Figure 5.5), $d_{p,50}$ of PVC, PET and PC further drops to 59, 67 and 91 μm, respectively. For the BCS, the sediment particles show a $d_{p,50}$ of 31 μm, while $d_{p,50}$ of PVC, PET and PC equals 111, 130 and 196 μm, respectively. Therefore, it seems that a decanter centrifuge is particularly unsuccessful in the separation of sediment particles with d_p values smaller than 63 μm (i.e. sediment scenario 1 or the mud size fraction) from a mixture with high-density microplastic particles (ranging from 1 μm to 5 mm).

Considering the low-density bio-fouled microplastic particles, the expected $d_{p,50}$ of sediment scenario 1 and 2 correspond to 161 and 355 μm, respectively. Therefore, little improvement in the separation performance of the decanter is observed for these particles. However, the $d_{p,50}$ of the bio-fouled microplastic particles associated with the BCS equals 362 μm and > 5 mm for sediment scenario 1 and 2, respectively. This implies that for a feed mixture corresponding to sediment scenario 2 and polluted with low-density bio-fouled microplastic particles, the decanter centrifuge is successful in isolating the microplastic particles in the effluent outlet, given the best-case scenario. The latter translates to a shape factor Ψ = 1 for sediment and Ψ = 0.01 for microplastic particles, which is solely true for foil or fibrous microplastic particles.
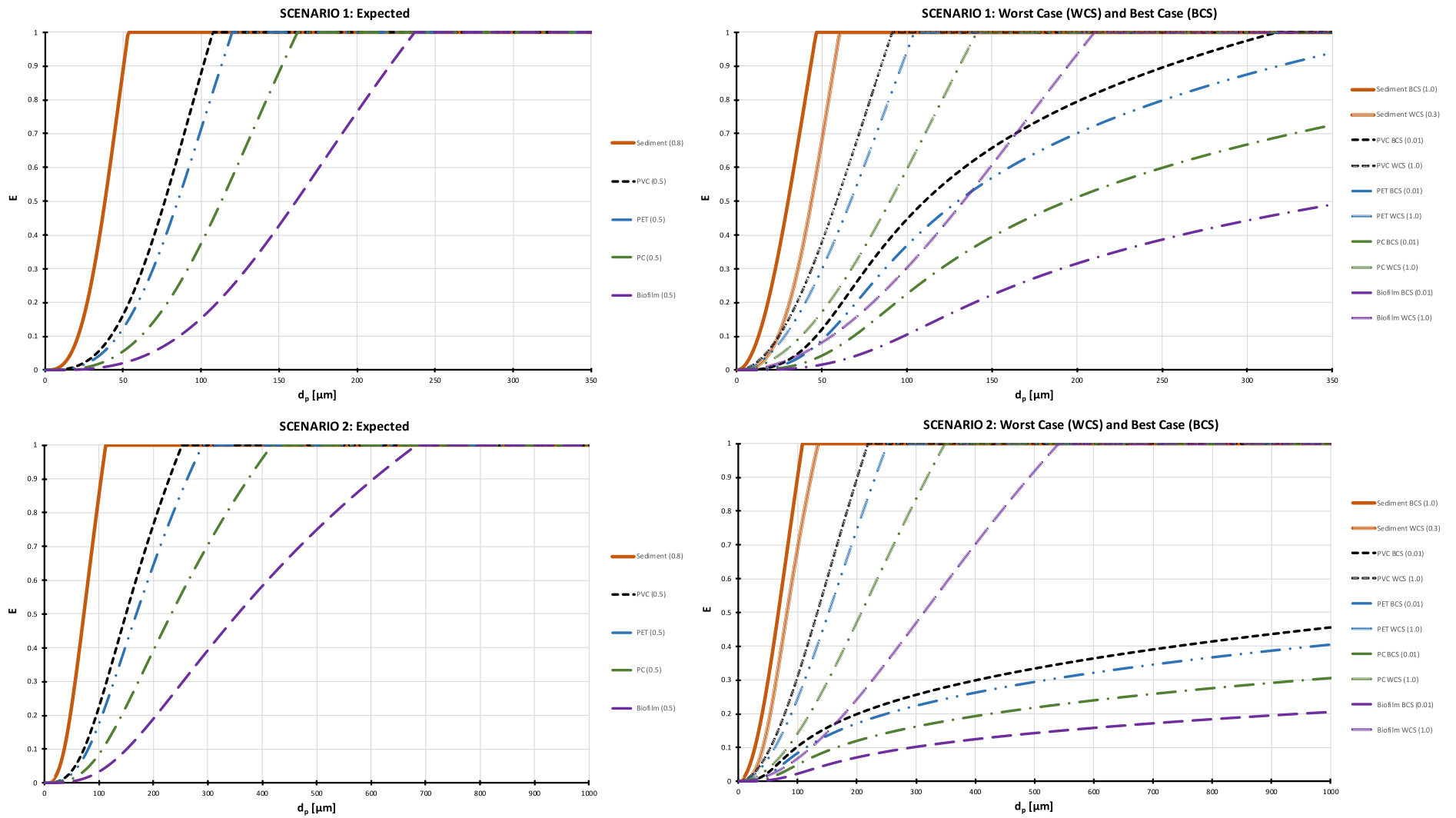
Figure 5.5: Overview of the theoretical grade efficiency curves associated with the considered decanter centrifuge subdivided in four graphs. The graphs at the top correspond to sediment scenario 1 (i.e. mud size fraction; < 63 μm), while the graphs at the bottom correspond to sediment scenario 2 (i.e. sand size fraction; 63 μm – 2 mm). Both the expected and the worst/best-case scenarios are discussed. The legend indicates the corresponding feed constituents with its assumed shape factor Ψ presented in parentheses, where *Biofilm* represents the low-density bio-fouled microplastic particles.

Furthermore, other processes next to biofouling contribute to the settling behaviour of initially floating microplastic particles in the marine environment, as elaborated in Subsection 2.2.4 and briefly discussed above in Subsection 5.2.3. This suggests that microplastic particles with a density lower than the surrounding seawater are also present in marine sediment mixtures. Moreover, due to the strong turbulent regime associated with the pumping of sediment and the rotating motion in the decanter centrifuge, it is hypothesized that the biofilms attached to bio-fouled microplastic particles will detach and therefore restore the original density of the corresponding particles. This hypothesis would imply that low-density microplastic particles, such as PP, LDPE and HDPE that account for approximately 60 % of the total worldwide non-fibre plastic production, are successfully removed in the decanter effluent (i.e. with a 100 % probability). Therefore, separation by means of centrifugal sedimentation might prove to be valuable for the remediation of microplastic particles from marine sediment mixtures to some extent. However, it must be recognized that this separation technique isolates microplastic particles indirectly, meaning that they are removed together with the bulk of the liquid medium. As a result, a secondary treatment is required to separate the microplastic particles from the liquid stream, which is seawater in this context.

To illustrate the findings discussed above, Table 5.6 was constructed providing a quantitative overview of the different in- and outlet streams of the decanter centrifuge based on the predictions of the grade efficiency curves for the expected scenario (i.e. not the BCS or WCS). It is assumed that the critical diameter $d_{p,50}$ determines the cut-off size of the corresponding particles that are separated in the decanter centrifuge. Therefore, particles with a size d_p smaller than the corresponding critical diameter are assumed to be discharged via the effluent outlet, while particles with a size d_p greater than the corresponding critical diameter are assumed to be discharged via the solids outlet. Moreover, the distinction between high-density and low-density microplastics is incorporated, where the critical diameter of the high-density microplastics is derived by calculating the average between the critical diameters of PVC and PET, which are the most produced high-density polymer types worldwide (Subsection 2.1.2). Low-density microplastics are assumed to escape with the effluent outlet with a 100 % probability, therefore excluding the effects of biofouling.

Table 5.6: Overview of the estimated composition of the different in- and outlet streams of a decanter centrifuge used as remediation technique for both high-density microplastics (*Microplastics: HD*) and low-density microplastics (*Microplastics: LD*) from two different types of marine sediment mixtures (i.e. scenario 1 and 2). High- and low-density refers to the density of the corresponding polymer type that is respectively higher or lower than the density of seawater.

	Feed inlet	**Effluent outlet**	**Solids outlet**
		SCENARIO 1[a]	
Sediment	Mud fraction (< 63 μm)	< 39 μm	39 μm – 63 μm
Microplastics: HD	1 μm – 5 mm	< 82 μm	82 μm – 5 mm
Microplastics: LD	1 μm – 5 mm	1 μm – 5 mm	None
		SCENARIO 2[b]	
Sediment	Sand fraction (63 μm – 2 mm)	None	63 μm – 2 mm
Microplastics: HD	1 μm – 5 mm	< 160 μm	160 μm – 5 mm
Microplastics: LD	1 μm – 5 mm	1 μm – 5 mm	None

[a]Decanter operated at $\Omega = 5400$ rpm and $Q_{in} = 10$ m³/h
[b]Decanter operated at $\Omega = 3500$ rpm and $Q_{in} = 30$ m³/h

5.4.2 Mass balance

For illustrative purposes, a quantitative description of the decanter separation process is presented by constructing a mass balance of sediment scenario 2 that roughly estimates the expected decanter outlets based on the results presented in Table 5.6. The starting point of the mass balance is the corresponding optimal inlet flow rate Q_{in} = 30 m³/h. Considering that the solids volume fraction ϵ of the feed mixture was determined as 0.2, which was based on information provided by dredging company Jan De Nul, the inlet flow rate can be divided in a liquid part and a solids part. The liquid part is assumed to be seawater and the solids part a combination of sediment and microplastic particles. To translate the volumetric flow rates to mass flow rates, a density of 1025 and 2650 kg/m³ is assumed for the seawater and the solid particles, respectively. The latter value is based on the average density of marine sediments (dry weight), as discussed above in Section 5.1, and neglects the density of microplastic particles assuming that, for simplification, their total mass is negligible compared to the total mass of sediment particles. Furthermore, a microplastic concentration of 100 particles/kg sediment is assumed, which corresponds to the global average concentration in intertidal sediments (Subsection 2.2.4). In addition, by estimating that the ratio between high-density and low-density microplastics in the feed mixture is $\frac{2}{3}$, which is based on the approximation that 60 % of the total worldwide plastic production is associated with low-density plastic types (Subsection 2.1.2), the number of low-density and high-density microplastics in the feed mixture per unit of time can be calculated.

To derive an estimation for the average mass of one microplastic particle, the average density is multiplied by the estimated average volume of a microplastic particle. The average density of high-density microplastics is assumed to be determined by the average densities of PVC and PET, while the average density of low-density microplastics is assumed to be determined by the average densities of PE and PP, which ultimately yields an average density of 1400 kg/m³ and 925 kg/m³, respectively. Regarding the average volume of a microplastic particle, three size classes of microplastics are defined based on Desforges *et al.* (2014), namely lower range small microplastics (LR-SMPs; < 500 μm), upper range small microplastics (UR-SMPs; 0.5 – 1 mm) and large microplastics (LMPs; 1 – 5 mm). The corresponding average particle diameter of LR-SMPs, UR-SMPs and LMPs is 250 μm, 750 μm and 3 mm, respectively (Everaert *et al.*, 2018). Assuming spherical microplastic particles, the following average volumes are derived: 0.008 mm³ for LR-SMPs, 0.221 mm³ for UR-SMPs and 14.137 mm³ for LMPs. Thus, the mass of one microplastic particle for each of the size classes was calculated. The corresponding results are given by Table 5.7. Furthermore, according to Desforges *et al.* (2014); Obbard *et al.* (2014) and Song *et al.* (2014), approximately 75 % of all floating marine microplastics are associated with LR-SMPs, 15 % with UR-SMPs and 10 % with LMPs. If a similar size distribution is assumed for the microplastics in marine sediments, the mass-contribution of each size category for both high-density and low-density microplastics in the feed mixture and the corresponding decanter outlet streams can be estimated. Finally, by assuming a cake dryness of 60 m%, which is common for decanter centrifuges, the water mass flow rates of the outlet streams are calculated. The results of this hypothetical mass balance calculation are depicted in Figure 5.6.

Table 5.7: Overview of the individual mass of high-density microplastics (*Microplastics: HD*) and low-density microplastics (*Microplastics: LD*). Three size classes are defined: lower range small microplastics (*LR-SMPs*; < 500 μm), upper range small microplastics (*UR-SMPs*; 0.5 – 1 mm) and large microplastics (*LMPs*; 1 – 5 mm).

	Microplastics: HD [mg]	Microplastics: LD [mg]
LR-SMPs	0.011	0.007
UR-SMPs	0.309	0.204
LMPs	19.792	13.077

Similar to the findings concluded in the discussion of the previous subsection, Figure 5.6 demonstrates in an alternative way that a decanter centrifuge is unable to separate all microplastic particles from a sediment mixture associated with sediment scenario 2. Moreover, it needs to be mentioned that the decanter performs better for sediment scenario 2 compared to sediment scenario 1, as elaborated in the previous subsection. It appears that, with respect to the described assumptions and the fact that the fraction of high-density microplastics smaller than 160 μm (Table 5.6) is set equal to the LR-SMPs class, the mass of microplastics per unit of time in the effluent and the solids outlet is approximately equal. In addition, the successfully isolated microplastics in the effluent seem to be extremely diluted, considering that for a little over 1 kg of microplastics that end up in the effluent, approximately 18 ton of seawater ($\pm$ 18 m^3) is drained via the effluent. This implies that a secondary large-scale treatment step would be required to isolate the microplastic particles from the seawater volume, as mentioned in the previous subsection. However, one has to acknowledge that the mass of microplastic particles might not be the most appropriate measure to evaluate remediation techniques, considering that the smallest microplastics might cause the most harm in the marine environment (Subsection 2.2.6). When the mass of microplastics in the effluent and the solids outlet are translated to number of particles, it appears that the abundance of microplastics isolated in the effluent is 9 times greater than the abundance of microplastics separated in the solids outlet. In absolute values, this translates to 1.431 million microplastic particles in the effluent outlet and 159 thousand in the solids outlet per hour. Note that despite the latter result argues in favor of a decanter centrifuge as a potential remediation technique for microplastic particles, a number of important assumptions were made to derive the corresponding mass balance. For instance, it was assumed that all low-density microplastics are 100 % isolated in the effluent, which might not be the case due to marine biofouling, and that 60 % of the microplastics present in the sediment mixture are low-density microplastics. In addition, only sediment particles larger than 63 μm (i.e. sediment scenario 2) were considered.

Feed inlet

30 m^3 h^{-1}

→ 6 m^3 h^{-1} ~ 15900 kg h^{-1} solids
24 m^3 h^{-1} ~ 24600 kg h^{-1} water

Effluent outlet

18242 kg h^{-1}

→ 0.000 kg h^{-1} sediment — ~ 49.98 m%
1.286 kg h^{-1} microplastics
18241 kg h^{-1} water — ~ 90.00 %

Solids outlet

22258 kg h^{-1}

→ 15897.426 kg h^{-1} sediment — ~ 50.02 m%
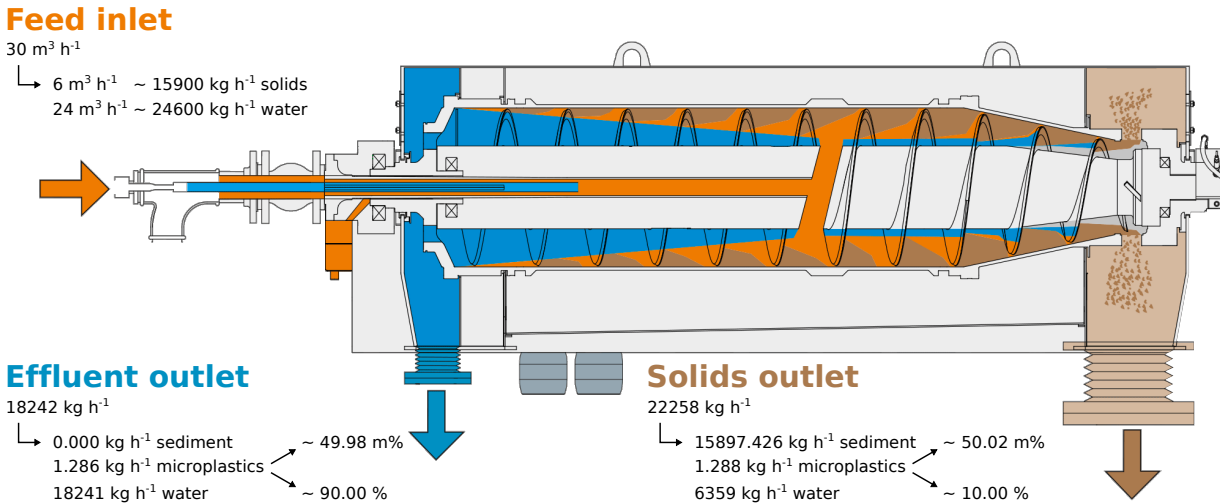1.288 kg h^{-1} microplastics
6359 kg h^{-1} water — ~ 10.00 %

Figure 5.6: Hypothetical mass balance concerning a decanter centrifuge rotating at $\Omega = 3500$ rpm with an inlet flow rate of $Q_{in} = 30$ m^3/h (i.e. the expected scenario) handling a feed mixture of sediment particles larger than 63 μm (i.e. sediment scenario 2) and microplastic particles in seawater at a solids volume fraction $\epsilon = 0.2$.

5.4.3 Conclusion

From the grade efficiency curves provided in Figure 5.5 for the case of a decanter centrifuge, it may be concluded that separation by means of centrifugal sedimentation is not suitable for (dredged) sediment mixtures polluted with high-density microplastic particles. The latter corresponds to particle densities greater

than the density of seawater. The main reason appears to be the significant overlap in size of the particles to be separated, considering the strong correlation between the particle diameter d_p and the grade efficiency E_{d_p} given by Equation 4.59. This quadratic relation can be deduced from Equation 4.51 that describes the settling velocity of a particle under the influence of a centrifugal force. Moreover, the difference in density between sediment and (high-density) microplastic particles seems to be insufficient to compensate for the overlap in particle diameter range. Consequently, no combination of structural and operational decanter parameters exists to effectuate a successful centrifugal separation of sediment mixtures polluted with high-density microplastic particles. On the other hand, low-density microplastic particles theoretically float in seawater and, as a result, are assumed to be isolated from the sediment particles with a 100 % probability. The latter implies that given a low-density microplastic particle that settled on the seabed due to density-modification caused by biofouling (Subsection 5.2.3), the biofilm is assumed to (partly) detach from the particle's surface during the separation process. This underlines the value of centrifugal sedimentation in the remediation of microplastic particles from marine sediments, considering that the majority of the total worldwide production of plastics is associated with low-density polymers. However, secondary treatment is required to separate the microplastic particles from the effluent of the decanter. In addition, considering that flow rates of dredging pumps commonly exceed 1500 m³/h, a significant amount of decanters would be required to process the dredged stream, and the grade efficiency curves would shift to the right under increasing flow rates, which decreases the performance of the separation process.

5.5 Separation performance of a novel flotation installation

5.5.1 Preliminary results

The conducted explorative experiments described in Subsection 4.4.3 provided valuable insights into the behaviour of sediment and microplastic particles in flotation systems. Moreover, it indicated the need for a more advanced flotation installation to achieve an appropriate separation performance.

Firstly, the experiments regarding the mechanical flotation cell revealed that using a mechanical impeller to introduce bubbles into the system causes a strong turbulent regime. As a consequence, both LDPE and PET microplastic particles were unable to be captured in the froth layer for a sufficient period of time. Therefore, less than half of the fed microplastic particles were recovered in the overflow. Moreover, the turbulence prevented the sediment particles to settle, which led to an overall poor separation performance. Secondly, the experiments with the pneumatic flotation column showed more promising results compared to the mechanical flotation cell. In the case that solely microplastic particles were added to the system, nearly all of them (i.e. both LDPE and PET) were recovered in the overflow assuming the most appropriate air flow rate. However, in the case that sediment particles were introduced into the system, the pores of the air sparger clogged almost immediately resulting in the absence of air bubbles. Therefore, the considered pneumatic flotation column was stated to be unable to process sediment mixtures. Thirdly, the experiments performed on the DAF installation indicated that the considered microplastic particle size of approximately 2 mm was too large to be captured by the microbubbles.

To conclude, each considered type of flotation system revealed relevant information that was used during the design phase of the proposed novel flotation installation. For instance, it appeared that the use of an air sparger is favoured in comparison to a mechanical impeller as bubble generation system. However, the introduction mechanism of the bubbles demands revision considering that the pneumatic flotation column appeared to be unable to process sediment mixtures due to clogging. In addition, the importance of bubble size was highlighted during the DAF experiments, considering that a distribution of solely micro-sized air

bubbles (i.e. < 100 μm) was unable to carry the relatively large microplastics (i.e. $\pm$ 2 mm) to the surface of the tank. Therefore, it is stated that a broad range in particle size of the particles to be separated demands a broad range in present bubble size. Some of these considerations were examined by means of graphical simulations discussed in the next subsection.

5.5.2   Simulations

The graphical simulations created to examine the effect of the number of tangential recycle inlets are provided in Figure 5.7. It appears that the use of four recycle inlets is associated with a high magnitude of flow velocity along the length of a flotation column with a diameter of 10 cm. Consequently, a strong turbulent flow is to be expected when implementing this configuration. In comparison, operating with two recycle inlets seems to correspond with a flow velocity magnitude that stabilizes over a smaller distance in the column flotation section of the installation. Furthermore, the use of a single recycle inlet corresponds to the largest zone of minimum flow velocity magnitude (i.e. the dark-blue zone in Figure 5.7), namely from $z = 70$ to $z = 100$ cm. However, the asymmetry associated with the use of only one recycle inlet seems to cause a less pronounced vortex effect as described in Subsection 4.4.4. Therefore, it was opted to install two tangential recycle inlets at opposite side of each other, with the possibility of deactivating one recycle inlet considering that an increase of the low-velocity or low-turbulent zone will hypothetically improve the separation performance.
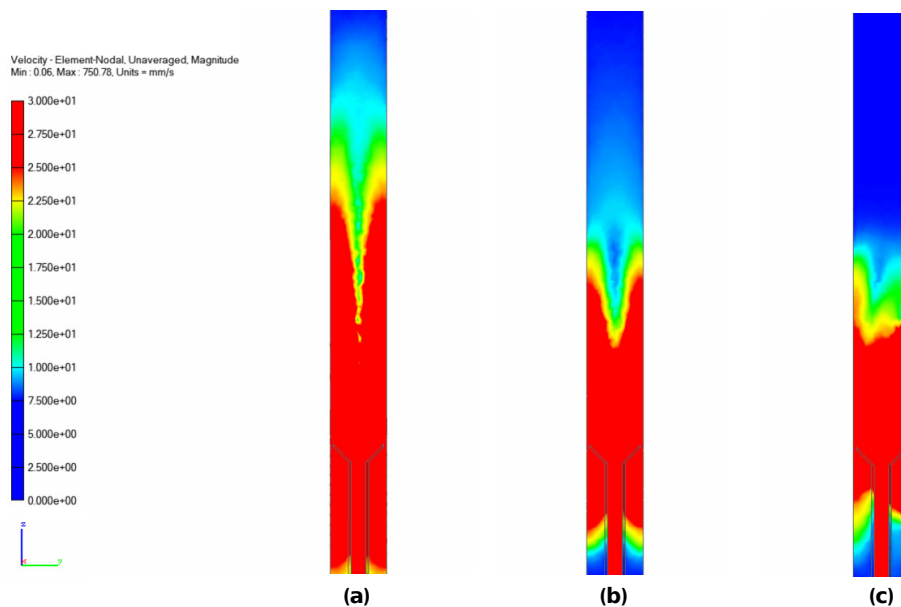

Figure 5.7: Graphical results of three different simulations illustrating the magnitude of the water flow velocity with regard to the novel flotation installation: (a) use of four recycle inlets, (b) use of two recycle inlets and (c) use of one recycle inlet.

5.5.3   Optimization

To recall the different experimental phases performed on the novel flotation installation, Table 5.8 was constructed. The first of the five consecutive experimental phases, which is the optimization phase of the operational parameters as described in Subsection 4.4.4, provided valuable insights into the dynamics of the novel flotation installation. For instance, it appeared that activating both venturi spargers caused too

much turbulence, which in turn led to a poor recovery rate ($< 50\%$) of the considered microplastic particles, most likely due to an increased detachment probability P_d. It is hypothesized that a bigger installation (i.e. column diameter > 10 cm) would benefit from a second venturi sparger owing to the increased requirement of bubble load and the elevated significance of asymmetry effects that would result from operating with only one venturi sparger. Furthermore, the addition and the corresponding position of the sieve plate affected the flow behaviour in the column considerably. In the absence of the sieve plate, the distribution of the bubbles in the flotation column was not homogenous. By adding the sieve plate, the homogeneity of the bubbles increased significantly, which resulted in a higher recovery rate of the microplastic particles, namely a difference of approximately 20 %. However, an optimal position of the sieve plate H_{sieve} was found. A sieve position too distant from the recycle inlet decreased the volume associated with a homogeneously distributed bubble flow, while a sieve position particularly close to the recycle inlet seemed to have little effect on the distribution of the bubbles. Therefore, an optimal sieve position relative to the fixed horizontal plain where the recycle flow enters the flotation column was defined as H_{sieve} = 10 cm.

Table 5.8: Overview of the different experimental phases performed on the novel flotation installation containing information about the involved polymer types, the addition of sediment, the number of iterations, the constant variables and the variables under consideration.

	Polymer type	Sediment	Dependent variables	Independent variables
Phase 1	PET	N/A	Microplastic recovery rate	$H_{recycle}$, H_{sieve}, Q_{air}, $N_{venturi}$
Phase 2	PP, LDPE, HDPE, PET, PS, PC	N/A	Microplastic recovery rate	Polymer type
Phase 3	PET, PS, PC	2 scenarios	Microplastic recovery rate and sediment entrainment	Polymer type, sediment scenarios
Phase 4	PET, PS, PC	2 scenarios	Microplastic recovery rate and sediment entrainment	Polymer type interaction, sediment scenarios
Phase 5	PET, PS, PC	2 scenarios	Microplastic recovery rate and sediment entrainment	Polymer concentration, sediment scenarios

In addition to the position of the sieve plate, the position of the recycle inlet $H_{recycle}$ appeared to have an important impact on the flotation process. Reducing the distance between the recycle inlet and outlet causes a large fraction of the bubbles generated by the venturi sparger(s) to be recycled by means of the submersible pump. As a consequence, the bubble size decreases under the influence of the shearing action caused by the pump. Increasing the distance between the recycle inlet and outlet seems to influence the amount of sediment particles that is able to enter the recycle flow. Moreover, beyond a certain distance between the recycle inlet and outlet, small sediment particles appeared to get stuck in an infinite recycle loop. Therefore, the optimal position of the recycle inlet relative to the recycle outlet was determined by $H_{recycle}$ = -15 cm, while additionally taking the maximization of the microplastic recovery rate into consideration.

Furthermore, changes in the inlet air flow rate of the venturi sparger were examined. By adjusting the needle valve of the flowmeter, the inlet air flow of the venturi could be controlled. A small air flow rate resulted in poor bubble generation, while a large air flow rate caused a turbulent regime that proved to be strong enough to disrupt the homogenous distribution of the bubbles induced by the addition of the sieve plate. Ultimately, a well-balanced combination of operating variables was derived with an optimized air flow rate Q_{air} = 0.3 m³/h.

To illustrate, Figure 5.8 provides a close-up image of the novel flotation installation and summarizes the optimal operational parameters obtained by means of experimental phase 1.
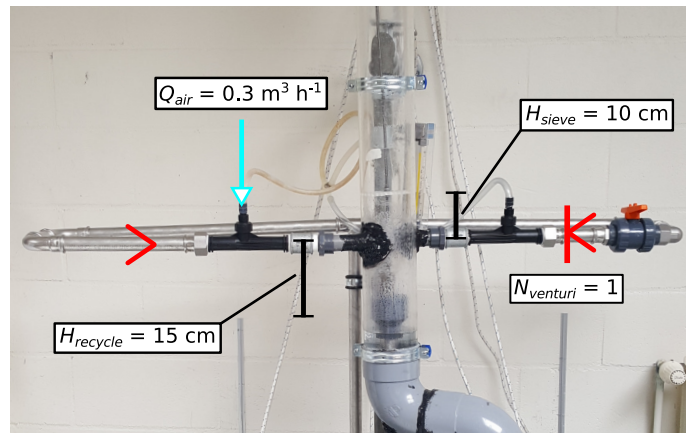

Figure 5.8: Close-up image of the constructed flotation installation added with the experimentally derived optimal operational conditions.

5.5.4   Microplastic recovery rate and sediment entrainment

A summary of the results involving experimental phase 2 is provided in Table 5.9. As expected, the recovery rate of microplastic particles that naturally float in water (i.e. PP, LDPE and HDPE) was consistently equal to 100 %. The microplastic recovery rates of the considered PET, PS and PC particles appeared to be less than 100 %, but higher than 98 % with little variation among the iterations. This implies a good separation performance of the novel flotation installation with an appropriate choice of operational variables.

Table 5.9: Summary of the results of experimental phase 2 performed on the novel flotation installation containing information about the microplastic recovery rate of different polymer types without the addition of sediment. All values are expressed as percentages.

	Phase 2
PP	100.00 ± 0.00
LDPE	100.00 ± 0.00
HDPE	100.00 ± 0.00
PET	98.40 ± 0.18
PS	99.20 ± 0.22
PC	98.80 ± 0.22

Table 5.10 provides a summary of the results of experimental phases 3 to 5. Considering the results of phase 3, it appears that the average microplastic recovery rates are comparable to phase 2. However, the corresponding standard deviations are approximately 10 times higher, yet still acceptable considering the relatively low number of repetitions. By comparing the microplastic recovery rates between the different sediment scenarios, solely for PET particles a minor increase (i.e. on average +0.67 %) from scenario 1 to scenario 2 was observed. In addition, scenario 2 was associated with an average sediment entrainment of merely 0.11 ± 0.01 m%, while the sediment entrainment corresponding to scenario 1 appeared to be significantly higher, namely 5.68 ± 0.50 m%. These findings imply that small sediment particles (i.e. $d_p < 63$ µm) have a higher probability to escape the system via the overflow rather than through the solids discharge at the bottom.

Table 5.10: Summary of the results of experimental phases 3 to 5 performed on the novel flotation installation containing information about the microplastic recovery rate (*PET*, *PS* and *PC*) and the sediment entrainment (*Sediment*). All values are expressed as percentages with sediment entrainment expressed as mass percentage.

Phase 3 $(1000{:}1)^a$	**Scenario 1**	**Scenario 2**
PET	97.33 ± 2.31	98.00 ± 2.00
PS	98.67 ± 2.31	98.67 ± 1.15
PC	98.67 ± 2.31	98.67 ± 1.15
Sediment	5.68 ± 0.50	0.11 ± 0.01
Phase 4 $(1000{:}1)$	**Scenario 1**	**Scenario 2**
PET + PS + PC	95.56 ± 2.04	96.00 ± 1.15
Sediment	5.93 ± 0.59	0.09 ± 0.01
Phase 5 $(100{:}1)$	**Scenario 1**	**Scenario 2**
PET + PS + PC	85.00 ± 1.47	86.11 ± 0.32
Sediment	4.34 ± 0.44	0.08 ± 0.01

$^a(X_1{:}X_2)$ expresses the concentration as X_1 microplastic particles per X_2 kg of sediment

The recovery rates resulting from the microplastic mixture covered in experimental phase 4 indicate an average decrease of approximately 2 % compared to the individual microplastic recovery rates observed during phase 3. The microplastic concentration in both phases was identical, namely 1000 microplastic particles for every kilogram of sediment. The only difference was that phase 4 combined the different polymer types in a single sediment mixture, while phase 3 covered individual polymer type mixtures. Therefore, it may be concluded that the interaction of different polymer types in a sediment mixture has a negative impact on the microplastic recovery rate of the installation. Considering that the standard deviations of the microplastic recovery rates vary around 2 %, this unexpected observation might be due to the relatively low number of performed iterations. Another explanation might be that the formation of microplastic clusters, as explained in Subsection 4.4.1 and illustrated in Figure 4.11, is facilitated for microplastic particles of the same polymer type and plays an important role in the flotation of microplastics. The sediment entrainment observed in phase 4 associated with both scenarios appeared to be comparable to those of phase 3.

The comparison of the recovery rate results of the microplastic mixtures between phase 4 and phase 5 revealed that lowering the microplastic concentration of phase 4 to the global average concentration of 100 microplastic particles for every kilogram of sediment is associated with a significant decrease. While the microplastic recovery rates of the experimental phases 1 to 4 did not drop under 95 %, phase 5 corresponds to a microplastic recovery rate of 85.00 ± 1.47 % and 86.11 ± 0.32 % for scenario 1 and 2, respectively. Moreover, this decrease of approximately 10 % seems to be primarily attributed to the PET particles, considering their average microplastic recovery rate of 70.00 ± 1.67 % and 71.67 ± 1.92 % for scenario 1 and 2, respectively. This suggests that among the considered polymer types, PET particles are the most difficult to separate by means of flotation, particularly when present in relatively low concentrations. This aligns with the findings summarized in Table 5.1 that indicate the relatively high density and low contact angle of PET compared to PS and PC, which both hinder effective flotation.

Furthermore, the results of Section 5.2 summarized in Table 5.2 suggest that bio-fouled (micro)plastic particles will be associated with low microplastic recovery rates due to the significant decrease in contact angle. However, no experiments were performed to confirm this prediction due to time restrictions. In

addition, it is hypothesized that a premixing step of the feed mixture by means of an agitator will cause the biofilms to (partly) detach from the surface of the particles. Therefore, the impact of biofouling on the separation performance of the novel flotation installation is yet to be examined.

5.5.5 Conclusion

In general, it may be concluded that the novel flotation installation shows an excellent separation performance when dealing with a sediment mixture that corresponds to the sand fraction (i.e. scenario 2) and a microplastic concentration of 1000 particles/kg sediment with a microplastic size of approximately 2 mm. For sediment mixtures associated with the mud fraction (i.e. scenario 1), the sediment entrainment increases from approximately 0.1 m% to 5 m%. Furthermore, feed mixtures with a microplastic concentration of 100 particles/kg sediment show a significantly lower microplastic recovery rate under the predefined operational conditions (i.e. from approximately 95 % to 85 %). Therefore, the lowest separation performance is expected when dealing with a low microplastic concentration sediment mixture related to the mud fraction. In addition, marine biofouling appears to have an important negative effect on the microplastic recovery rate, yet further research is required to quantify the corresponding impact on the separation performance of the novel flotation installation. In contrast to separation by means of centrifugal sedimentation discussed in the previous section, this novel flotation installation seems to perform well for both low-density and high-density microplastic particles.

6

Conclusion

During this thesis, two promising separation technologies were chosen and evaluated based on their ability to isolate microplastic particles from marine sediment mixtures. To that end, the sinking behaviour of microplastic particles obtained by fragmentation of municipal plastic waste products was analyzed, and the shape-dependent drag model that predicts the terminal settling velocity of the corresponding microplastics most accurately was identified. Next to the traditional shape descriptor of sphericity, it appeared that a measure of circularity is essential to appropriately account for the irregular shape of microplastic particles, in particular fibrous particles. From a total of 10 different drag models, it was experimentally demonstrated that the one proposed by Dioguardi *et al.* (2018) performed best for the established dataset. This drag model includes a measure of both sphericity and circularity. Furthermore, the effect of marine biofouling on physical and chemical properties of plastics, in particular the contact angle and density, was examined. It was found that, based on the contact angle, bio-fouled plastic particles shift from a predominantly hydrophobic behaviour towards a prominently hydrophilic behaviour. In addition, it was calculated that biofouling might cause initially floating marine microplastic particles to settle on the seabed due to density-modification. This was stated to hold true for thin foil microplastic particles of all sizes, yet seemed very unlikely for spherical microplastic particles associated with the millimetre-range.

After an appropriate characterization of the feed mixture with the focus on dredged sediment, separation by means of centrifugal sedimentation was concluded to be an ineffective remediation technique for high-density microplastic particles based on theoretical calculations regarding a decanter centrifuge. This was primarily due to the significant overlap of the inherent particle diameter ranges of sediment and microplastic particles. Moreover, the considerable difference in density between these two solid feed constituents appeared to be insufficient to compensate for the overlap of particle diameter range. For low-density microplastic particles, which by definition hold a smaller density compared to seawater, centrifugal sedimentation is expected to be a successful remediation technique. However, this assumes that in case a low-density microplastic particle ends up on the seabed due to density-modification caused by biofouling (or any other phenomenon), the initial plastic density is (partly) restored during the separation process. The latter implies that low-density microplastic particles present in marine sediments must ultimately exhibit floating behaviour in a seawater medium during centrifugal sedimentation to achieve successful separation. With respect to separation by means of froth flotation, the same performance is expected regarding low-density microplastic particles, yet this technique appeared to be more effective for high-density microplastic particles as well. In addition, froth flotation is a more selective separation technique in the sense that microplastic particles are isolated at a significantly higher concentration compared to centrifugal sedimentation where the microplastic particles are removed via the bulk of the effluent. Despite the effectiveness of traditional froth flotation techniques for marine sediment remediation of both high- and low-density microplastic particles,

the corresponding separation process was determined to be inefficient. Therefore, a novel flotation installation was designed based on the principles of a cyclonic-static microbubble flotation column (FCSMC) applied in the mining industry.

A first prototype of this novel flotation installation was constructed, and the operational variables were optimized. For a microplastic concentration of 1000 particles/kg sediment, a recovery rate of over 95 % for high-density microplastics with a diameter > 2 mm was found. The corresponding sediment entrainments for the mud fraction (i.e. particle size < 63 μm) and the sand fraction (i.e. particle size between 63 μm and 2 mm) were approximately 5 m% and 0.1 m%, respectively. Therefore, it is said that the installation holds an excellent separation performance for high-density microplastics larger than 2 mm in diameter at a concentration of 1000 particles/kg sediment. Moreover, it was derived that the microplastic recovery rate is independent of the size distribution of the sediment particles, yet decreases to approximately 85 % for a microplastic concentration of 100 particles/kg sediment, which corresponds to the global average microplastic concentration of sediments in intertidal areas, with no significant changes in sediment entrainment for both the mud and the sand fraction. For low-density microplastics, a consistent recovery rate of 100 % was confirmed. Furthermore, the examined effect of marine biofouling on the contact angle of plastics suggests that bio-fouled microplastic particles will exhibit a significantly lower recovery rate. However, by implementing a continuous feed system in the design of a second prototype that incorporates severe premixing by means of agitators, the biofilms might detach from the surface of the particles. Therefore, the impact of biofouling on the separation performance of the novel flotation installation is currently uncertain.

In general, the obtained results indicate that separation by means of froth flotation is favoured compared to centrifugal separation regarding the objective to isolate all microplastic particles from marine sediment mixtures. In particular, the proposed flotation design demonstrates a promising separation performance. Despite the hypothesis that the flexibility of the applied venturi spargers as bubble generation system provides the constructed flotation installation with the ability to capture microplastic particles with diameters smaller than 2 mm, further experiments are required to analyze the effect of particle size on the corresponding microplastic recovery rate.

Nevertheless, this thesis was the first to analyze large-scale remediation techniques for the removal of microplastics from (dredged) marine sediments. To that end, the first representative experimental study on the sinking behaviour of microplastic particles was performed and documented, which led to the identification of the most accurate shape-dependent drag model to predict their terminal settling velocity. In addition, the unknown effect of marine biofouling on the surface chemical properties of plastics was revealed. All these results are of paramount importance to understand the dynamic behaviour and fate of microplastic particles in the marine environment and might serve as a stepping stone towards the development of other promising remediation techniques.

To conclude, the two potential remediation techniques presented in this thesis aimed towards large-scale applications and considered the characteristics of dredged sediment during the evaluation of their separation process. It is clear that further optimization and research is required to achieve a successful integration of sediment remediation of microplastics and traditional dredging operations, yet the first step towards this valuable synergistic collaboration is made. Considering the continuous marine plastic waste infiltration and the growing concerns regarding the impact of the associated microplastic particles, these potential large-scale solutions that actively contribute to prevent further accumulation of marine microplastics and simultaneously aim towards an accessible, short-term integration with current industries, might prove to be fundamental for the protection of human health and the well-being of marine organisms.

7

Recommendations for future research

Considering the promising results regarding sediment remediation techniques for microplastics presented in this thesis, in particular with respect to the novel flotation design, and the strong urge to cope with the growing accumulation of marine microplastics, this chapter provides a description of the main recommendations for future research.

For the decanter centrifuge, it is recommended to initiate pilot testing to evaluate the separation performance in a real system. In particular, the effect of biofouling of low-density microplastics requires an experimental approach to confirm theoretical hypotheses. By means of a pilot installation, it is possible to quantify the fraction of bio-fouled low-density microplastics that regains their initial density prior to biofouling, and thus exhibits floating behaviour in a seawater medium.

With respect to the novel flotation installation, in particular the first prototype, the microplastic recovery rate over the entire corresponding size range is yet to be experimentally evaluated, as mentioned in the previous chapter. However, the development of a second prototype that is able to operate continuously and includes a premixing step of the feed mixture is essential to appropriately examine the impact of biofouling on the microplastic recovery rate of the installation. In addition, optimization of the froth layer collection mechanism to complement the continuous flotation process will offer a more pragmatic indication regarding the sediment entrainment. For instance, the implementation of a secondary overflow trough or the use of scrapers might increase the separation performance. Furthermore, experimental data that allows to derive the separation performance as a function of the inlet flow rate of the feed mixture is crucial to prepare a large-scale feasibility study. Depending on the result of that study, upscaling of the flotation installation is recommended to provide confirmation of the large-scale ability to separate microplastic particles from marine sediment mixtures.

To further promote successful integration of the proposed remediation technique for microplastics with traditional dredging operations, it is advised to explore the impact of an unstable or vibrating surface area, as occurs on board of a dredging vessel, on the separation performance of the installation. Lastly, it is clear that international regulations should encourage this innovative concept to efficiently mitigate the microplastic infiltration into the marine environment. Therefore, an estimation of both investment and operational costs to attract financial support should contribute to the realisation of this objective.

8

Bibliography

Adriaens R, Zeelmaekers E, Fettweis M, Vanlierde E, Vanlede J, Stassen P, Elsen J, Srodon J, and Vandenberghe N. Quantitative clay mineralogy as provenance indicator for recent muds in the southern North Sea. *Marine Geology*, 2018.

Albertson M. Effect of shape on the fall velocity of gravel particles. *Proceedings of the 5th Iowa Hydraulics Conference*, pages 243–261, 1953.

Aldridge J, Bergman M, Bolam T, Craeymeersch J, Degraer S, Duineveld G, Eggleton J, Goethals P, Hillewaert H, Irion G, Kershaw P, Kröncke I, Lavaleye M, Mason C, Rachor E, Rees H, Reiss H, Rumohr H, Schratzberger M, Smith R, Vanden Berghe E, Van Hoey G, Vincx M, and Willems W. Structure and Dynamics of the North Sea Benthos. Technical report, International Council for the Exploration of the Sea (ICES), 2007.

American Chemistry Council. Plastics — How Plastics Are Made, 2005.

American Chemistry Council. Plastics Make it Possible — What are Plastics: the Chemistry, 2011.

Anderson P. J, Warrack S, Langen V, Challis J. K, Hanson M. L, and Rennie M. D. Microplastic contamination in Lake Winnipeg, Canada. *Environmental Pollution*, 225:223–231, 2017.

Andrady A. Microplastics in the marine environment. *Marine Pollution Bulletin*, 62(1596-1605), 2011.

Angu E, Drelich J, Laskowski J, and Mittal K. *Apparent and Microscopic Contact Angles*. VSP, Utrecht, The Netherlands, 2000.

Antunes J, Frias J, Micaelo A, and Sobral P. *Resin pellets from beaches of the Portuguese coast and adsorbed persistent organic pollutants*, volume 130. sep 2013.

Arthur C, Baker J, and Bamford H. Proceedings of the International Research Workshop on the Occurrence, Effects and Fate of Microplastic Marine Debris. *NOAA Technical Memorandum NOS-OR&R-30*, (January):530, 2009.

Baeyens W. F. J, Eck B. V, Lambert C, Wollast R, and Goeyens L. General description of the Scheldt estuary. *Kluwer Academic Publishers*, pages 1–14, 1998.

Bagheri G and Bonadonna C. On the drag of freely falling non-spherical particles. *Powder Technology*, 301:526–544, 2016.

Baranya S, Józsa J, Török G, and Rüther N. A comprehensive field analysis of a river confluence. (January), 2012.

Barnes D, Galgani F, Thompson R, and Barlaz M. Accumulation and fragmentation of plastic debris in global environments. *Philosophical Transactions of the Royal Society B: Biological Sciences*, 364(1985-1998), 2009.

Beer S, Garm A, Huwer B, Dierking J, and Nielsen T. G. No increase in marine microplastic concentration over the last three decades – A case study from the Baltic Sea. *Science of the Total Environment*, 621:1272–1279, 2018.

Bell G. R. A. *Analysis and Development of a Decanter Centrifuge: Power consumption analysis, development of a composite bowl, and feed accelerator analysis*. PhD thesis, University of Canterbury, 2013.

Bergmann M, Peeken I, Beyer B, Krumpen T, Primpke S, Tekman M, and Gerdts G. Vast Quantities of Microplastics in Arctic Sea Ice - A Prime Temporary Sink for Plastic Litter and a Medium of Transport. *MICRO 2016: Fate and Impact of Microplastics in Marine Ecosystems*, pages 75–76, jan 2017.

Bergmann M, Gutow L, and Klages M. *Marine Anthropogenic Litter*. Springer, 2015.

Besseling E, Wegner A, Foekema E. M, van den Heuvel-Greve M. J, and Koelmans A. A. Effects of microplastic on fitness and PCB bioaccumulation by the lugworm Arenicola marina (L.). *Environmental Science & Technology*, 2013.

BIR. World Steel Recycling in Figures. Technical report, Bureau of International Recycling: Ferrous Division, 2018.

Biron M. *Thermosets and Composites: Material Selection, Applications, Manufacturing and Cost Analysis*. Elsevier, 2013.

Blight L. K and Burger A. E. Occurrence of plastic particles in seabirds from the eastern North Pacific. *Marine Pollution Bulletin*, 34(5):323–325, 1997.

Bolgar M, Hubball J, Groeger J, and Meronek S. *Handbook for the Chemical Analysis of Plastic and Polymer Additives*. CRC Press, 2 edition, 2015.

Borysenko A, Clennell B, Sedev R, Burgar I, Ralston J, Raven M, Dewhurst D, and Liu K. Experimental investigations of the wettability of clays and shales. *Journal of Geophysical Research: Solid Earth*, 114(July 2008): 1–11, 2009.

Brazel C. S and Rosen S. L. *Fundamental Principles of Polymeric Materials*. Wiley, 3 edition, 2012.

Browne M, Galloway T, and Thompson R. Microplastic – an emerging contaminant of potential concern? *Integrated Environmental Assessment and Management*, 3 (559-561), 2007.

Browne M. A, Dissanayake A, Galloway T. S, Lowe D. M, and Thompson R. C. Ingested Microscopic Plastic Translocates to the Circulatory System of the Mussel , Mytilus edulis (L .). *Environmental Science & Technology*, 42(13):5026–5031, 2008.

Browne M. A, Galloway T. S, and Thompson R. C. Spatial Patterns of Plastic Debris along Estuarine Shorelines. *Environmental Science & Technology*, 44(9): 3404–3409, may 2010.

Browne M. A, Crump P, Niven S. J, Teuten E, Tonkin A, Galloway T, and Thompson R. Accumulation of microplastic on shorelines worldwide: Sources and sinks. *Environmental Science & Technology*, 45(21):9175–9179, 2011.

Browne M. A, Niven S. J, Galloway T. S, Rowland S. J, and Thompson R. C. Microplastic moves pollutants and additives to worms, reducing functions linked to health and biodiversity. *Current Biology*, 23(23):2388–2392, 2013.

Camenen B. Simple and General Formula for the Settling Velocity of Particles. *Journal of Hydraulic Engineering*, 133(February):229–233, 2007.

Carbery M, O'Connor W, and Palanisami T. Trophic transfer of microplastics and mixed contaminants in the marine food web and implications for human health. *Environment International*, 115(March):400–409, 2018.

Carpenter E. J and Smith K. *Plastics on the Sargasso Sea Surface*. Science, New York, 1972.

CCB. Microplastic pollution originating from Textiles and Paints: Environmental impacts and solutions. Technical report, Coalition Clean Baltic, Uppsala, Sweden, 2017.

Cheng N.-S. Simplified Settling Velocity Formula for Sediment Particle. *Journal of Hydraulic Engineering*, 123:149–152, 1997.

Chua E. M, Shimeta J, Nugegoda D, Morrison P. D, and Clarke B. O. Assimilation of Polybrominated Diphenyl Ethers from Microplastics by the Marine Amphipod, Allorchestes Compressa. *Environmental Science & Technology*, 48(14):8127–8134, jul 2014.

Claessens M, De Meester S, Landuyt L. V, Clerck K. D, and Janssen C. R. Occurrence and distribution of microplastics in marine sediments along the Belgian coast. *Marine Pollution Bulletin*, 62(10):2199–2204, 2011.

Clift R and Gauvin W. H. Motion of entrained particles in gas streams. *The Canadian Journal of Chemical Engineering*, 49(4):439–448, 1971.

Cole M, Lindeque P, Halsband C, and Galloway T. S. Microplastics as contaminants in the marine environment: A review. *Marine Pollution Bulletin*, 62(12): 2588–2597, 2011.

Cole M, Webb H, Lindeque P. K, Fileman E. S, Halsband C, and Galloway T. S. Isolation of microplastics in biota-rich seawater samples and marine organisms. *Scientific Reports*, 4:4528, mar 2014.

Collignon A, Hecq J. H, Glagani F, Voisin P, Collard F, and Goffart A. Neustonic microplastic and zooplankton in the North Western Mediterranean Sea. *Marine Pollution Bulletin*, 64(4):861–864, 2012.

Costa M, Ivar do Sul J, Silva-Cavalcanti K, Araùjo M, Spengler A, and Tourinho P. On the importance of size of plastic fragments and pellets on the strandline: a snapshot of a Brazilian beach. *Environmental Monitoring and Assessment*, 168(299-204), 2010.

Coterio V. R, Luttrell G. H, and Adel G. T. *Optimization of air-injection spargers for column flotation applications*. PhD thesis, Virginia Polytechnic Institute and State University, 2016.

Cowie J. M. G and Arrighi V. *Polymers: Chemistry and Physics of Modern Materials*. CRC Press, 3 edition, 2007.

Cozar A, Echevarria F, Gonzalez-Gordillo J. I, Irigoien X, Ubeda B, Hernandez-Leon S, Palma A. T, Navarro S, Garcia-de Lomas J, Ruiz A, Fernandez-de Puelles M. L, and Duarte C. M. Plastic debris in the open ocean. *Proceedings of the National Academy of Sciences*, 111(28):10239–10244, 2014.

Crawford C. B and Quinn B. Microplastic separation techniques. In *Microplastic Pollutants*, pages 203–218. Elsevier, 2017.

Curray J and Griffiths J. Sphericity and roundness of quartz grains in sediments. *Geological Society of America Bulletin*, 66, 1955.

Dai Z, Fornasiero D, and U J. R. Particle-bubble collision models: a review. pages 231–256, 2000.

De Blauwe Cluster. Over — De Blauwe Cluster, 2018.

De Brauwer, Verfaillie E, Du Four I, Van Lancker V, Maes F, and Schrijvers J. Dredging and disposal of dredged material. Technical report, Marine Geology, Marine Institute, 2005.

Dellino P, Mele D, Bonasia R, Braia G, Volpe L. L, and Sulpizio R. The analysis of the influence of pumice shape on its terminal velocity. *Geophysical Research Letters*, 32(October):2–5, 2005.

Deng Y, Wang H, and Lu H. The contact angle of water on feldspar in a reservoir rock. *Chinese Science Bulletin*, 63:3137–3145, 2018a.

Deng Y, Xu L, Lu H, Wang H, and Shi Y. Direct measurement of the contact angle of water droplet on quartz in a reservoir rock with atomic force microscopy. *Chemical Engineering Science*, 177:445–454, 2018b.

Derraik J. G. The pollution of the marine environment by plastic debris: a review. *Marine Pollution Bulletin*, 44: 842–852, 2002.

Desforges J. P. W, Galbraith M, Dangerfield N, and Ross P. S. Widespread distribution of microplastics in subsurface seawater in the NE Pacific Ocean. *Marine Pollution Bulletin*, 79(1-2):94–99, 2014.

Dietrich W. E. Settling Velocity of Natural Particles. *Water Resources Research*, 18(6):1615–1626, 1982.

Dioguardi F and Mele D. A new shape dependent drag correlation formula for non-spherical rough particles. Experiments and results. *Powder Technology*, 277, 2015.

Dioguardi F, Survey B. G, Mele D, and Dellino P. A New One-Equation Model of Fluid Drag for Irregularly Shaped Particles Valid Over a Wide Range of Reynolds Number: Aerodynamic drag of irregular particles (corrected). *Journal of Geophysical Research: Solid Earth*, 123:144–156, 2018.

Doghri I, Rodrigues S, Bazire A, Dufour A, Akbar D, Sopena V, Sablé S, and Lanneluc I. Marine bacteria from the French Atlantic coast displaying high forming-biofilm abilities and different biofilm 3D architectures. *BMC Microbiology*, 15(231):1–10, 2015.

Doyle M. J, Watson W, Bowlin N. M, and Sheavly S. B. Plastic particles in coastal pelagic ecosystems of the Northeast Pacific ocean. *Marine Environmental Research*, 71(1):41–52, 2011.

Dubaish F and Liebezeit G. Suspended microplastics and black carbon particles in the Jade system, southern North Sea. *Water, Air, and Soil Pollution*, 224(2), 2013.

Dyachenko A, Mitchell J, and Arsem N. Extraction and identification of microplastic particles from secondary wastewater treatment plant (WWTP) effluent. *Analytical Methods*, (9), 2017.

Ebewele R. O. D. o. C. E. *Polymer Science and Technology*. CRC Press, Boca Raton, New York, 2000.

Edmondson S and Gilbert M. Brydson's Plastics Materials. In Gilbert M, editor, *Elsevier*, page 892. Butterworth-Heinemann, 8 edition, 2017.

Eerkes-Medrano D, Thompson R. C, and Aldridge D. C. Microplastics in freshwater systems: A review of the emerging threats, identification of knowledge gaps and prioritisation of research needs. *Water Research*, 75: 63–82, 2015.

El Fishawi N. Roundness and sphericity of the delta coastal sands. *Acta Mineralogica-Petrographica*, pages 235–245, 1984.

Elias H. G. *An Introduction to Plastics*. Wiley, 2 edition, 2003.

Emerson Z. I. *Particle and bubble interactions in flotation systems*. PhD thesis, Auburn Univrsity, 2007.

Eriksen M, Mason S, Wilson S, Box C, Zellers A, Edwards W, Farley H, and Amato S. Microplastic pollution in the surface waters of the Laurentian Great Lakes. *Marine Pollution Bulletin*, 77(1-2):177–182, 2013.

Eriksen M, Lebreton L. C, Carson H. S, Thiel M, Moore C. J, Borerro J. C, Galgani F, Ryan P. G, and Reisser J. Plastic Pollution in the World's Oceans: More than 5 Trillion Plastic Pieces Weighing over 250,000 Tons Afloat at Sea. *PLoS ONE*, 9(12):1–15, 2014.

Essel R, Engel L, and Carus M. Sources of microplastics relevant to marine protection in Germany. *Umweltbundesamt*, page 48, 2015.

Estahbanati S and Fahrenfeld N. L. Influence of wastewater treatment plant discharges on microplastic concentrations in surface water. *Chemosphere*, 162:277–284, 2016.

Ethington E. F. Interfacial contact angle measurements of water, mercury, and 20 organic liquids on quartz, calcite, biotite, and Ca-montmorillonite substrates. Technical report, US Department of the interior geological survey, 1990.

Eunomia. Plastics in the Marine Environment. Technical Report June, Eunomia Research and Consulting Ltd, 2016.

European Bioplastics. BIOPLASTICS: Facts and Figures. Technical report, Nova-Institute, 2017.

European Union. Horizon 2020 Work Programma for Research & Innovation. Technical report, 2017.

European Union. The 2018 Annual Economic Report on EU Blue Economy. Technical report, 2018.

Everaert G, Van Cauwenberghe L, De Rijcke M, Koelmans A. A, Mees J, Vandegehuchte M, and Janssen C. R. Risk assessment of microplastics in the ocean: Modelling approach and first conclusions. *Environmental Pollution*, 242:1930–1938, 2018.

Farrell P and Nelson K. Trophic level transfer of microplastic: Mytilus edulis (L.) to Carcinus maenas (L.). *Environmental Pollution*, 177:1–3, 2013.

Fendall L. S and Sewell M. A. Contributing to marine pollution by washing your face: Microplastics in facial cleansers. *Marine Pollution Bulletin*, 58(8):1225–1228, 2009.

Feng H, Zhang W, Zhu Y.-l, Lei Z.-y, and Ji X.-m. Sampling surface particle size distributions and stability analysis of deep channel in the Pearl River Estuary. *China Ocean Engineering*, (June), 2017.

Fischer V, Elsner N. O, Brenke N, Schwabe E, and Brandt A. Plastic pollution of the kuril-kamchatka trench area (NW pacific). *Deep-Sea Research Part II: Topical Studies in Oceanography*, 111:399–405, 2015.

Folk R. Student operator error in determination of roundness, sphericity and grain size. *Journal of Sedimentary Petrology*, 25:297–301, 1955.

Francis A. Wall Effect in Falling Ball Method for Viscosity. *Physics*, 4:403–406, 1933.

Fraunholcz N. *Plastics Flotation*. PhD thesis, Technische Universiteit Delft, 1997.

Free C. M, Jensen O. P, Mason S. A, Eriksen M, Williamson N. J, and Boldgiv B. High-levels of microplastic pollution in a large, remote, mountain lake. *Marine Pollution Bulletin*, 85(1):156–163, 2014.

Frias J. P, Sobral P, and Ferreira A. M. Organic pollutants in microplastics from two beaches of the Portuguese coast. *Marine Pollution Bulletin*, 60(11):1988–1992, 2010.

Gaines R. V, Catherine H, Skinner W, Foord E. E, Mason B, and Rosenzweig A. *Dana's New Mineralogy*, volume 120. Wiley, 8 edition, 1998.

Gall S and Thompson R. The impact of debris on marine life. *Marine Pollution Bulletin*, 92(1-2):170–179, mar 2015.

Ganser G. H. A rational approach to drag prediction nonspherical particles. *Powder Technology*, 77:143–152, 1993.

Geankoplis C. J. *Transport Processes and Unit Operations*. Transport Processes and Unit Operations. Bukupedia, third edit edition, 1993.

GESAMP. Sources, fate and effects of microplastics in the marine environment: part 2 of a global assessment. *The Joint Group of Experts on Scientific Aspects of Marine Environmental Protection*, Working Gr, 2015.

Geyer R, Jambeck J. R, and Law K. L. Production, uses, and fate of all plastics ever made. *Science Advances*, 3 (7):5, 2017.

Gleiss M. Development of a Dynamic Process Model for the Mechanical Fluid Separation in Decanter Centrifuges. (1):19–26, 2018.

Goel S and Jameson G. J. Detachment of particles from bubbles in an agitated vessel. *Minerals Engineering*, 36-38:324–330, 2012.

Goldstein M. C and Goodwin D. S. Gooseneck barnacles (Lepas spp.) ingest microplastic debris in the North Pacific Subtropical Gyre. *PeerJ*, 1:17, 2013.

Goossens D. A drag coefficient equation for natural, irregularly shaped particles. *Catena Verlag*, 14:73–99, 1987.

Gouin T, Roche N, Lohmann R, and Hodges G. A thermodynamic approach for assessing the environmental exposure of chemicals absorbed to microplastic. *Environmental Science and Technology*, 45(4):1466–1472, 2011.

Graf W. *Hydraulics of sediment transport*. McGraw-Hill, New York, 1971.

Graham E. R and Thompson J. T. Deposit- and suspension-feeding sea cucumbers (Echinodermata) ingest plastic fragments. *Journal of Experimental Marine Biology and Ecology*, 368(1):22–29, 2009.

Gregory J. *Particles in water: properties and processes*. CRC Press, 2006.

Gregory M. Plastic "scrubbers" in hand cleansers: a further (and minor) source for marine pollution identified. *Marine Pollution Bulletin*, 32(867-871), 1996.

Gupta A and Yan D. *Mineral Processing Design and Operations*. Elsevier, 2 edition, 2016a.

Gupta A and Yan D. Chapter 17 - Magnetic and Electrostatic Separation. In Gupta A and Yan D, editors, *Mineral Processing Design and Operations (Second Edition)*, pages 629–687. Elsevier, Amsterdam, second edi edition, 2016b.

Haff P. K. Technology as a geological phenomenon: implications for human well-being. *Geological Society, London, Special Publications*, 395(1):301–309, 2014.

Haider A and Levenspiel O. Drag Coefficient and Terminal Velocity of Spherical and Nonspherical Particles. *Powder Technology*, 58:63–70, 1989.

Heskett M, Takada H, Yamashita R, Yuyama M, Ito M, Geok Y. B, Ogata Y, Kwan C, Heckhausen A, Taylor H, Powell T, Morishige C, Young D, Patterson H, Robertson B, Bailey E, and Mermoz J. Measurement of persistent organic pollutants (POPs) in plastic resin pellets from remote islands: Toward establishment of background concentrations for International Pellet Watch. *Marine Pollution Bulletin*, 64(2):445–448, 2012.

Hidalgo-Ruz V, Gutow L, Thompson R. C, and Thiel M. Microplastics in the Marine Environment: A Review of the Methods Used for Identification and Quantification. *Environmental Science & Technology*, 16, 2012.

Hiller. Functional Principle of a decanter centrifuge, 2019.

Hirai H, Takada H, Ogata Y, Yamashita R, Mizukawa K, Saha M, Kwan C, Moore C, Gray H, Laursen D, Zettler E. R, Farrington J. W, Reddy C. M, Peacock E. E, and Ward M. W. Organic micropollutants in marine plastics debris from the open ocean and remote and urban beaches. *Marine Pollution Bulletin*, 62(8):1683–1692, 2011.

Huggett R. J. *Fundamentals of Geomorphology*. Routledge, third edit edition, 2011.

ICFPA. Sustainability Progress Report. Technical report, International Council of Forest and Paper Associations, 2015.

IEA and OECD. World Energy Outlook. Technical report, 2015.

Inaba T, Hori T, Aizawa H, Ogata A, and Habe H. Architecture , component , and microbiome of bio fi lm involved in the fouling of membrane bioreactors. *npj Biofilms and Microbiomes*, 3(5), 2017.

Kang J.-h, Youn O, Lee K.-w, Kyoung Y, and Joon W. Marine neustonic microplastics around the southeastern coast of Korea. *Marine Pollution Bulletin*, 96:304–312, 2015.

Karak N. *Fundamentals of Polymers: Raw Materials to Finish Products*. Prentice Hall India (PHI), 2009.

Koelmans A. A, Besseling E, Wegner A, and Foekema E. M. Erratum: Plastic as a carrier of POPs to aquatic organisms: A model analysis (Environmental Science and Technology (2013) 47 (7812-7820) DOI: 10.1021/es401169n). *Environmental Science and Technology*, 47(15):8992–8993, 2013.

Koelmans A. A, Besseling E, and Foekema E. M. Leaching of plastic additives to marine organisms. *Environmental Pollution*, 187:49–54, 2014.

Koelmans A. A, Besseling E, and Shim W. J. Nanoplastics in the Aquatic Environment. Critical Review. In *Marine Anthropogenic Litter*, chapter 12, pages 325–240. Springer, doi 10.100 edition, 2015.

Kooi M, Van Nes E. H, Scheffer M, and Koelmans A. A. Ups and Downs in the Ocean: Effects of Biofouling on Vertical Transport of Microplastics. *Environmental Science and Technology*, 51(14):7963–7971, 2017.

Kowalczuk P. B, Akkaya C, Ergun M, Janicki J, Sahbaz O, and Drzymala J. WATER CONTACT ANGLE ON CORRESPONDING SURFACES OF FRESHLY FRACTURED FLUORITE , CALCITE AND MICA.

Physicochemical Problems of Mineral Processing, 53 (1):192–201, 2017.

Kowalski N, Reichardt A. M, and Waniek J. J. Sinking rates of microplastics and potential implications of their alteration by physical, biological, and chemical factors. *MPB*, 109(1):310–319, 2016.

Krumbein W. C. Measurement and geological significance of shape and roundness of sedimentary particles. *Journal of Sedimentary Petrology*, 11:64–72, 1941.

Kubota M. A mechanism for the accumulation of floating marine debris north of Hawaii. *Journal of Physical Oceanography*, 1994.

Kubota M, Takayama K, and Namimoto D. Pleading for the use of biodegradable polymers in favor of marine environments and to avoid an asbestos-like problem for the future. *Applied Microbiology and Biotechnology*, 67(4):469–476, 2005.

Lassen C, Hansen S. F, Magnusson K, Hartmann N. B, Rehne Jensen P, Nielsen T. G, and Brinch A. *Microplastics Occurrence, effects and sources of releases*. Danish Environmental Protection Agency, Copenhagen, Denmark, 2015.

Lattin G. L and Moore C. J. A comparison of neustonic plastic and zooplankton at different depths near the southern California shore. *Marine Pollution Bulletin*, 49:291–294, 2004.

Law K. L, Morét-Ferguson S, Maximenko N. A, Proskurowski G, Peacock E. E, Hafner J, and Reddy C. M. Plastic accumulation in the North Atlantic subtropical gyre. *Science*, 329(5996):1185–1188, 2010.

Leggett J. K. *Marine Clastic Sedimentology: Concepts and Case Studies*. Springer, 2012.

Lehaitre M, Delauney L, and Compere C. *Biofouling and underwater measurements*, pages 463–493. 2008.

Leslie H. A, van Velzen M. J. M, and Vethaak A. D. Microplastic survey of the Dutch environment. *IVM Institute for Environmental Studies*, 476(September), 2013.

Li C, Zhang Y, and Yehuda C. RSC Advances Individual based modeling of Pseudomonas aeruginosa bio fi lm with three detachment. *RSC Advances*, (5):79001–79010, 2015.

Li J, Liu H, and Paul Chen J. Microplastics in freshwater systems: A review on occurrence, environmental effects, and methods for microplastics detection. *Water Research*, 137:362–374, 2018.

Li X, Xu H, Liu J, Zhang J, Li J, and Gui Z. Cyclonic state micro-bubble flotation column in oil-in-water emulsion separation. *Separation and Purification Technology*, 165:101–106, 2016.

Liebezeit G and Dubaish F. Microplastics in beaches of the East Frisian Islands Spiekeroog and Kachelotplate. Technical Report 1, 2014.

Liska I. *The Danube River Basin*. The Handbook of Environmental Chemistry. Springer, 2015.

Liu J. Cyclone-static micro-bubble flotation apparatus & method, 2002.

Lozano L. R and Mouat J. Marine litter in the North-East Atlantic Region. Technical report, 2009.

Luis M, Nascimento F, and Aparicio C. Data classification with the Vogel – Fulcher – Tammann – Hesse viscosity equation using correspondence analysis. 398:71–77, 2007.

Lusher A. L, Burke A, O'Connor I, and Officer R. Microplastic pollution in the Northeast Atlantic Ocean: Validated and opportunistic sampling. *Marine Pollution Bulletin*, 88(1-2):325–333, 2014.

MacArthur Foundation. The New Plastics Economy: Rethinking the future of plastics. *World Economic Forum*, (January):120, 2016.

Maes T, Meulen M. D. V. D, Devriese L. I, Leslie H. A, Huvet A, Frère L, Robbens J, and Vethaak A. D. Microplastics Baseline Surveys at the Water Surface and in Sediments of the North-East Atlantic. *Frontiers in Marine Science*, 4(5):1–13, 2017.

Magnusson K and Norén F. Screening of microplastic particles in and down-stream a wastewater treatment plant. *IVL Swedish Environmental Research Institute*, C 55(C):22, 2014.

Mani T, Hauk A, Walter U, and Burkhardt-Holm P. Microplastics profile along the Rhine River. *Scientific Reports*, 5(December):1–7, 2015.

Martin J, Lusher A, Thompson R. C, and Morley A. The Deposition and Accumulation of Microplastics in Marine Sediments and Bottom Water from the Irish Continental Shelf. *Scientific Reports*, 7(1):1–9, 2017.

Martinez E, Maamaatuaiahutapu K, and Taillandier V. Floating marine debris surface drift: Convergence and accumulation toward the South Pacific subtropical gyre. *Marine Pollution Bulletin*, 58(9):1347–1355, 2009.

Mateo-Sagasta J, Raschid-Sally L, and Thebo A. Global Wastewater and Sludge Production, Treatment and Use. In Drechsel P, Qadir M, and Wichelns D, editors, *Wastewater*. Springer, Dordrecht, 2015.

Mathalon A and Hill P. Microplastic fibers in the intertidal ecosystem surrounding Halifax Harbor, Nova Scotia. *Marine Pollution Bulletin*, 81(1):69–79, 2014.

Mato Y, Isobe T, Takada H, Kanehiro H, Ohtake C, and Kaminuma T. Plastic resin pellets as a transport medium for toxic chemicals in the marine environment. *Environmental Science & Technologychnology*, 35(2): 318–324, 2001.

Maximenko N, Hafner J, and Niiler P. Pathways of marine debris derived from trajectories of Lagrangian drifters. *Marine Pollution Bulletin*, 65(1-3):51–62, 2012.

McCabe W. L, Smith J. C, and Harriott P. *Unit Operations Of Chemical Engineering*. Mcgraw-Hill Education - Europe, 7 edition, 2004.

McDermid K. J and McMullen T. L. Quantitative analysis of small-plastic debris on beaches in the Hawaiian archipelago. *Marine Pollution Bulletin*, 48(7-8):790–794, 2004.

McDevitt J. P, Criddle C. S, Morse M, Hale R. C, Bott C. B, and Rochman C. M. Addressing the Issue of Microplastics in the Wake of the Microbead-Free Waters Act - A New Standard Can Facilitate Improved Policy. *Environmental Science and Technology*, 51(12):6611–6617, 2017.

Minaker V. Prospects For Future Developments in Screw-Conveyor Sedimentation Centrifuges (Decanters): A Discussion. *Chemical and Petroleum Engineering*, 31 (4):200–207, 1995.

Mintenig S, Int-Veen I, Löder M, Primpke S, and Gerdts G. Identification of microplastic in effluents of waste water treatment plants using focal plane array-based micro-Fourier-transform infrared imaging. *Water Research*, 108:365–372, jan 2017.

Mittal K. *Adhesion Aspects of Thin Films*. VSP, Zeist, The Netherlands, 2001.

Mittal K. *Contact Angle, Wettability and Adhesion*. VSP, Utrecht, edition 3 edition, 2003.

Moore C. J. A comparison of neustonic plastic and zoo-plankton abundance in southern California ' s coastal waters. *Marine Pollution Bulletin*, 44:1035–1038, 2002.

Moore C. J, Moore S. L, Leecaster M. K, and Weisberg S. B. A comparison of plastic and plankton in the North Pacific Central Gyre. *Marine Pollution Bulletin*, 42(12):1297–1300, 2001.

Moore C. J. Synthetic polymers in the marine environment: A rapidly increasing, long-term threat. *Environmental Research*, 108(2):131–139, oct 2008.

MSFD Technical Subgroup on Marine Litter. *Guidance on Monitoring of Marine Litter in European Seas*. Number 1. European Union, institute edition, 2013.

Murphy F, Ewins C, Carbonnier F, and Quinn B. Wastewater Treatment Works (WwTW) as a Source of Microplastics in the Aquatic Environment. *Environmental Science & Technology*, 50(11):5800–5808, 2016.

Murray F and Cowie P. R. Plastic contamination in the decapod crustacean Nephrops norvegicus (Linnaeus, 1758). *Marine Pollution Bulletin*, 62(6):1207–1217, 2011.

Nerland I. L, Halsband C, Allan I, and Thomas K. V. Microplastics in marine environments: Occurrence, distribution and effects. Technical report, Oslo, 2014.

Ng K. L and Obbard J. P. Prevalence of microplastics in Singapore's coastal marine environment. *Marine pollution bulletin*, 52(7):761–7, 2006.

Nicholson J. W. *The Chemistry of Polymers*. Royal Society of Chemistry, 5 edition, 2017.

NIIR Board of Consultants and Engineers. *The Complete Technology Book on Plastic Extrusion, Moulding and Mould Designs*. Asia Pacific Business Press, 2006.

Norén F. Small plastic particles in Coastal Swedish waters. Technical Report 3-4, Sweden, 2007.

Norén F, Norén K, and Magnusson K. Marint mikroskopiskt skrap. Undersokning langs svenska vastkusten 2013 & 2014. Technical report, IVL. Rapport 2014:52. Lansstyrelsen i Vastra Gotalands lan, Vattenvardsenheten., 2014.

Notebaert B, Houbrechts G, Verstraeten G, Broothaerts N, Haeckx J, Reynders M, Govers G, Petit F, and Poesen J. Fluvial architecture of Belgian river systems in contrasting environments : Implications for reconstructing the sedimentation history. *Geologie en Mijnbouw*, (May 2014), 2011.

NOVA Chemicals. NOVA Chem: Joffre Expansion - What We Make, 2017.

Obbard R. W, Sadri S, Wong Y. Q, Khitun A. A, Baker I, and Thompson R. C. Global warming releases microplastic legacy frozen in Arctic Sea ice. *Earth's Future*, 2(6):315–320, 2014.

Ozdemir O, Karaguzel C, Nguyen A. V, Celik M. S, and Miller J. D. Contact angle and bubble attachment studies in the flotation of trona and other soluble carbonate salts. *Minerals Engineering*, 22(2):168–175, 2009.

Patel M, Goyal B, Bhadada S, Bhatt J, and Amin A. Getting into the brain: approaches to enhance brain drug delivery. *CNS Drugs*, 23(33-58), 2009.

Perry R. H and Green D. W. *Perry's Chemical Engineers' Handbook*. Mcgraw-Hill Education - Europe, 1997.

Pettijohn F. *Sedimentary Rocks*. Harper and Row, New York, third edit edition, 1975.

Pfeiffer T, Costa A, and Macedonio G. A model for the numerical simulation of tephra fall deposits. *Journal of Volcanology and Geothermal Research*, 140:273–294, 2005.

Pita F and Castilho A. Separation of plastics by froth flotation . The role of size , shape and density of the particles. *Waste Management*, 60:91–99, 2017.

PlasticsEurope. What are Plastics — How are Plastics Made; A Large Family,, 2018.

Porter A, Lyons B. P, Galloway T. S, and Lewis C. Role of Marine Snows in Microplastic Fate and Bioavailability. *Environmental Science and Technology*, 52(12):7111–7119, 2018.

Powers M. A new roundness scale for sedimentary particles. *Journal of Sedimentary Petrology*, 32:117–119, 1953.

Powers V. The Bakelizer. *American Chemical Society National Historic Chemical Landmarks*, pages 1–2, 1993.

Prakash R, Majumder S. K, and Singh A. Chemical Engineering & Processing : Process Intensi fi cation Flotation technique : Its mechanisms and design parameters. (March), 2018.

Records A and Sutherland K. *Decanter Centrifuge Handbook*. Elsevier, 2001.

Reed S, Clark M, Thompson R, and A Hughes K. *Microplastics in marine sediments near Rothera Research Station, Antarctica*, volume 133. aug 2018.

Reisser J, Shaw J, Wilcox C, Hardesty B. D, Proietti M, Thums M, and Pattiaratchi C. Marine plastic pollution in waters around Australia: Characteristics, concentrations, and pathways. *PLoS ONE*, 8(11), 2013.

Remo J. W. F, Heine R. A, and Ickes B. S. Geomorphology Particle size distribution of main-channel-bed sediments along the upper Mississippi River , USA. *Geomorphology*, 264:118–131, 2016.

Rhodes M. *Introduction to Particle Technology*. Wiley, Monash University, Australia, second edi edition, 2008.

Richardson J. F and Zaki W. N. The sedimentation of a suspension of uniform spheres under conditions of viscous flow. *Chemical Engineering Science*, 3(2):65–73, 1954.

Richardson P. N. *Introduction to Extrusion*. Society of Plastics Engineers, Greenwich, 1974.

Riley N. A. Projection Sphericity. 11(2):94–97, 1941.

Ro K. S and Neethling J. B. Biofilm Density for Biological Fluidized Beds. *Research Journal of the Water Pollution Control Federation*, 63(5):815–818, 1991.

Rochman C. M, Hoh E, Kurobe T, and Teh S. J. Ingested plastic transfers hazardous chemicals to fish and induces hepatic stress. *Scientific Reports*, 3:1–7, 2013.

Rochman C. M, Kurobe T, Flores I, and Teh S. J. Early warning signs of endocrine disruption in adult fish from the ingestion of polyethylene with and without sorbed chemical pollutants from the marine environment. *Science of the Total Environment*, 493:656–661, 2014.

Rochman C. M, Kross S. M, Armstrong J. B, Bogan M. T, Darling E. S, Green S. J, Smyth A. R, and Veríssimo D. Scientific Evidence Supports a Ban on Microbeads. *Environmental Science and Technology*, 49(18):10759–10761, 2015.

Rosato D. V, Rosato D. V, and Rosato M. V. Plastic Product Material and Process Selection Handbook. In Rosato D. V, Rosato D. V, and Rosato M. V, editors, *Elsevier*, page 618. Elsevier, Oxford, 2004.

Ryan P. G, Moore C. J, Van Franeker J. A, and Moloney C. L. Monitoring the abundance of plastic debris in the marine environment. *Philosophical Transactions of the Royal Society B: Biological Sciences*, 364 (1526):1999–2012, 2009.

Salta M, Wharton J, Blache Y, Stokes K. R, and Briand J.-f. Marine Biofilms on artificial surfaces : Structure and

dynamics Minireview Marine biofilms on artificial surfaces : structure and dynamics. *Environmental Microbiology*, 15(11):2879–2893, 2013.

Saunders K. J. *Organic Polymer Chemistry: An Introduction to the Organic Chemistry of Adhesives, Fibres, Paints, Plastics and Rubbers*. Springer Science, 2 edition, 1988.

Setälä O, Fleming-Lehtinen V, and Lehtiniemi M. Ingestion and transfer of microplastics in the planktonic food web. *Environmental Pollution*, 185:77–83, 2014.

Shang J, Flury M, Harsh J. B, and Zollars R. L. Comparison of different methods to measure contact angles of soil colloids. *Journal of Colloid Interface Sciences*, 328:299–307, 2008.

Shen H, Forssberg E, and Pugh R. J. Selective flotation separation of plastics by particle control. 33:37–50, 2001.

Smart P. Particle Shape Statistics Revisited. 2013.

Sneed E and Folk R. Pebbles in the lower Colorado River, Texas, a study in particle morphogenesis. *Journal of Geology*, 66:114–150, 1958.

Song Y. K, Hong S. H, Jang M, Kang J. H, Kwon O. Y, Han G. M, and Shim W. J. Large accumulation of micro-sized synthetic polymer particles in the sea surface microlayer. *Environmental Science Technology*, 48(16):9014–9021, 2014.

Stokes G. G. On the Effect of the Internal Friction of Fluids on the Motion of Pendulums. *Transactions of the Cambridge Philosophical Society*, pages 8–106, 1851.

Strand J and Tairova Z. Microplastic particles in North Sea sediments 2015. *DCE - Danish Centre for Environment and Energy*, (178):20pp., 2016.

Strand J, Lassen P, Shashoua Y, and Andersen J. Microplastic particles in sediments from Danish waters. Technical report, ICES Annual Science Conference, Reykjavik, Iceland, 2013.

Stringham G, Simons D, and Guy H. The behaviour of large particles falling in quiescent liquids. *Geological Survey*, page 36, 1969.

Sundt P, Schultze P.-E, and Syversen F. Sources of microplastic-pollution to the marine environment. Technical Report M-321—2015, Norwegian Environment Agency (Miljødirektoratet), 2014.

Swamee P and Ojha C. Drag coefficient and fall velocity of nonspherical particles. *Journal of Hydraulic Engineering*, 117(5):660–667, 1991.

Talsness C. E, Andrade A. J. M, Kuriyama S. N, Taylor J. A, and vom Saal F. S. Components of plastic: experimental studies in animals and relevance for human health. *Philosophical transactions of the Royal Society of London. Series B, Biological sciences*, 364 (1526):2079–2096, jul 2009.

Talvitie J and Heinonen M. Preliminary study on Synthetic microfibers and particles at a municipal waste water treatment plant. Technical report, 2014.

Talvitie J, Mikola A, Setälä O, Heinonen M, and Koistinen A. How well is microlitter purified from wastewater? – A detailed study on the stepwise removal of microlitter in a tertiary level wastewater treatment plant. *Water Research*, 109:164–172, 2017.

Tarleton E. S and Wakeman R. J. Solid/liquid separation equipment. In Tarleton E. S and Wakeman R. J, editors, *Solid/Liquid Separation*, pages 1–77. Butterworth-Heinemann, Oxford, 2007.

Tekman M. B, Krumpen T, and Bergmann M. Marine litter on deep Arctic seafloor continues to increase and spreads to the North at the HAUSGARTEN observatory. *Deep-Sea Research Part I: Oceanographic Research Papers*, 120(November 2016):88–99, 2017.

Thompson R. C. *Plastic debris in the marine environment:Consequences and solutions*, volume 193. jan 2006.

Thompson R. C, Olson Y, Mitchell R. P, Davis A, Rowland S. J, John A. W, McGonigle D, and Russell A. E. Lost at Sea: Where Is All the Plastic? *Science*, 304 (5672):838, 2004.

Thompson R. M. Microplastics in the Marine Environment: Sources, Consequences and Solutions. In *Marine Anthropogenic Litter*. Springer, 2015.

Toorman E. Sediment Transport Modelling : Modelling : from particle and Kolmogorov scales to geomorphological scales Outline Introduction Multi-scales. Technical Report September, Hydraulics Laboratory Civil Engineering Department KU Leuven, 2009.

Tourinho P. S, Ivar do Sul J. A, and Fillmann G. Is marine debris ingestion still a problem for the coastal marine biota of southern Brazil? *Marine Pollution Bulletin*, 60 (3):396–401, 2010.

Ugolini A, Ungherese G, Ciofini M, Lapucci A, and Camaiti M. Microplastic debris in sandhoppers. *Estuarine, Coastal and Shelf Science*, 129:19–22, 2013.

Ulrich H. *Raw Materials for Industrial Polymers*. Oxford University Press, 1988.

UNEP. Plastics in Cosmetics. Technical report, United Nations Environment Programme, 2015.

Van Cauwenberghe L. *Occurrence, effects and risks of marine microplastics*. Thesis submitted in fulfilment of the requirements for the degree of doctor (phd) in applied biological sciences., Ghent University, 2015.

Van den Eynde D, Lauwaert B, Martens C, and Pirlet H. Dredging and dumping. Technical report, Royal Belgian Institute of Natural Sciences (RBINS), Operational Directorate Natural Environment (MUMM), Ostend, Belgium, 2015.

van Franeker J. A, Blaize C, Danielsen J, Fairclough K, Gollan J, Guse N, Hansen P. L, Heubeck M, Jensen J. K, Le Guillou G, Olsen B, Olsen K. O, Pedersen J, Stienen E. W, and Turner D. M. Monitoring plastic ingestion by the northern fulmar Fulmarus glacialis in the North Sea. *Environmental Pollution*, 159(10): 2609–2615, 2011.

van Oss C. J. *Interfacial Forces in Aqueous Media*. CRC Press, second edi edition, 2006.

Van Sebille E, England M. H, and Froyland G. Origin, dynamics and evolution of ocean garbage patches from observed surface drifters. *Environmental Research Letters*, 7(4), 2012.

Vianello A, Boldrin A, Guerriero P, Moschino V, Rella R, Sturaro A, and Da Ros L. Microplastic particles in sediments of Lagoon of Venice, Italy: First observations on occurrence, spatial patterns and identification. *Estuarine, Coastal and Shelf Science*, 130:54–61, 2013.

VLAIO. Spearhead clusters — Agentschap Innoveren en Ondernemen, 2018.

Von Moos N, Burkhardt-Holm P, and Köhler A. Uptake and effects of microplastics on cells and tissue of the blue mussel Mytilus edulis L. after an experimental exposure. *Environmental Science & Technology*, 46(20): 11327–11335, 2012.

Wagner M and Lambert S. Microplastics Are Contaminants of Emerging Concern in Freshwater Environments: An Overview. In *The Handbook of Environmental Chemistry*, page 302. Springer, 2018.

Wagner M, Scherer C, Alvarez-Muñoz D, Brennholt N, Bourrain X, Buchinger S, Fries E, Grosbois C, Klasmeier J, Marti T, Rodriguez-Mozas S, Urbatzka R, Vethaak A. D, Winther-Nielsen M, and Georg R. Microplastics in freshwater ecosystems: what we know and what we need to know. *Environmental Sciences Europe*, (12), 2014.

Walker G. P. L, Wilson L, and Bowell E. L. G. Explosive Volcanic Eruptions-I The Rate of Fall of Pyroclasts. *Geophysical Journal of the Royal Astronomical Society*, 22(4):377–383, 1971.

Waller C. L, Griffiths H. J, Waluda C. M, Thorpe S. E, Loaiza I, Moreno B, Pacherres C. O, and Hughes K. A. Microplastics in the Antarctic marine system: An emerging area of research. *Science of the Total Environment*, 598:220–227, 2017.

Walstra D.-j, Hoyng C, Tonnon P, and Van Rijn L. Experimental study investigating various shoreface nourishment designs. *Coastal Engineering Proceedings*, (January), 2011.

Wang C.-q, Wang H, Fu J.-g, and Liu Y.-n. Flotation separation of waste plastics for recycling — A review. *Waste Management*, 41:28–38, 2015.

Weber M and Paddock D. Interceptional and gravitational collision efficiencies for single collectors at intermediate Reynolds numbers. *Journal of Colloid Interface Sciences*, 94(2):328–335, 1983.

Weir C. L. *Introduction to Molding*. Society of Plastics Engineers, 1975.

Wenzel R. N. Resistance of solid particles to wetting by water. *Industrial & Engineering Chemistry*, 28(8): 988–994, aug 1936.

Willis K. A, Eriksen R, Wilcox C, and Hardesty B. D. Microplastic Distribution at Different Sediment Depths in an Urban Estuary. *Frontiers in Marine Science*, 4 (December), 2017.

Wills B and Finch J. *Wills' Mineral Processing Technology: An Introduction to the Practical Aspects of Ore Treatment and Mineral Recovery*. Elsevier, edition 8 edition, 2016.

Wilson L and Huang T. C. The influence of shape on the atmospheric settling velocity of volcanic ash particles. *Earth and Planetary Science Letters*, 44(2):311–324, 1979.

WM. Waste Management Announces Second Quarter Earnings. Technical report, 2015.

Woodall L. C, Sanchez-Vidal A, Canals M, Paterson G. L. J, Coppock R, Sleight V, Calafat A, Rogers A. D, Narayanaswamy B. E, and Thompson R. C. The deep sea is a major sink for microplastic debris. *Royal Society Open Science*, 1:140317, 2014.

Wright S. L, Rowe D, Thompson R. C, and Galloway T. S. Microplastic ingestion decreases energy reserves in marine worms. *Current Biology*, 23(23):R1031–R1033, 2013.

Yang W.-C. *Handbook of Fluidization and Fluid-Particle Systems*. CRC Press, first edit edition, 2003.

Yuan Y and Lee T. R. Contact Angle and Wetting Properties. In Bracco G and Holst B, editors, *Surface Science Techniques*, chapter 1. Springer, 2013.

Zaichik L. I, Pershukov V. A, Kozelev M. V, and Vinberg A. A. Modeling of Dynamics , Heat Transfer , and Combustion in Two-Phase Turbulent Flows : 1 . Isothermal Flows. 1777(97):291–310, 1997.

Zalasiewicz J, Williams M, Waters C. N, Barnosky A. D, and Haff P. The technofossil record of humans. *Anthropocene Review*, 1(1):34–43, 2014.

Zalasiewicz J, Waters C. N, Ivar do Sul J. A, Corcoran P. L, Barnosky A. D, Cearreta A, Edgeworth M, Gałuszka A, Jeandel C, Leinfelder R, McNeill J. R, Steffen W, Summerhayes C, Wagreich M, Williams M, Wolfe A. P, and Yonan Y. The geological cycle of plastics and their use as a stratigraphic indicator of the Anthropocene. *Anthropocene*, 13:4–17, 2016.

Zettler E. R, Mincer T. J, and Amaral-Zettler L. A. Life in the "plastisphere": Microbial communities on plastic marine debris. *Environmental Science and Technology*, 47(13):7137–7146, 2013.

Zhao J, Ran W, Teng J, Liu Y, Liu H, Yin X, Cao R, and Wang Q. Microplastic pollution in sediments from the Bohai Sea and the Yellow Sea, China. *Science of the Total Environment*, 640-641:637–645, 2018.

Zhao S, Zhu L, Wang T, and Li D. Suspended microplastics in the surface water of the Yangtze Estuary System, China: First observations on occurrence, distribution. *Marine Pollution Bulletin*, 86(1-2):562–568, 2014.

Zheng Y and Zaoui A. Wetting and nanodroplet contact angle of the clay 2:1 surface: The case of Na-montmorillonite (001). *Applied Surface Science*, 396: 717–722, 2017.

Zhou Q, Zhang H, Fu C, Zhou Y, Dai Z, Li Y, Tu C, and Luo Y. The distribution and morphology of microplastics in coastal soils adjacent to the Bohai Sea and the Yellow Sea. *Geoderma*, 322(March):201–208, 2018.

Ziccardi L. M, Edgington A, Hentz K, Kulacki K. J, and Kane Driscoll S. Microplastics as vectors for bioaccumulation of hydrophobic organic chemicals in the marine environment: A state-of-the-science review. *Environmental Toxicology and Chemistry*, 35(7):1667–1676, 2016.

Zisman W. Relation of the Equilibrium Contact Angle to Liquid and Solid Constitution. *Fowkes: Contact Angle, Wettability, and Adhesion*, page 51, 1964.

Zitko V and Hanlon M. Another source of pollution by plastics: skin cleansers with plastic scrubbers. *Marine Pollution Bulletin*, 22(41-42), 1991.

A

Extra Tables and Figures

Table A.1: Summary of the main performance properties of the most common plastic types
(Adapted from Willis *et al.*, 2017; Rosato *et al.*, 2004).

Polymer type	Properties
Polypropylene	High chemical resistance, high fatigue resistance, high elasticity, high toughness, high insulation
Low-density polyethylene	High flexibility, high ductility, low tensile strength
High-density polyethylene	Moderate stiffness, high tensile strength, high rigidity
Polyvinyl chloride	High flexibility or high rigidity, very high tensile strength
Polyethylene terephthalate	Very high chemical resistance, high recyclability, high strength to weight ratio, shatterproof
Polyurethane	Very high adaptability, high tensile strength and high rigidity or high flexibility and high toughness
Polystyrene	Convertibility to foams, high insulation, low impact resistance
Polyamide	High adaptability, high heat resistance
Polycarbonate	Very high impact resistance, high tensile strength, high insulation

Table A.2: Overview of some common applications corresponding to the plastic types discussed in Table 2.1 along with their recognizable recycling codes (Adapted from Edmondson and Gilbert, 2017).

Polymer type	Recycling code	Applications
Polypropylene	05 PP	Folders, food packaging, automotive bumpers, microwave containers, external prostheses, ropes, living hinges, bottle caps and strapping
Low-density polyethylene	04 PE-LD	Films for food packaging, agricultural films, house wrap, grocery bags and reusable bags
High-density polyethylene	02 PE-HD	Toys, milk bottles, pipes and fuel tanks
Polyvinyl chloride	03 PVC	Window frames, flooring, pipes, sheathing for electrical cables, containers and garden hoses
Polyethylene terephthalate	01 PET	Bottles, strapping, textiles and tape applications
Polyurethane	07 O	Mattresses, cushions, insulation panels, inside refrigerators and freezers as insulation foams and sponges
Polystyrene	06 PS	Spectacle frames, packaging, plastic cups, utensils, CD cases, license plate frames, Petri dishes and Styrofoam
Polyamide	07 O	Textiles
Polycarbonate	07 O	Electrical hardware, DVD's, dome-lights, sound walls, safety glazing, police riot gear, protection films on displays and signs, motorcycle windscreens and smartphone cases

Table A.3: Characterisation of microplastic particles in sediments worldwide. The location (*Site*), polymer type (*PT*), most frequently observed particle size (*PS*) and particle morphology are provided. For the latter, pellets and granules (as discussed in subsection 2.2.2) are considered as similar and termed *Spherical*.

Site	PT [type;%]	PS [μm]	Particle morphology [%]			Reference
			Fibres	Spherical	Other	
North-East Atlantic	N/A	<300	41	59	0	Maes *et al.* (2017)
North Sea	N/A	<300	41	0	59	Strand and Tairova (2016)
North Atlantic	N/A	<300	N/A	N/A	N/A	Mathalon and Hill (2014)
Australian waters	N/A	<300	87	1	12	Willis *et al.* (2017)
Deep sea trench	N/A	<300	75	0	25	Fischer *et al.* (2015)
Dutch waters	N/A	<300	dominant	N/A	N/A	Leslie *et al.* (2013)
Antarctic waters	N/A	N/A	dominant	N/A	N/A	Reed *et al.* (2018)
Belgian waters	PS, PP, PE and nylon	<300	59	37	16	Claessens *et al.* (2011)
Irish waters	PA;23, PET;11, PP;3, AC;2	**	85	0	15	Martin *et al.* (2017)
Venetian Lagoon	PE;48, PP;34, PES;4, PS;4,	<300	11	1	88	Vianello *et al.* (2013)
Yellow Sea and Bohai Sea	RY;61, PE;16, PET;12, PP;7, PA;3	<500	94	2	4	Zhao *et al.* (2018)
Atlantic Ocean, Indian Ocean and Mediterranean Sea	RY;57, PES;23, PA;15, AC;5	<1000	100	0	0	Woodall *et al.* (2014)
Worldwide	PES;56, AC;23, PP;7, PE;6, PA;3	N/A	N/A	N/A	N/A	Browne *et al.* (2011)

Table A.4: Script of the Matlab function containing the iterative algorithm used to derive the approximated particle Reynolds numbers according to Dioguardi *et al.* (2018) from input values for d_p, ρ_p, ρ_f, μ, Ψ and an inital prediction for Re_p.

```matlab
function [Re] =  ReynoldsNumber_Dioguardi(d_p, rho_p, Psi, rho_f,...
    mu_f, Re_start)

%Constant values:
g=9.81;
tol=1.e-1000;
exp1=0.25;
exp2=0.08;
exp3=-5.05;

%Preallocation:
Re_old=zeros(1,length(d_p));
Cd_old=zeros(1,length(d_p));
wt_old=zeros(1,length(d_p));

%Iterative algorithm:
for j=1:length(d_p)

Re_old(j)=Re_start;
Cd_old(j)=(24/Re_old(j))*(((1-Psi)/Re_old(j))+1)^exp1+...
    (24/Re_old(j))*0.1806*(Re_old(j)^0.6459)*...
    Psi^(-(Re_old(j)^exp2))+0.4251/(1+(6880.95/(Re_old(j)*...
    (Psi^exp3)))));
wt_old(j)=sqrt((4*g*d_p(j)*(rho_p-rho_f))/(3*Cd_old(j)*rho_f));

    for i=1:10
        Cd_new=(24/Re_old(j))*(((1-Psi)/Re_old(j))+1)^exp1+...
            (24/Re_old(j))*0.1806*(Re_old(j)^0.6459)*...
            Psi^(-(Re_old(j)^exp2))+0.4251/(1+(6880.95/(Re_old(j)*...
            (Psi^exp3)))));
        wt_new=sqrt((4*g*d_p(j)*(rho_p-rho_f))/(3*Cd_new*rho_f));
        Re_new=(rho_f*wt_new*d_p(j))/mu_f;
        res_Re=abs(Re_new-Re_old(j));
        if(res_Re<=tol)
            break
        else
            Re_old(j)=Re_new;
            Cd_old(j)=Cd_new;
            wt_old(j)=wt_new;
            continue
        end
    end

%Assign solution to output:
Re(j)=Re_new;

end
end
```
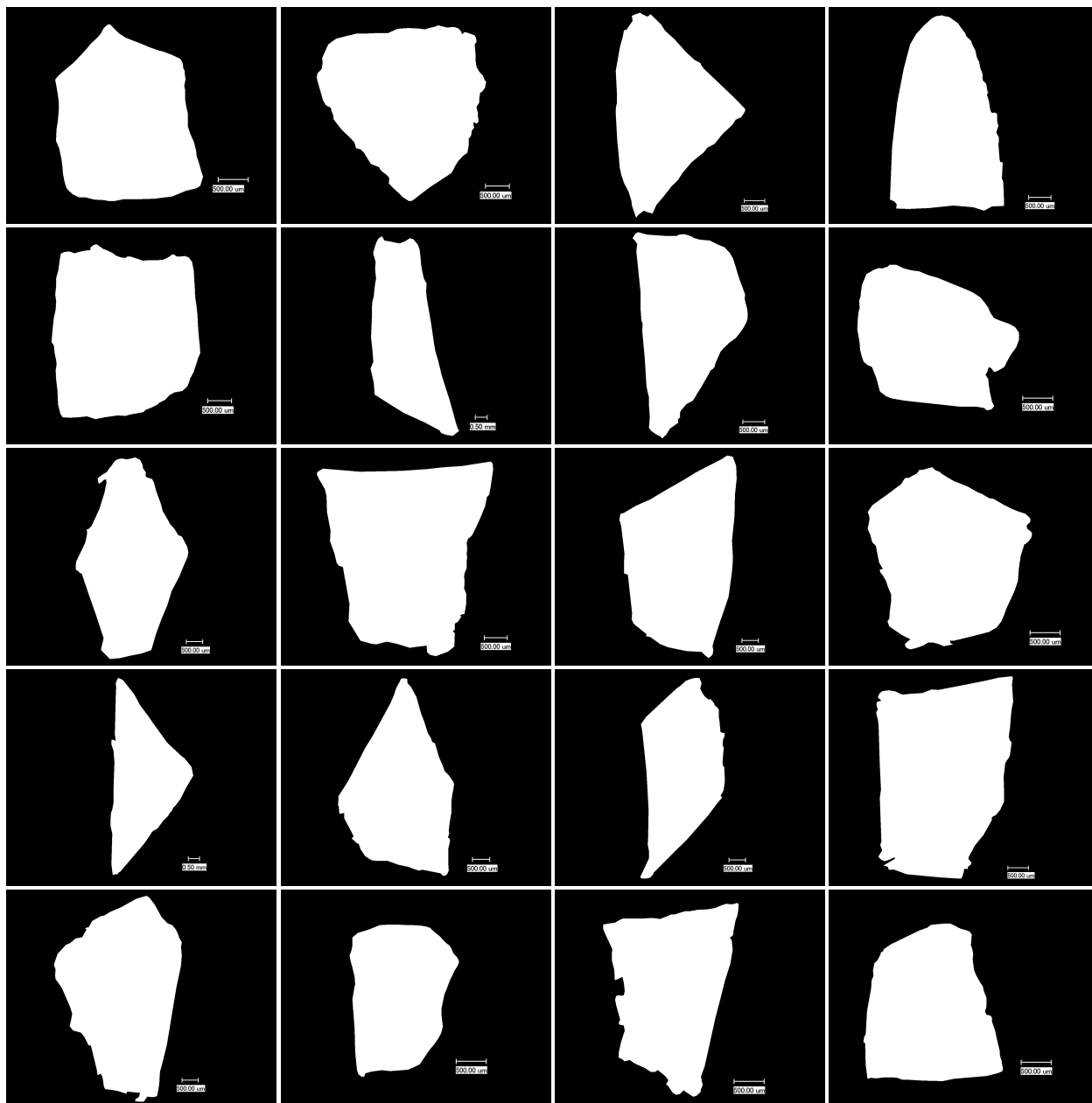
Figure A.1: Post-processed 2D-images of 20 different microplastic particles originating from discarded Cola-Cola bottles, captured by means of a Keyence VHX-500FE Digital Microscope and processed by the image analysis software ImageJ.
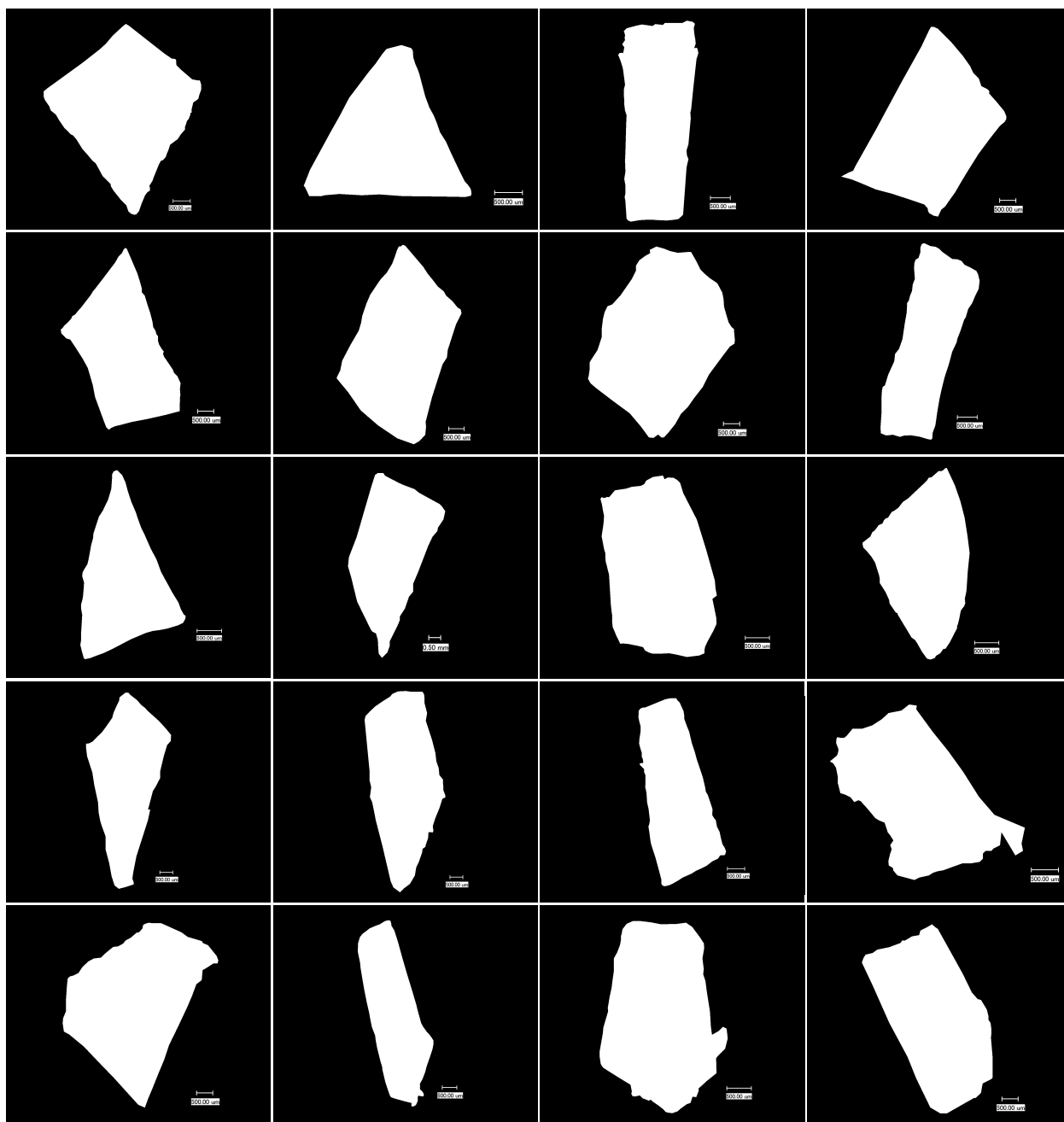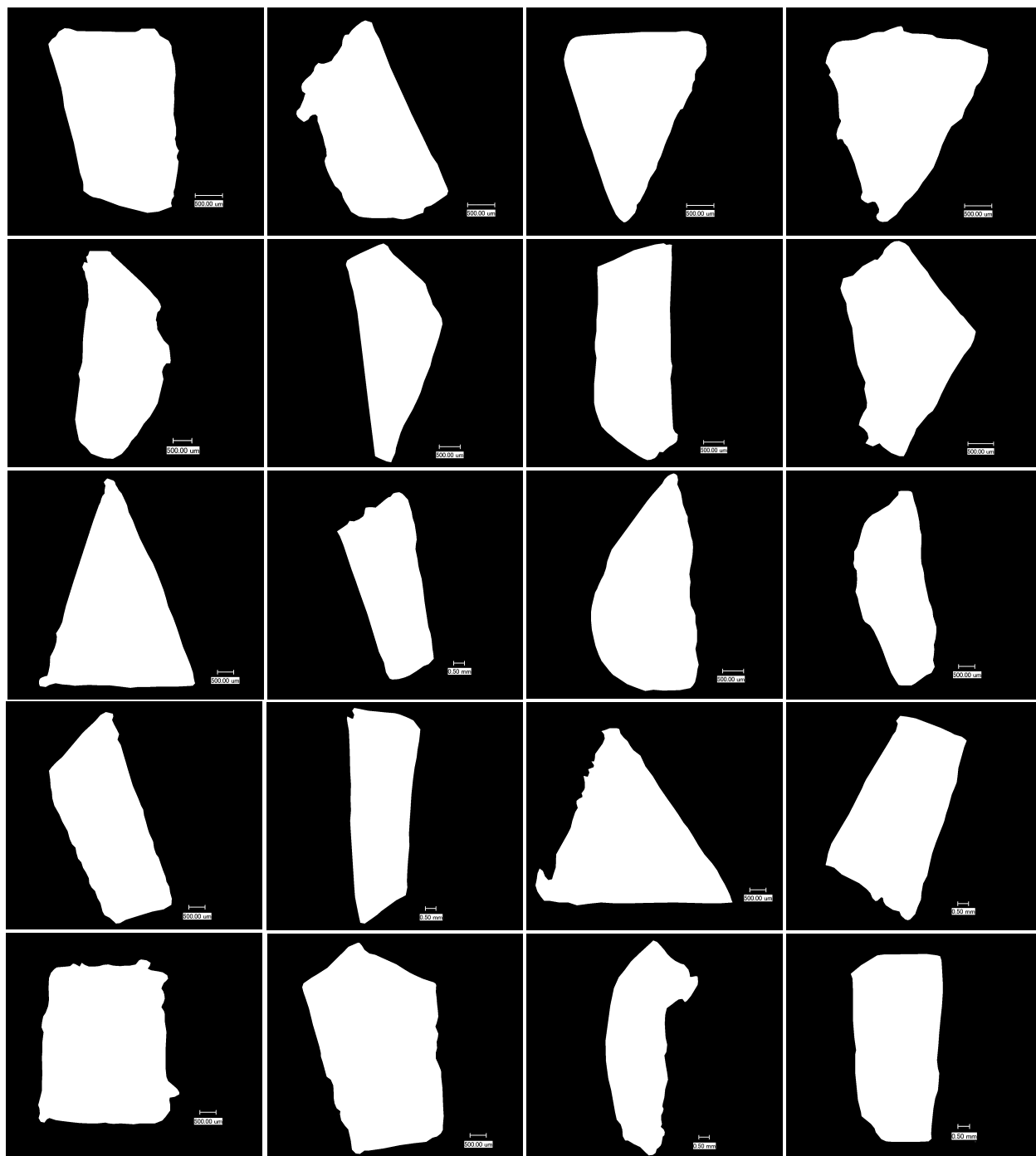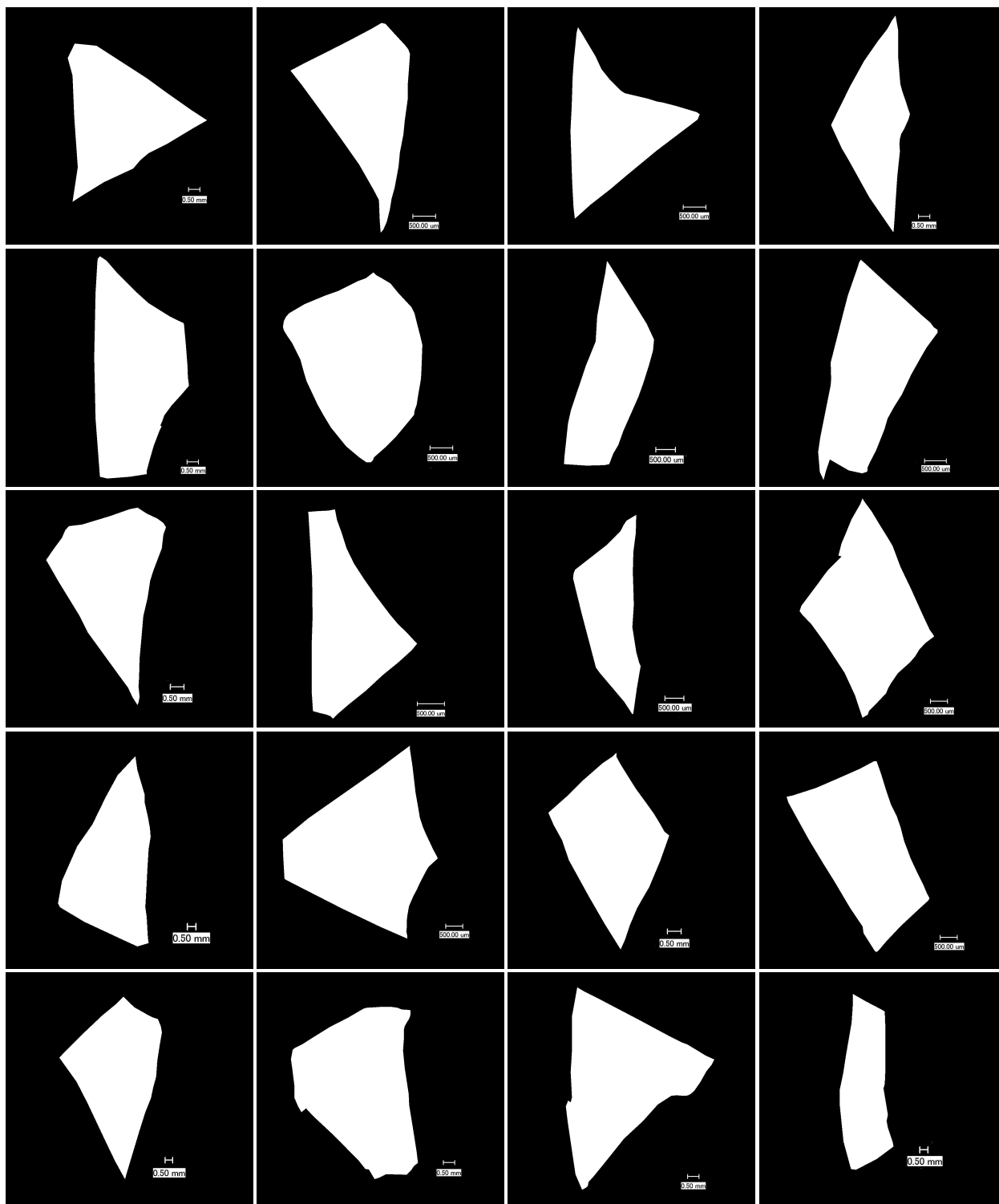
Figure A.2: Post-processed 2D-images of 20 different microplastic particles originating from discarded flowerpots, captured by means of a Keyence VHX-500FE Digital Microscope and processed by the image analysis software ImageJ.
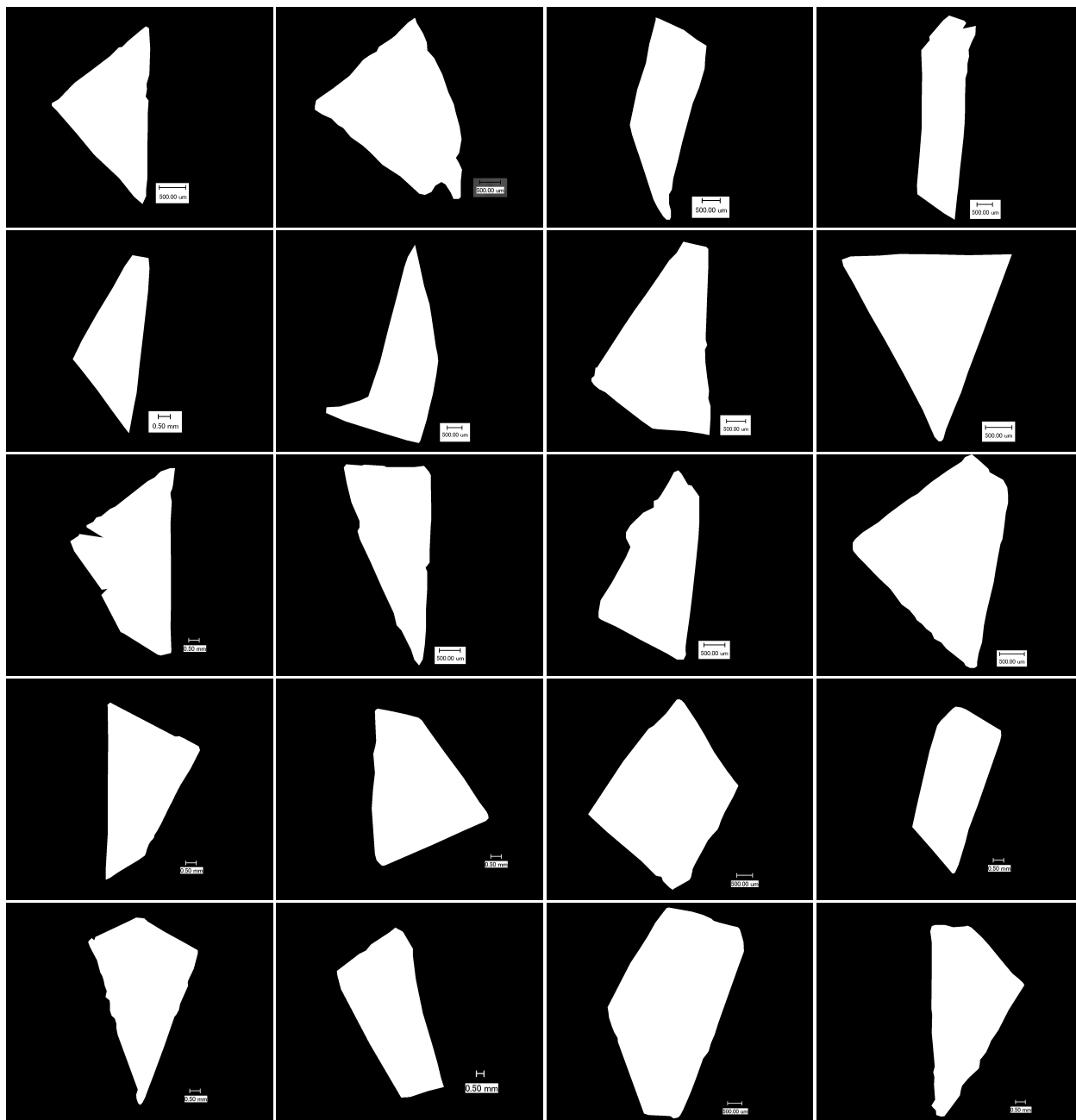
Figure A.3: Post-processed 2D-images of 20 different microplastic particles originating from discarded Dash bottles, captured by means of a Keyence VHX-500FE Digital Microscope and processed by the image analysis software ImageJ.
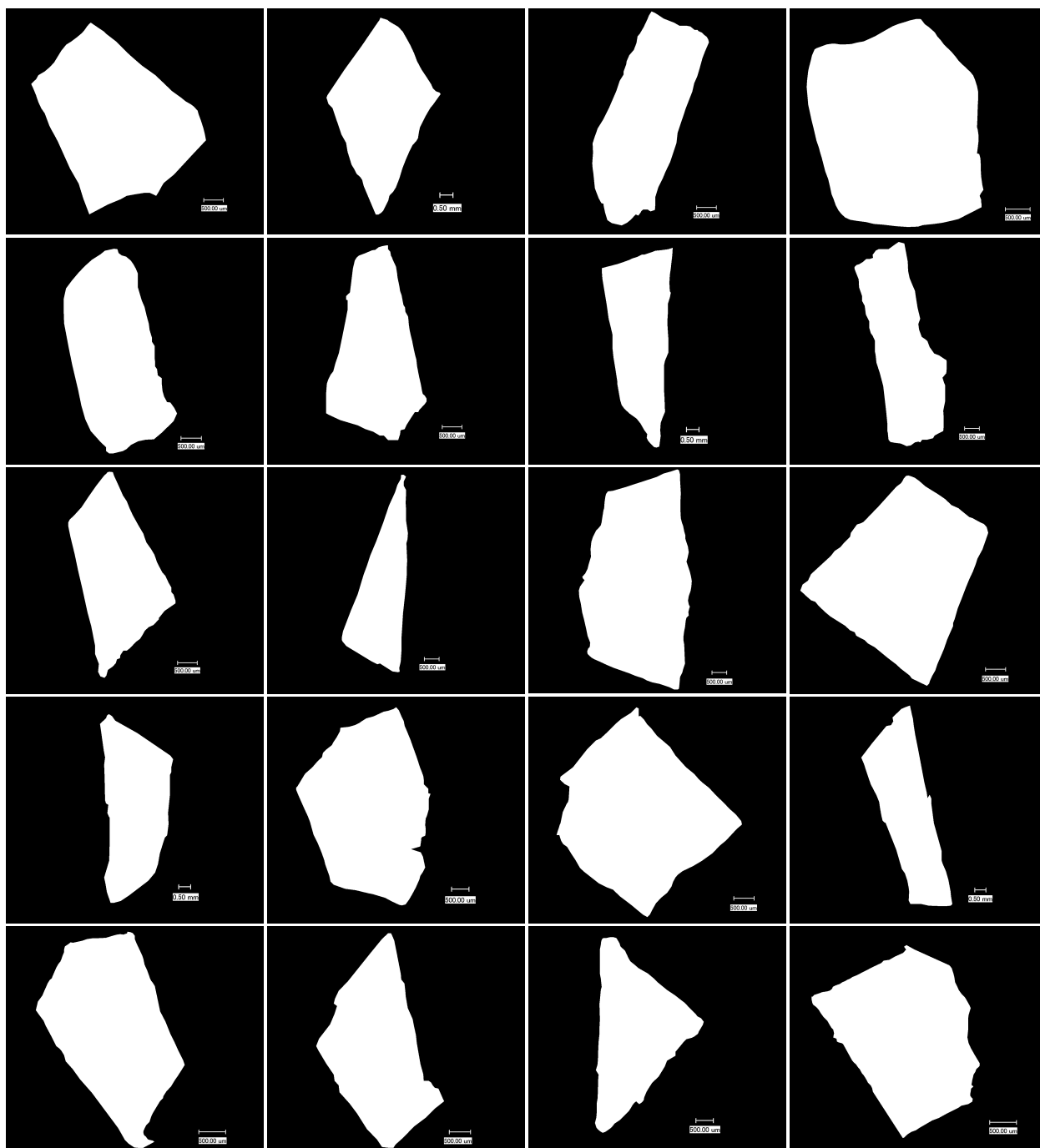
Figure A.4: Post-processed 2D-images of 20 different microplastic particles originating from discarded Lotus Speculoos packages, captured by means of a Keyence VHX-500FE Digital Microscope and processed by the image analysis software ImageJ.

Figure A.5: Post-processed 2D-images of 20 different microplastic particles originating from discarded Jupiler shrink wrap, captured by means of a Keyence VHX-500FE Digital Microscope and processed by the image analysis software ImageJ.

Figure A.6: Post-processed 2D-images of 20 different microplastic particles originating from discarded mushroom containers, captured by means of a Keyence VHX-500FE Digital Microscope and processed by the image analysis software ImageJ.
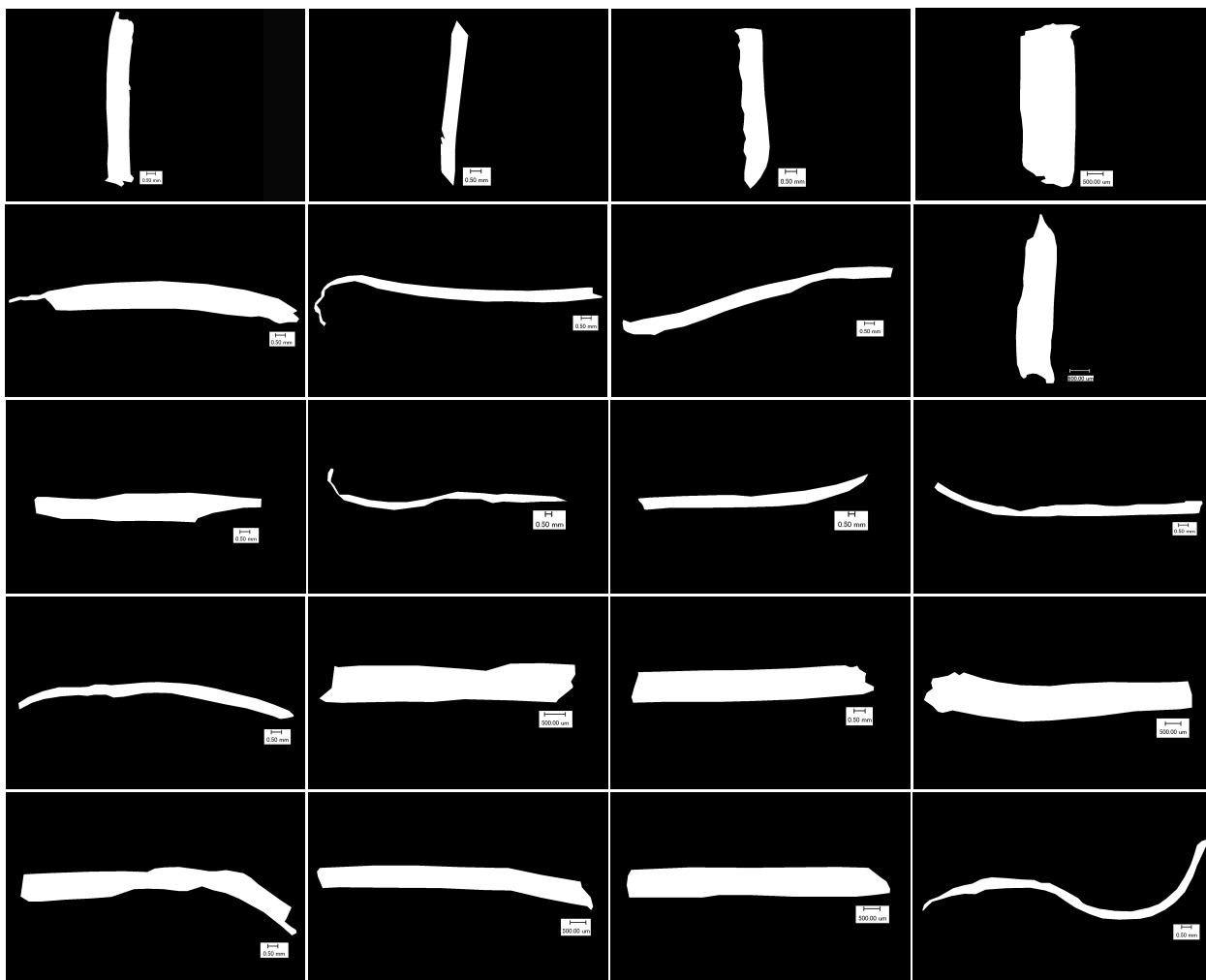
Figure A.7: Post-processed 2D-images of 20 different microplastic particles originating from discarded PVC-pipes, captured by means of a Keyence VHX-500FE Digital Microscope and processed by the image analysis software ImageJ.
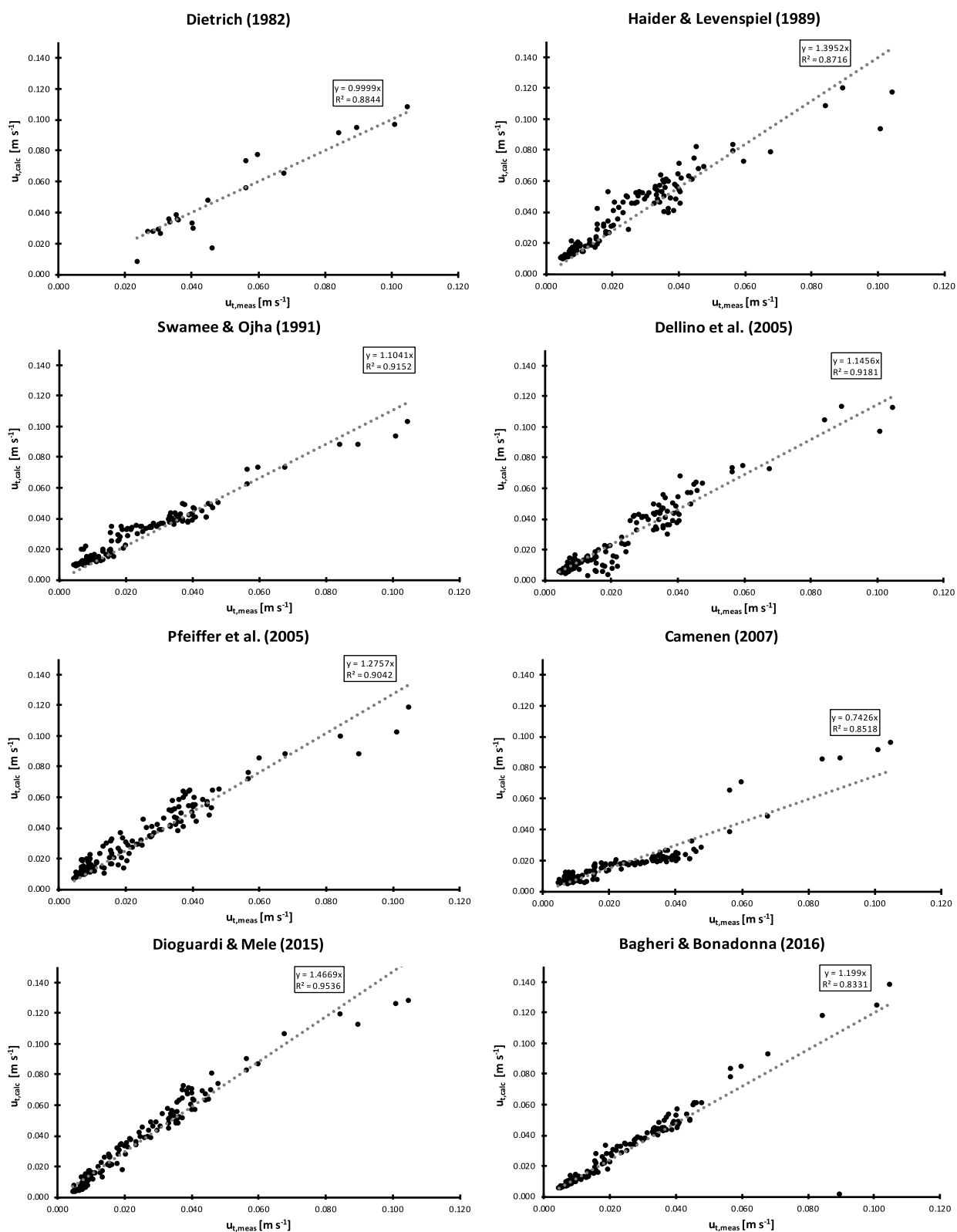
Figure A.8: Scatter plots of $u_{t,calc}$ versus $u_{t,meas}$ calculated by the shape-dependent drag laws discussed in this thesis, excluding the ones provided in Figure 5.4. Dotted grey lines represent the linear regression lines of the type $y = ax$ with R^2 the corresponding correlation coefficient.
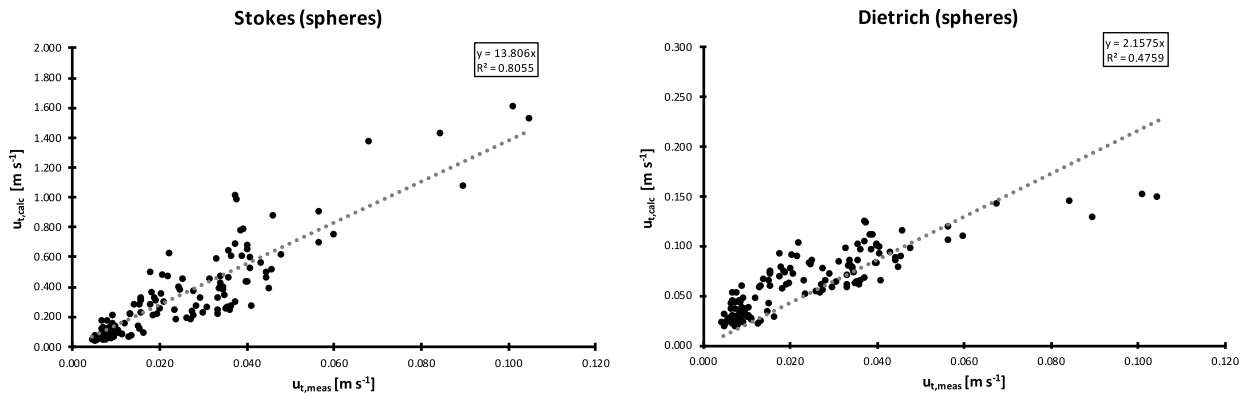
Figure A.9: Scatter plots of $u_{t,calc}$ versus $u_{t,meas}$ comparing the theoretical terminal velocity calculated by the drag laws for spherical particles proposed by Stokes (1851) (left) and Dietrich (1982) (right). Dotted grey lines represent the linear regression lines of the type $y = ax$ with R^2 the corresponding correlation coefficient.